Hybrid Electric Powertrain Design and Control with Planetary Gear Sets for Performance and Fuel Economy

by

Oguz H. Dagci

A dissertation submitted in partial fulfillment
of the requirements for the degree of
Doctor of Philosophy
(Electrical Engineering: Systems)
in The University of Michigan
2018

Doctoral Committee:

Professor Jessy W. Grizzle, Co-Chair
Professor Huei Peng, Co-Chair
Professor Bogdan Epureanu
Professor Jing Sun

Oguz H. Dagci

oguzhada@umich.edu

ORCID iD: 0000-0003-1753-2137

ACKNOWLEDGEMENTS

I would like to express my sincerest appreciation to both of my advisors, Professor Jessy W. Grizzle and Professor Huei Peng, for their support and guidance over the past five years. I will never forget the day I spoke to Professor Grizzle about my PhD application. On that day, after carefully listening to me about my background, motivation, and goals, he accepted me as his PhD student without any hesitation. I am highly grateful to him for his trust in me. I am also thankful to Professor Peng for helping me find my research topic and progress in the right direction with positive attitude and constructive feedback.

I would like to give my special thanks to Becky Turanski and Professor David L. Neuhoff for their guidance on how to meet PhD requirements and milestones as a part-time PhD student.

Last, but not least, I would like to thank to my mother, Sevinc Dagci, and my wife, Olcay Bilgic Dagci. My mother has kept my morale high at difficult times with her endless love and wise perspectives. My wife has always had full confidence in my abilities and has encouraged me when I needed motivation, challenged me when I needed to be pushed, and made sacrifices to let me pursue my dreams.

TABLE OF CONTENTS

LIST OF FIGURES

Figure

LIST OF TABLES

Table

ABSTRACT

Planetary gear sets (PGs) play a key role in hybrid electric vehicle (HEV) design by enabling a variety of unique architectures using a limited number of powertrain components. Leveraging the capability of this mechanical device, this study introduces an automated design process for PG-based HEV systems focusing on both fuel economy and performance, while also deriving the necessary analysis and synthesis tools. First, the design process generates all possible modes in an HEV design with a given set of powertrain components. The data structure and the derivation method of speed and torque relationships of each mode enable an exhaustive search of the large design space that grew with all the component topology and PG gear ratio combinations. Second, all powertrain types realizable with a given set of components are mathematically shown, and each feasible mode is classified under one of these powertrain types. Third, computationally efficient linear programming solvers suitable for vector operations are developed for each powertrain type to assess the forward- and backward-speed gradeability, long-hauling torque, and acceleration time of each mode for all PG gear ratio combinations. Fourth, the combination of modes that meets the performance requirements, along with the number and location of clutches that make these mode transitions possible, are identified. As a result, each potent mode combination, the clutches necessary for the mode transition, and the auxiliary modes established through all clutch state combinations constitute a design that meets the performance criteria. Last, the fuel economy improvement potential of each design is evaluated using an algorithm that approximates dynamic programming optimization. The results show that light-duty truck performance requirements can

be met by many two-PG HEV designs without sacrificing fuel economy if the right analysis and synthesis techniques for exploring the entire design space are developed. In addition to the design process, the feasibility of mode transitions and the effect of mode transitions on the fuel economy simulation results are investigated. For this purpose, the dynamics of mode transition is analyzed, and control algorithms achieving the transitions without interrupting the desired vehicle torque are developed. Then, these analysis and synthesis techniques are automated so that they can be integrated into the fuel economy simulation algorithm. The simulation results reveal that some mode transitions have a negative effect on fuel economy and the assumption of mode transition feasibility at any operating point is not valid.

CHAPTER I

Introduction

1.1 Motivation

The history of hybrid electric vehicles (HEVs) dates back to the late 1890s [1]. These vehicles were either parallel or series type. Their purpose was to complement the technological deficiencies in internal combustion engines with lead acid batteries rather than to improve fuel economy. Advancements in internal combustion engines in terms of power density and reliability, and the expansion of a gasoline supply network made HEVs disappear from the market by the end of World War I.

In the U.S., the resurrection of HEVs occurred in the 1990s thanks to the advancements in power electronics, battery technology, and government funded research programs such as Partnership for New Generation Vehicles (PNGV). The hybrid electric vehicles developed by U.S. automotive original equipment manufacturers (OEMs) stayed at the research stage, however, due to low oil prices, shifting customer demand towards low efficiency sport-utility vehicles (SUVs), lack of financial feasibility for the additional cost of vehicle hybridization, and an emphasis on full electric vehicles by regulatory bodies in the U.S. In this market environment, Toyota introduced the world's first mass-produced HEV, which possessed a state-of-the-art hybrid electric vehicle architecture in Japan in 1997, and worldwide in 2000. Despite initial skepticism, the Toyota Prius was a big success due to its high fuel economy, reliability, and

popular image. Due to the Prius's market success, rising oil prices, and increasing fuel economy regulations in the 2000s, other OEMs followed the trend and introduced their own HEV models. As of the end of 2016, the share of HEVs in the U.S. light-duty vehicle market was 2.0%, 85% of which belonged to vehicles that use powertrain architectures realized with the planetary gearsets similar to those of the Prius [2]. Of the remaining 15%, most used parallel hybrid architectures. The high percentage share of planetary gearset-based powertrain architectures was an indication of their success in the market and showed a need for further research to improve their capabilities, explore their limits, and achieve high impact research results.

Switching the perspective from the past of HEVs to their future also indicates a need for further research on hybrid architectures with planetary gearsets. Fuel economy standards set by the U.S. Environmental Protection Agency (EPA) and the Department of Transportation's National Highway Traffic Safety Administration (NHTSA) in 2012 require that the corporate average fuel economy (CAFE) for new light-duty vehicles be 36.6 miles per gallon (mpg) and 54.5mpg in 2017 and 2025, respectively, as shown in Figure 1.1 [3]. Thus far, automotive OEMs have met current regulations with limited electrification/hybridization in the small and midsize vehicle segments, and incremental efficiency improvements in the conventional powertrain technologies for cars and light-duty trucks.

As seen in Figure 1.1, the gap between target CAFE and projected achieved CAFE (without credits) will widen every year between 2018 and 2025 [4]. The EPA projects that this gap can be closed with the application of new technologies to conventional engines, and the introduction of a higher number of HEVs, plug-in hybrid electric vehicles (PHEVs), and electric vehicles (EVs) [5]. The Center for Automotive Research (CAR) also predicts a major shift to HEVs and PHEVs by 2025 [6]. Furthermore, an analysis conducted by researchers at MIT researchers reveals that major contributors to fuel economy improvements will likely come from

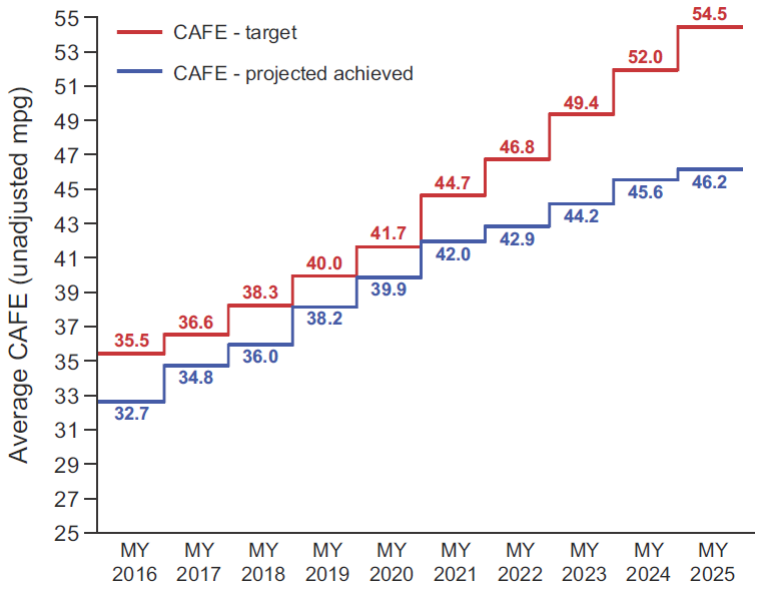

Figure 1.1: Average fleet-wide CAFE performance targets and the corresponding projected achieved performance levels (without credits) for model years 2016 through 2025 [4].

HEV, PHEV, and EV technologies, and that the 2025 targets can be achieved with at least a 21% HEV market share [7].

According to the new regulations, the annual increase in fuel economy for light-duty trucks is to be, on average, 3.5% from 2017 to 2021, and 5% from 2022 to 2025 [8]. Since the market share of light-duty trucks and large sports utility vehicles (SUVs) in the U.S. reached 40% at the beginning of 2017 [9], OEMs with large light-duty truck market shares must consider not only incremental technologies but also advanced powertrain technologies such as electrification/hybridization. Moreover, there are incentives (additional credits) for game changing technologies including hybridization of light-duty pickup trucks, in the new regulations for the years between 2017 and 2025 [5]. However, due to the usage profiles and performance requirements of these vehicle classes, simple hybrid electric powertrain designs either provide insufficient benefits or require the use of costly and bulky electrical components. Despite these difficulties, OEMs and research institutions have yet to tackle this problem thoroughly, aside from an unsuccessful product with advanced hybrid architecture [10]. In light of

the current state of the field, deriving analytical results and designing new hybrid architectures with planetary gearsets for both superior performance and fuel economy are an exciting and open field, and have the potential for high impact on both the progress of automotive technology and a cleaner environment for future generations.

1.2 Background

In this section, the fundamentals of hybrid electric powertrain types and planetary gearsets are described so as to ease the understanding of the following chapters in this study.

1.2.1 Hybrid Electric Powertrain Types

A hybrid electric vehicle (HEV) is a vehicle that combines conventional internal combustion engine propulsion with electric propulsion. Powertrain types used in HEVs have been categorized in the literature into three groups, according to how the engine and electric machine(s) are configured to propel a vehicle (see description following). As will be shown in this dissertation, this categorization is insufficient for describing all powertrain types realizable with PGs.

1.2.1.1 Parallel Hybrid Electric Powertrain Type

In the parallel hybrid type shown in Figure 1.2, the vehicle can be propelled by both an engine and an electric machine. Generally, the main driver is the engine and the electric machine assists as an additional torque source. Although designing such a powertrain is not difficult, a major disadvantage is that the engine speed is not decoupled from the vehicle speed. Thus, the engine cannot be operated at its optimum point for every vehicle speed, and the fuel economy benefit achieved with this type is thus limited.

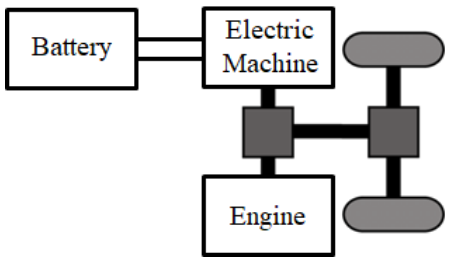

Figure 1.2: Parallel Hybrid Electric Powertrain Type.

1.2.1.2 Series Hybrid Electric Powertrain Type

In the series hybrid type shown in Figure 1.3, the vehicle is propelled by an electric machine via a single- or multi-step gear transmission. Energy to the electric machine comes from the battery and/or the generator driven by a conventional engine. The disadvantages of this type are the need for high power, and thus a large electric machine (as it is the sole driver to the wheels), and the inefficiencies resulting from the repeated energy conversions (first mechanical to electrical and then electrical to mechanical).

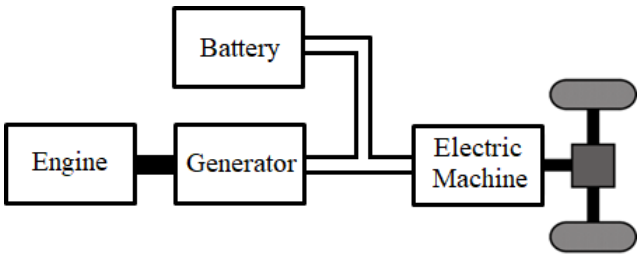

Figure 1.3: Series Hybrid Electric Powertrain Type.

1.2.1.3 Power-Split Hybrid Electric Powertrain Types

The power-split hybrid type shown in Figure 1.4 relies on the use of planetary gearsets (PGs), which provide the mechanical connections between the engine, electric machines, and vehicle output shaft. It has the advantages of both parallel and series types, since engine speed can be set to a desired speed at any vehicle speed (within system constraints) to maintain optimal efficiency (as in the series type), and part

of the engine mechanical power may be directly transferred to the wheels (as in the parallel type). The main disadvantages of a power-split type are design and control complexities, which are the focus of this dissertation.

Because engine speed is set to a desired value independent of the vehicle speed via the control of electric machines in the power-split type, it is called an electronically controlled continuously variable transmission (eCVT). Furthermore, in power-split type terminology, *mechanical point* is defined as the condition in the system where all the power of the engine is transferred mechanically to the wheels. This condition usually occurs when the speed of one of the electric machines reaches zero.

Power-split hybrid types are classified in the literature into three sub-categories (input-split, output-split, compound-split) depending on whether the electric machine is coupled to the engine or to the output shaft. Details on the three types of power-split powertrains are explained in the following subsections.

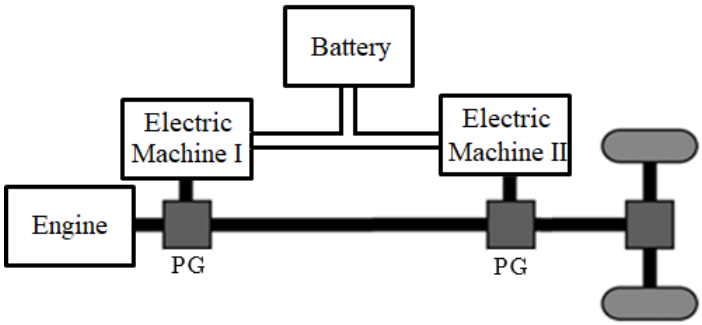

Figure 1.4: Power-Split Hybrid Electric Powertrain Type.

Input-Split Hybrid Electric Powertrain

In the input-split system, one of the electric machines is coupled to the vehicle output shaft. Thus, the speed of that electric machine becomes zero only at zero vehicle speed. This electric machine is represented as Electric Machine II in Figure 1.4. The speed of Electric Machine I in this figure is determined by both engine speed and vehicle speed. At low vehicle speed, Electric Machine I acts as a generator, that is, it

produces electricity using some of the engine's mechanical power. Electric Machine II uses the electric energy generated by the Electric Machine I and battery to produce the mechanical power delivered to the wheels. The remaining mechanical power of the engine that is not used by the Electric Machine I is also delivered to the wheels. As a result, the engine power is split between the generator and the wheels. As the vehicle speed increases, Electric Machine I passes its mechanical point, and Electric Machines I and II exchange roles. In this case, Electric Machine II performs the electric generation role, while Electric Machine I acts as an electric motor. This change is not desirable, however, due to the drop in overall system efficiency [11].

Output-Split Hybrid Electric Powertrain

In the output-split system, one of the electric machines, represented as Electric Machine I in Figure 1.4, is coupled to the engine. Thus, its speed never becomes zero except at zero engine speed. The speed of the second electric machine, Electric Machine II in the same figure, is determined by both engine speed and vehicle speed. At low vehicle speed, Electric Machine II acts as a generator. Electric Machine I consumes the electric energy generated by Electric Machine II to produce the mechanical power added to the engine mechanical power. The sum of the engine power and Electric Machine I power is delivered to the output shaft of the vehicle. Some portion of the mechanical power is consumed by Electric Machine II, acting as a generator. The remaining portion is delivered to the wheels. Since the total mechanical power is split at the output stage, this type of power-split architecture is called output-split hybrid electric powertrain. As the vehicle speed increases, Electric Machine II reaches its mechanical point, and the electric generation role between Electric Machine I and II switches. This change is desirable due to the overall increase in system efficiency [11].

Compound-Split Hybrid Electric Powertrain

In the compound-split system, the speed of both electric machines is determined

by the engine speed and the vehicle speed. Thus, two mechanical points exist in the system. As will be shown subsequently, a major advantage of this type of architecture is the low electric machine power requirement during the eCVT mode when the system operates between two mechanical points. When it operates outside the range of the mechanical points, the overall system efficiency drops significantly.

1.2.2 Planetary Gearset Basics

The planetary gearset shown in Figure 1.5 is a mechanical device that consists of four parts called the sun gear, the planet gears and their carrier, and the ring gear. The ring gear, which is the outer gear, rotates around the sun gear, which is at the center. The mechanical connection between the ring gear and sun gear is established through the planet gears (a.k.a. pinion), which are held together by the carrier. There are three axes rotating in the system (ring, carrier, sun), whose relative motions to one another are governed by Eqs. (1.1a)-(1.1e). In these equations, N_R and N_S are the tooth number on the ring and sun gears; ω_R, ω_C, ω_S are the rotational speed of the ring, carrier, and sun gears, and T_R, T_C, T_S are the respective torques applied to these gears. As observed from these equations, the degrees of freedom in a planetary gearset are two, where the speed values of any two gears determine the speed of the third gear.

For simplicity, the planetary gearset will henceforth be represented as a lever, shown in Figure 1.6 [12]. The lengths between R-C and C-S points on the lever are taken as 1 and α, where the latter is the ratio of N_R to N_S.

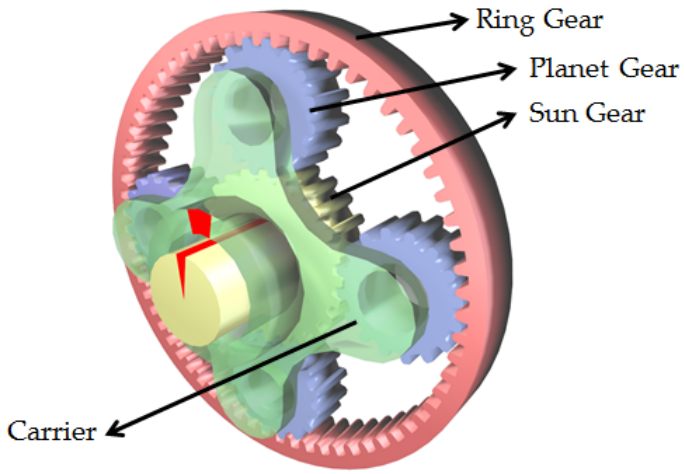

Figure 1.5: Planetary Gearset [13].

Figure 1.6: Symbolic Representation of a Planetary Gearset.

$$\alpha = \frac{N_R}{N_S} \tag{1.1a}$$

$$\omega_C = \frac{N_R}{N_R + N_S}\omega_R + \frac{N_S}{N_R + N_S}\omega_S = \frac{\alpha}{1+\alpha}\omega_R + \frac{1}{1+\alpha}\omega_S \tag{1.1b}$$

$$T_C + T_R + T_S = 0 \tag{1.1c}$$

$$T_R = -\frac{N_R}{N_R + N_S}T_C = -\frac{\alpha}{1+\alpha}T_C \tag{1.1d}$$

$$T_S = -\frac{N_S}{N_R + N_S}T_C = -\frac{1}{1+\alpha}T_C \tag{1.1e}$$

1.2.3 Multi-mode Hybrid Electric Powertrain

In this study, a configuration is defined as a powertrain entity that is constructed by assigning predefined components including clutches to the PG nodes. Figure 1.7 shows a configuration example. In contrast to a configuration, modes are generated by assigning predefined components that do not include clutches to the PG nodes. A mode corresponds to the dynamics for a given state of the clutches in a configuration. Figure 1.8 shows one mode of the configuration in Figure 1.7, where Clutches B and C are closed while Clutch A is open.

A powertrain design is required to meet its fuel economy and performance targets at all reasonable vehicle speeds and road load conditions. However, in a hybrid electric powertrain design with one mode, electric machines may reach their speed limits due to system constraints and/or the engine may no longer be able to stay at its most efficient operating point as vehicle speed and road load vary. Furthermore, as explained in subsections 1.2.1.3 and 1.2.1.3, the overall system efficiency drops significantly during the eCVT mode if the vehicle speed exceeds or falls below a certain level. As a result, a single-mode powertrain cannot sustain maximum efficiency at every vehicle speed and road load condition due to either the speed or power limits of the system components. To overcome this deficiency, an HEV powertrain must be designed with multiple modes.

Multiple modes, each of which fits best to a different operating condition, can be put together using clutches in a multi-mode design. However, to make the transition from one mode to another seamless requires the coordination of engine and electric machine torque such that the torque at the vehicle output shaft remains undisturbed. How to achieve this coordination is investigated in this dissertation as well.

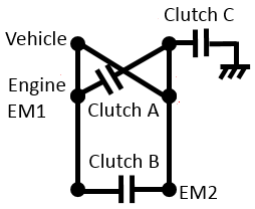

Figure 1.7: Configuration Example.

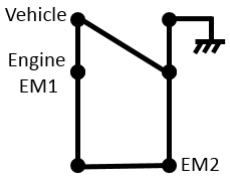

Figure 1.8: Mode Example.

1.3 Literature Review

Exploiting the full potential of PGs in HEV design requires a design process with the following characteristics:

1. Design candidates should be evaluated against both fuel economy and performance criteria (gradeability, launch torque, long-hauling torque, acceleration time between various speed intervals, top speed, backward driving capability) used in a full-fledged HEV powertrain design.

2. The design candidates that can be generated with a given set of components should be manageable in size.

3. The synthesis and analysis tools should be suitable for component sizing studies.

4. Not one single HEV powertrain type should be excluded from the process.

In this section, the literature review will be conducted from the perspective of these four criteria above.

Furthermore, the problem of designing, optimizing, and controlling an HEV powertrain requires developments in four pillars. The first pillar is the availability of analysis methodologies to derive the kinematic constraints and dynamic equations of a design candidate. The second pillar is the development of new techniques to evaluate a design candidate in terms of meeting design requirements (for example, acceleration, backward-speed operation, gradeability). The third pillar is the evaluation of the fuel economy improvement potential of feasible, implementable design candidates to benchmark the designs that are capable of meeting performance requirements. The fourth pillar is the development of control methods to achieve mode transitions without deteriorating drivability. The four sections of the literature review cover each of these pillars.

1.3.1 PG-based Hybrid Electric Powertrain Modeling Techniques

Several methods exist for deriving and analyzing kinematic and dynamic equations of mechanical systems with planetary gearsets. The first common method is the application of multi-body dynamic analysis techniques to the problem [14]. This approach, together with the Lagrange equations and constraint Jacobian matrix, is used to derive the dynamic equations of automatic transmission systems in [15]. The simplified version of this methodology described in [16] is also applicable to automatic transmission systems. The second approach in multi-body system analysis is Kane's method [17]. Graph representation and fundamental circuit techniques are also employed for kinematics, static force, and torque analyses of planetary gearsets [18, 19]. The fourth method is the lever diagram, which is widely used in planetary gearset analysis thanks to its practicality and intuitiveness [12]. The bond graph method as the fifth approach is a graphical tool to describe relations between speed, torque and power in a mechanical system [20]. Another technique for deriving the dynamic equations of a mechanical system with planetary gearsets is to analyze it as

a free body diagram and to then apply speed and torque constraints [21].

Some of these modeling techniques have already been applied to the study of HEV powertrains designed with planetary gearsets. Kane's method is applied to derive a dynamic model of a power-split hybrid architecture with two modes in [22]. Mechanical losses are also considered in that model. The dynamic model of the power-split hybrid design employed in the Chevrolet Tahoe model is developed by [23] using the bond graph representation method. This model is also validated through vehicle tests, and integrated into the popular vehicle and powertrain simulation tool called Powertrain System Analysis Toolkit (PSAT). The bond graph method is also used to model the kinematics and dynamics of the Toyota Prius, Chevrolet Tahoe and Renault power-split hybrid architectures [24]. Furthermore, the same method is applied to analyze the power flow of these designs. The free body diagram technique is utilized to derive the dynamic equations of the Toyota Prius and Ford Escape power-split designs in [25, 26]. The lever diagram technique is used mostly to investigate the speed and/or torque relationships of a HEV design at steady-state conditions. This technique is applied to the Toyota Prius, Chevrolet Tahoe, and Chevrolet Volt HEV powertrains by [25, 27, 28].

The modeling techniques described thus far are analytically powerful tools. However, except for [15, 16], they rely on human involvement in the system analysis and derivation of equations, and are thus not suitable for computerized modeling. When the number of HEV designs that need to be evaluated is large, an automated modeling technique is required. Such a technique specific for HEV designs has been developed by [29]. In this method, the characteristic information of a design is held in a matrix, and the dynamic equations are derived through matrix operations. This technique is suitable for automation since the characteristic matrix and subsequent matrix operations can be easily calculated by computer. Its drawbacks, however, are the difficulty obtaining the key features of a design from its characteristic matrix and

the unsuitability for component sizing studies because of the computational penalty of matrix inverse operations.

The modeling technique introduced in this dissertation is suitable for automating the process, deriving analytical results, and performing component sizing studies.

1.3.2 PG-based Hybrid Electric Powertrain Design and Performance Analysis Techniques

Although several HEV design methodologies have been introduced in the last 10 years [30, 29, 31, 32, 33, 34, 35, 36, 37, 38], they fall short in meeting all the requirements in the guidelines specified at the beginning of this section.

In the first attempt to introduce PG-based hybrid electric powertrain design methodology, the number of PGs, clutches, brakes, and electric machines are initially determined, and then all possible kinematic combinations of these elements are analyzed using graph theory and algebraic design techniques [30]. Since the authors of [30] are employed in the industry, however, their work is not presented in sufficient detail due to intellectual property protection considerations. Moreover, vehicle performance, fuel economy, and component sizing are not taken into account in their work. This gap is partially filled in [29] by taking 0-50mph time and fuel economy improvement potential of design candidates into account in the process after generating the dynamic model of each possible configuration with two planetary gearsets in a matrix form and assessing its feasibility by analyzing the structure of its dynamic model. Unfortunately, only power-split designs without other performance criteria are evaluated. Furthermore, constant vehicle power is assumed for 0-50mph time evaluation, and a computationally inefficient exhaustive search of all possible operating points of components at a given vehicle speed needed to be performed to assess the acceleration performance of a design candidate.

In [39], all possible configurations of a power-split hybrid powertrain with a single

planetary gearset are investigated, and all potential feasible locations for clutch installations are identified to explore better designs than Toyota Prius and Chevrolet Volt. It shows that the fuel economy and acceleration performance of the Toyota Prius configuration can be improved in urban driving with an additional clutch, and the removal of two clutches from the Chevrolet Volt configuration does not significantly affect its fuel economy. The process in [29] is improved in [32, 35] by developing an automatic modeling and screening process that conducts an exhaustive search of all designs with different configurations, clutch locations, operating modes, and powertrain types. However, the method for generating the design space is based on evaluating all possible configurations, which will grow to unmanageable numbers if the variation of component sizes is considered. Furthermore, the method for deriving the speed and torque relationships is not suitable for PG gear ratio variation, and only 0-60mph time is analyzed for drivability by assuming that engine speed acceleration is linearly proportional to the vehicle speed acceleration.

A mode-based design approach is adopted in [37, 38] by slightly modifying the work of [32, 35]. Since that work is using the same automatic modeling and screening process, all of its drawbacks are inherited. Moreover, categorizing the feasible modes as fuel saving and high performance modes in [38] is not appropriate because a mode's behavior can change with respect to vehicle speed. In contrast to the exhaustive design approaches, a generalized representation of a power-split configuration with two PGs is proposed by [31, 40]. They show that an arbitrary nonsingular kinematic relation can be realized by the proper selection of gear ratios in two generalized power-split configurations. In the first configuration, an input-coupled powertrain type is connected to an output-coupled type, while the second configuration is a compound power-split type. However, that method is applicable only to power-split designs and cannot generate unique multi-mode designs. This concept is improved in [36] by using genetic algorithms and sequential quadratic programming to identify kinematic

relationships of superior power-split or full-electric single or two-mode designs. But that approach requires a large number of initial population and does not guarantee convergence to the optimal design. Moreover, since a description of the performance evaluation is skipped in the paper, an oversimplified performance analysis should be expected.

In contrast to to all these complete design frameworks, the study in [34] proposes only an automatic topology generator based on constraint logic programming without taking the component sizes, fuel economy, and performance into account. Hence, that work should be extended to be comparable to other design frameworks. The paper that emphasizes accurate performance analysis as much as fuel economy implements an instantaneous optimization for full load analysis [33]. Because it evaluates torque and speed combinations of all components in a design candidate at each simulation step during 0-60mph time calculation, computational load is heavy and only a small design space can be handled in practice. As a result, this approach is applied only to power-split designs with a single PG.

1.3.3 Hybrid Electric Powertrain Fuel Economy Analysis Techniques

Exploring feasible HEV designs and analyzing whether they meet design requirements and the components operating within their physical limits are one aspect of the design problem. The other aspect is to assess the potential for improved fuel economy of a design candidate.

Dynamic programming (DP) is a numerical method for solving optimal control problems [41, 42]. Solutions obtained via DP are guaranteed to be globally optimal. Drawbacks of this method, however, are the requirement to know future reference points and states (noncausality), and the exponential growth of the computational load as the number of state and control variables increases (the curse of dimensionality).

Fuel economy numbers of light-duty vehicles are typically determined by running them on known reference vehicle speed profiles called drive cycles, and measuring their total fuel consumption. The fuel economy improvement potential of a given HEV design should, therefore, be evaluated when the control applied to the actuators in the system are optimized while following a drive cycle. DP suits this optimization problem well. The noncausality of DP is not an issue thanks to the known reference vehicle speed profile and the assumption of a lack of unknown disturbances. The curse of dimensionality might not be an issue if the total number of states and control inputs does not exceed two, and the number of simulation runs is limited. As these assumptions hold true for parallel, series, and single mode power-split designs, DP has been applied several times to fuel economy evaluation studies [43, 25, 44, 45, 46, 47, 48]. DP cannot be utilized in the simulation of multi-mode HEV designs, however, due to the curse of dimensionality.

To overcome the noncausality of DP and to increase the computational efficiency, the equivalent consumption minimization strategy (ECMS) is introduced in [49, 50]. The main idea behind this concept is that every variation in battery state of charge (SOC) should be compensated in the future by engine operations. At each time instant, a cost function as the sum of fuel energy and battery SOC variation multiplied by the battery energy to the fuel energy equivalency coefficient is optimized. Since this optimization is an instantaneous optimization rather than a time-horizon optimization as with DP, it is computationally efficient. Finding the equivalency factor in the cost function, however, requires multiple simulations, and there is no guarantee that it will be constant. Although several studies show the conditions for making the solution of ECMS globally optimal [51, 52, 53], they fail to provide a solution for estimating the equivalency factor in the cost function and applying this methodology to multi-mode HEV designs.

In the quest to find computationally efficient optimal control solutions in the fuel

economy evaluation of HEV designs, quadratic programming has also been used by approximating the engine fuel rate as a convex quadratic function of battery power [47]. Furthermore, in [54, 55, 56, 57], the convex optimization method is applied to calculate the fuel optimal control for parallel, series, and power-split designs by modeling the fuel and electrical power as a convex function of engine torque and electric machine torque. The drawbacks of these approaches are the distortions in the efficiency maps of the system components due to the approximations, and the inability of quadratic and convex optimization algorithms to make integer decisions such as engine on/off control and hybrid mode control.

The problem is that when the search space of a design problem is large, neither of the aforementioned methods can give computationally efficient results. Thus, a near-optimal method that is orders of magnitude faster than DP is proposed [58]. They introduce a concept called power-weighted efficiency analysis for rapid sizing (PEARS), which relies on the analysis of the efficiency of powertrain components at each mode, and their instantaneous optimization. The researchers, however, have not provided any analytical results proving how close the proposed method approaches the optimal results. In this study, after some robustness improvements are applied, this method, which is suitable for multi-mode design simulations and high execution speed, is used in fuel economy simulations.

1.3.4 Hybrid Electric Powertrain Control for Mode Transitions

In all fuel economy evaluation algorithms (DP, ECMS, PEARS), the mode that produces the lowest cost is determined at each time instant of the drive cycle. Hence, the result of the fuel economy simulations is the sequence of modes, each of which has its own operating points independent of the other time points. However, since the feasibility and cost of the mode transition between consecutive time instants are not taken into account in these algorithms, fuel economy simulation results might not

reflect the real world numbers.

The equivalent term of the mode transition is the gear shift in conventional transmissions. This topic and related clutch control mechanisms have been studied to a certain extent in the literature [16, 59, 60, 61, 62]. Because engine is the only torque generating source in conventional transmissions, the degrees of freedom are limited during a gear shift. In contrast to conventional transmissions, HEV powertrains have electric machine(s) as additional torque sources, thus enabling more flexibility in controlling the clutch torque and vehicle output torque during mode transitions. In the literature, most of the related work deals with the control of the clutchless transition from EV to HEV [63, 64] or the control of one-clutch mode transition, which connects an engine to a transmission [65, 66, 67, 68, 69]. However, little research has been done on the general multi-clutch mode shift analysis in HEV powertrains, as the existing work performs only two-clutch mode transitions for a specific HEV powertrain through a fixed control sequence similar to conventional transmissions [70, 71, 72, 73, 74].

1.4 Objective and Approach

1.4.1 Objective

The goal of this study is to develop a systematic hybrid electric powertrain design methodology that includes the automatic generation of design candidates, their computerized steady-state and dynamic equation derivations, automated feasibility and powertrain type determination algorithms, and design candidate performance and fuel economy evaluation algorithms suitable to component sizing. The methodology will be applied to exploring the viable hybrid electric powertrain concepts with two planetary gearsets, two electric machines, one battery pack, one internal combustion engine, and at least two operational modes for light-duty truck applications.

1.4.2 Approach

The design methodology aims to explore hybrid electric powertrain concepts that meet or exceed light-duty truck performance requirements while having superior fuel economy benefits compared to an equivalent conventional powertrain. Performance requirements of light-duty trucks are demanding as they need to be able to tow loads greater than the vehicle curb weight. An HEV powertrain shall meet these requirements with electric machines, whose maximum power is limited due to weight, cost, efficiency, and packaging constraints.

Before deriving the design methodology, the first question to be answered is which components need to be included in the design process. Assuming the target application is either a front-wheel or rear-wheel drive vehicle, one component must be a vehicle output shaft. Since the focus of this study is a hybrid electric powertrain design, one engine should also be included. If one electric machine is used to provide electric propulsion functionality, the series powertrain type and the eCVT operation of the power-split powertrain types, which require two electric machines cannot be realized. To cover a wide range of design candidates, two electric machines are used in this study. Planetary gearsets with their simplicity and functionality in generating design candidates are also included in the component list. In determining the number of PGs, the first option is to use a single PG, which has three nodes. Since the number of components is four (engine, output shaft, two electric machines), and only one of the electric machines can share a node with other components, 54 modes can be generated. Moreover, a one PG design excludes the possibility of designing a compound-split mode, which has a competitive advantage in providing eCVT operation with low power requirements for the electric machines at medium to high vehicle speed levels. In contrast to single PG designs, two-PG designs not only facilitate the inclusion of compound-split modes but also considerably increase the number of feasible modes in the design space. Thus, the design process begins with two PGs in this

dissertation. If two PGs do not provide enough feasible designs to meet all the vehicle requirements at the end of the process, then three-PG designs can be explored. The maximum number of brakes that will be used in the generation of design candidates is determined to be three because more than three brakes in a two-PG mode would lock every PG node.

After determining the number of PGs in the design, the next research question is how many modes to include in a design. A fixed-gear mode not mated with a transmission cannot meet all the performance requirements at a wide vehicle speed range. EV and series HEV powertrain modes are similar, as electric machines serve as the primary propulsion elements. Since electric machines used in the design have limited power, they cannot meet towing requirements alone. Moreover, since the energy supply in EVs is a battery with limited energy capacity, they cannot be used in long haul towing. Series HEVs do not have this problem, as there is a generator. A problem that both EVs and series HEVs share is the inflexibility of controlling the operating points of the propulsion electric machine as they are completely dependent on the driver's torque demand and current vehicle speed. Hence, operating the powertrain at its most efficient point is impossible, considering the various towing conditions ranging from an empty to a fully loaded vehicle at any vehicle speed. Similar arguments are valid for parallel HEV modes as well. Since the speed of the electric machine is dependent on the vehicle speed in a parallel HEV mode, the degrees of freedom in control authority are reduced. As a result, a parallel HEV can only be efficient under all towing conditions if it is mated to a transmission with multiple gears.

Power-split HEV modes are the right candidates for meeting the performance requirements of a light-duty truck since they allow the flexibility of controlling operating points of the components to desired states for changing operating conditions. As will be shown, an input-split type mode might meet performance requirements at low to medium vehicle speeds very well. As vehicle speed increases beyond a certain level,

however, electric machine power requirements exceed the allowed power limits. On the other hand, the output-split and compound split types are weak in meeting performance requirements at low vehicle speed but their performance increases as vehicle speed rises. Even if a power-split mode meets all performance requirements, a second mode will be needed to provide backward speed capability. Thus, the hypothesis in this study is that all performance requirements can be met across a wide range of vehicle speeds by using at least two modes.

The proposed design approach in this dissertation first creates all possible modes that can be generated with one vehicle output shaft, one engine, two electric machines, two PGs and at most three brakes. PG gear ratios are also included as design variables. Selecting powertrain modes as the design candidates creates a relatively smaller design space compared to other methods in the literature. The process then performs an exhaustive search through the strategic ordering of evaluation steps, where as many modes as possible are eliminated in the early design stages. An exhaustive search eliminates the risk of missing any competent design candidate in the process. Computationally heavy performance evaluations are accelerated through the introduction of new algorithms. Moreover, extremely time-consuming fuel economy simulations are conducted at the last stage of the process so as to handle just a small group of designs.

1.5 Contributions

The following contributions have been made in this dissertation to the design and control of HEV powertrains:

- Development of a systematic and practical design process that aims to maximize both fuel economy and performance.
- Automation of the static and dynamic equation derivations of planetary gearset

systems, and developing an analytical method to determine their feasibility and powertrain type.

- Derivation of both automated and manual methods to assess the forward- and backward-speed capability of each mode.
- Formulation and solution of the maximum acceleration problem for all powertrain types through linear programming technique.
- Formulation and solution of the x-y mph time problem for all powertrain types through linear programming and one-step predictive control.
- Analytical results for the acceleration capability of input-split and output-split HEV powertrain types.
- Derivation of the required electric machine power formulas for the power-split powertrain types during eCVT operation.
- Inclusion of PG gear ratios in the design process.
- Improvement of the fuel economy simulation software (PEARS) for better accuracy, robustness, and wider powertrain type coverage.
- Development of algorithms to analyze mode transition feasibility and control along with their integration into the PEARS software.

1.6 Organization

Chapter II evaluates the HEV powertrain design problem from a higher perspective by describing the design philosophy and building the design process. In Chapter III, the procedure for generating the design space and modeling the steady-state and dynamic equations of all design modes is explained. Chapter IV introduces the mode screening and powertrain type identification processes. Chapter V describes

the methods that efficiently evaluate the modes with respect to PG gear ratio variations and forward/backward speed capability. The performance criteria and related analysis and synthesis algorithms for long-hauling, gradeability, and x-y mph time are explained in Chapter VI. Chapter VII first reviews the steps for creating the competent designs and then conducts the fuel economy simulations of competent designs, presenting the best designs and their characteristics. Chapter VIII explains the algorithms for analyzing and controlling mode transitions in HEV powertrain designs and implements these algorithms in the fuel economy simulations of the ten best competent designs. Finally, the dissertation is completed with the concluding remarks and suggestions for future studies.

CHAPTER II

Design Framework

The design framework consists of two major parts: (1) the strategic thinking and design philosophy that will lead to a rigorous but efficient design process; and (2) the phases of the design process generated according to these.

2.1 Design Space

Determining the elements the design space is composed of is crucial because this decision has a major effect on the success of the design process. Three options are possible for the design space elements: component-, configuration-, and mode-based elements. In the component-based case, the design elements are the components that may be used in a hybrid powertrain such as engine, electric machines, planetary gearbox, differential, clutches. The disadvantage of this approach, however, is that it generates an extremely large design space due to the fine granularity. Component-based design space is used only in [34], with an incomplete design process, where component sizes, fuel economy, and performance are not taken into account. The realistic approaches are configuration- and mode-based designs, where the design elements are at a coarser granularity. In configuration-based design, predefined components, including clutches, are assigned to the PG nodes. Each combination is named as one configuration and is a complete hybrid transmission design by itself. In the litera-

ture, the focus is mainly on configuration-based design processes [30, 32, 35, 75]. In contrast to a configuration, modes are generated by assigning predefined components that do not include clutches to the PG nodes. A mode corresponds to the dynamics for a given state of clutches in a configuration. In the mode-based design approach, once all modes are generated in the design space, the groups of modes that collectively meet the design specifications are first identified. If the modes in a group can transition to each other with the predetermined number of clutches, this mode group constitutes a valid design and is evaluated for other criteria such as fuel economy. In this study, the mode-based design approach is chosen. Since mode-based design and its advantages over other approaches are not explored well enough in the literature, the rationale behind this decision is explicitly described below.

- Design space in the mode-based design is much smaller than in the other approaches. In this study, the designs that can be generated with two PGs, one engine, two electric machines, one vehicle output shaft, and at most three brakes/clutches are investigated. For the configuration-based design, three clutches can be assigned to the PG nodes as $C_{15}^{3}+C_{15}^{2}+C_{15}^{1} = 575$ different ways. If we constrain the engine and vehicle output to not be on the same PG node, all components can be assigned to six PG nodes as $6\times5\times6\times6 = 1,080$ ways. As a result, the design space for the configuration-based approach becomes $621,000$. In the mode-based design approach, the modes can be grouped according to the number of connections between two PGs. For one, two, and three connections between two PGs, we can generate 9, 36, and 44 different connections, respectively. The components can be assigned to the PG nodes for these three types of connections as $5 \times 4 \times 5 \times 5 \times 2^3 = 4,000$, $4 \times 3 \times 4 \times 4 \times 2^2 = 768$, and $3\times2\times3\times3\times2^1 = 108$ ways. 2^x terms in these calculations come from the possibility of assigning a brake to the PG nodes, to which engine or vehicle is not assigned. Based on these results, the design space for the mode-based approach

becomes 68,832, which is almost ten times smaller than the configuration-based design space. When another design variable such as a PG gear ratio is introduced to the design problem, the design space grows even further and the advantage of the mode-based design becomes even more apparent.

- In the configuration-based design, the assignment of the components to the PG nodes is fixed in a design candidate. In the mode-based design, this constraint does not exist, and a design can consist of two modes with a component assigned to different PG nodes.

- The configuration-based design is not computationally efficient, because a unique mode can exist in multiple configurations and would thus be evaluated multiple times in a configuration-based design. In contrast, in the mode-based design, a unique mode is evaluated just once.

- Mode-based design leverages the symmetries inherent in multiple modes that have the same performance. Hence, the number of modes under evaluation can be easily compressed with proper techniques.

- Configuration-based design should limit the number of clutches in a design due to the large number of design candidates. Mode-based design, on the other hand, applies the constraint of clutch number only at the last stage of the design process, which means that any two modes can be in a design as long as they provide superior performance and fuel economy.

- Mode-based design is an incremental design technique, where a design first starts with a single mode and gradually adds other modes until the design criteria are met. Hence, mode-based design delivers the simplest design. Configuration-based design determines the number of clutches in advance and tries to find the best designs given the fixed number of clutches.

- Mode-based design is more flexible in terms of incremental design improvements, because the superior designs can be augmented with other modes to meet additional criteria. How to expand a design is not clear in the configuration-based design.

- Since mode-based design focuses on individual modes, the derivation of analytical results for powertrain types is more intuitive and straight-forward.

- The discrete nature of the clutch states in a configuration-based design disallows the use of computationally efficient vector operations for component sizing studies. In the mode-based design approach, on the other hand, each mode can be rapidly evaluated with the proper analysis techniques.

2.2 Design Philosophy

In the design optimization studies, three optimal design techniques are available: nested, alternating, and simultaneous. In the hybrid electric powertrain design, the nested method shown in Figure 2.1 has been extensively used [76], where plant design consists of topology generation and component sizing, and control design is the fuel economy evaluation of the plant. In the nested design, control design is reoptimized for every plant design variation. Due to the large design space in the HEV powertrain design, two simplification methods are applied. In the first method, the design space is made smaller by eliminating the component sizing portion of the plant design or by focusing solely on a subset of available topologies or powertrain types. In the second method, the plant is simplified, and some optimization techniques are applied. However, the simplified model and the limitations of the optimization techniques do not allow for an accurate assessment of the design space. In this study, a different approach with four pillars is taken.

1. Instead of generating complete plants, the modes that constitute the plants are

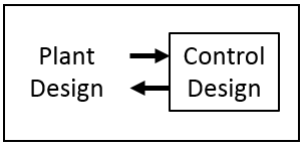

Figure 2.1: Nested System Level Optimization.

evaluated. At this step, a significant reduction in the design space is achieved. Moreover, eliminating the infeasible modes at the initial stage makes the design space even smaller, as shown in the conceptual Figure 2.2.

2. Computationally efficient performance evaluation methods suitable for component-sizing studies are derived. They are applied to all feasible modes before performing any fuel economy simulation. In this stage, many incompetent modes are eliminated from the design space. The powertrain designs that can be constructed with the competent modes are assessed for fuel economy, shown as the green box in Figure 2.2.

3. The power ratings of electric machines are chosen as the maximum of the allowable range, because if a mode does not meet the performance criteria with powerful electric machines, it cannot meet the same criteria with lower power rated ones. Thus, electric machine sizing is postponed to the fuel economy evaluation stage, where a much smaller design space remains.

4. This pillar was not derived at the beginning of this study. It is the result of the analysis of the design process outputs. It has been observed that PG gear ratio variation causes the fuel economy of a design to change between 0.2mpg and 1.0mpg. Therefore, the fuel economy simulation of each competent design can be conducted with just one PG gear ratio variation, with 1mpg added to the result, assuming the selected PG gear ratio gives the worst result. Those designs that cannot exceed the predetermined threshold are eliminated from the design

space without further fuel economy simulations. Fuel economy simulations are performed on the remaining designs for varying PG gear ratios. In this way, extremely computationally heavy fuel economy simulations are minimized.

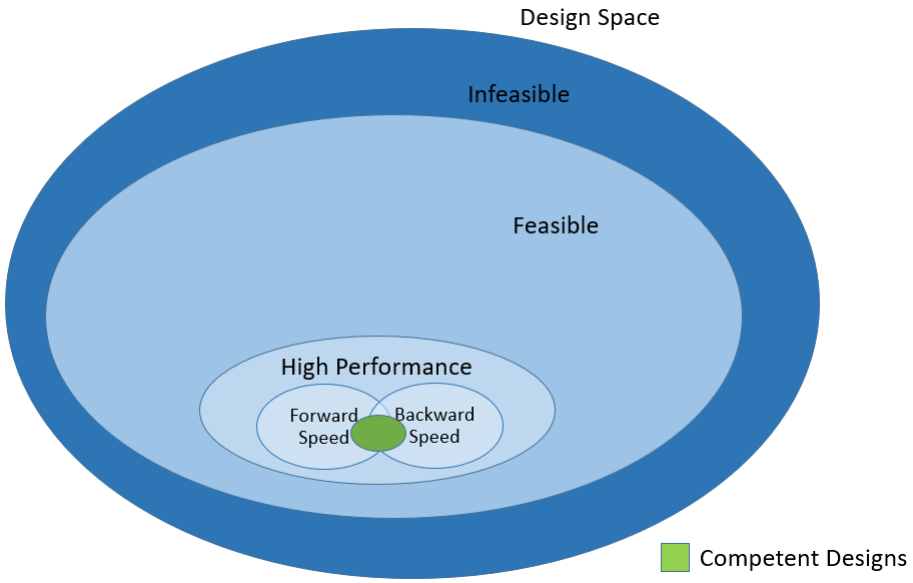

Figure 2.2: Strategic Design Approach.

2.3 Design Process

In this section, the design process created by following the design guidelines in the previous section is explained. Figure 2.3 shows each step in the proposed process for designing a superior HEV powertrain in terms of performance and fuel economy. These steps can be described in the order of execution as follows:

1. The design space is populated with all modes that can be generated with two PGs, one engine, one vehicle output shaft, two electric machines, and at most three brakes. To reduce the number of modes that will be evaluated for feasibility, a special compression technique that enables multiple modes to be represented by a single mode is developed.

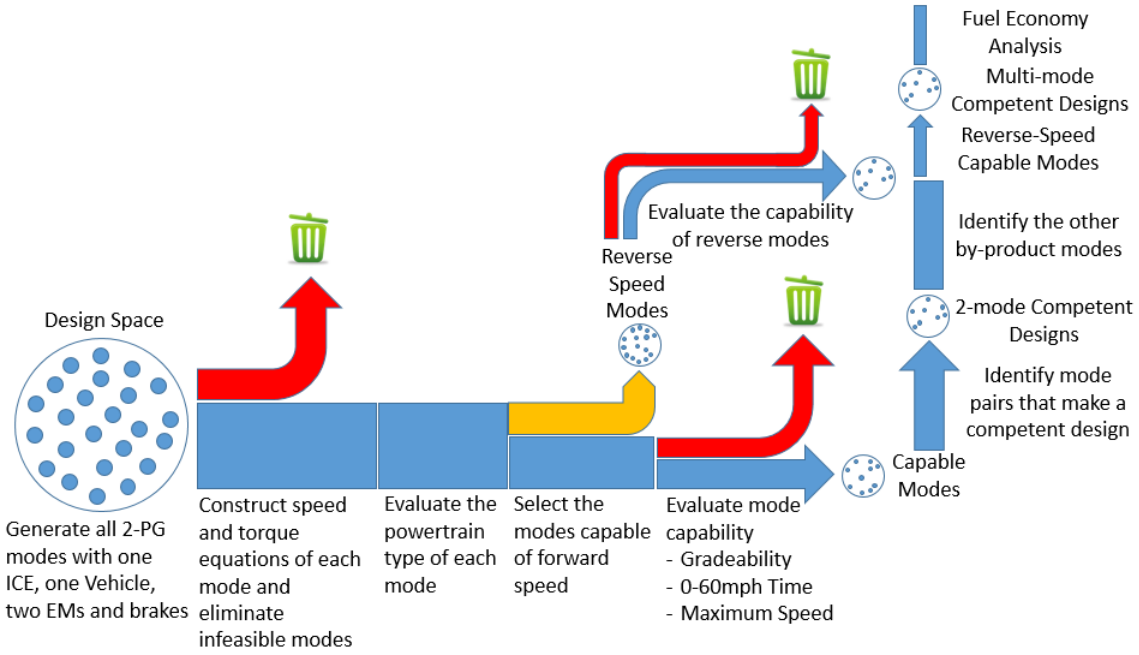

Figure 2.3: Proposed Design Process.

2. Steady-state speed and torque equations of each mode are derived in a format such that computationally efficient vector operations can be performed in the later stages for component-sizing studies. The modes that cannot deliver any vehicle torque or are stuck at 0 vehicle speed are defined as infeasible modes and are excluded from the process. The remaining modes are deemed feasible modes and are decompressed to revert to their original form.

3. Feasible modes are classified according to the structure of their torque and speed equations so that proper analysis techniques specific to each powertrain type can be applied.

4. All feasible modes are categorized into forward-speed and backward-speed groups, where forward-speed capable means that positive engine torque propels the vehicle in the forward direction. In the previous steps, all modes are evaluated for one PG gear ratio combination since PG gear ratio does not affect the behavior

of a mode. But forward- or backward-speed capability of a mode depends on the PG gear ratio. Therefore, in this step, each mode is evaluated for four PG gear ratio combinations, each of which takes either a maximum or minimum PG gear ratio value. The reason for taking just four gear ratio combinations will be explained in detail in Chapter V.

5. Forward-speed capable modes are assessed against gradeability, long-hauling, maximum speed, and x-y mph time tests, where $x \in [0, 50]$, $y \in [10, 60]$, and y-$x = 10$mph for all PG gear ratio combinations. The modes that cannot pass any of the predefined performance tests with any PG gear ratio combination are eliminated. Applying the challenging performance tests early in the process makes the design space much smaller for further processing.

6. Backward-speed capable modes are evaluated against backward-speed gradeability targets for all PG gear ratio combinations. The modes that cannot meet any performance target for any PG gear ratio are eliminated from the design space.

7. The individual modes or mode pairs that can meet all performance criteria collectively for the same PG ratios are identified to establish the core of the competent designs.

8. The clutch numbers and their locations are calculated to achieve the transition between two modes in each competent mode pair. The mode pairs that can transition to each other with less than a certain number of clutches are selected for further processing. Moreover, the other modes that can be generated for each combination of clutch states are also identified and analyzed. A determination is made as to whether any of these modes has backward-speed capability. If not, the modes in the backward-speed capable group that can be

transitioned without exceeding the clutch number constraint are incorporated into the design.

9. At the beginning of this stage, all competent designs have already been identified. The fuel economy improvement potential of the competent designs for each valid PG ratio is evaluated in this step. Since these designs had to pass many demanding performance design criteria beforehand, computationally complex fuel economy analysis is applied only to a limited number of designs. Finally, the competent designs with superior fuel economy become the end product of the proposed process.

In the following chapters, these steps will be explained in detail with accompanying analysis, synthesis techniques and analytical derivations.

CHAPTER III

Generation of Design Space

The first step in the HEV design process is to create the design space, which includes all modes that can be created with the given set of components. The second step is to derive the steady-state speed and torque equations and dynamic equations of the modes in the design space in order to quantify their characteristics. Since the analytical results that will be introduced in this dissertation depend primarily on the steady-state speed and torque equations, emphasis will be given to them. However, a method for deriving the dynamic equations will also be shown, as they are used in fuel economy simulations, 0-60mph time evaluation, and mode transition control.

3.1 Design Modes

Although the derived results are applicable to HEV designs with any number of planetary gearsets, the focus will be on hybrid electric modes with two planetary gearsets (PGs), one engine, two electric machines, and at most three brakes, as justified in Section 1.4.2. Since each PG has three nodes, the number of connections between two PGs can vary between one and three. Three connections between two gearsets generate modes with one degree of freedom and all speeds in the mode become the same. Thus, three-connection modes do not allow any useful design. As a result, only one- and two-connection modes shown in Figure 3.1 are investigated further.

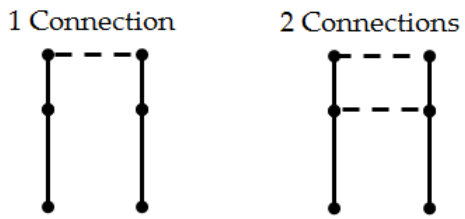

Figure 3.1: Modes with One and Two Connections.

3.1.1 One-Connection Modes

In the one-connection case, one of the three nodes of the first PG is connected to one of the three nodes of the second PG. Thus, there are 9 connection options and 5 available PG nodes, to which the components (engine, two electric machines, vehicle output shaft, brakes) can be assigned. Engine and vehicle cannot be assigned to the same node but electric machines can be assigned to any node, regardless of whether that node is assigned to another component. Similar to the electric machines, brakes can also be assigned to any node except engine and vehicle. Since assigning brakes is optional and three nodes are available for this assignment, they can be assigned 2^3 ways to a mode. As a result, the total number of modes that needs to be evaluated becomes $9 \times 5 \times 4 \times 5 \times 5 \times 2^3 = 36,000$.

3.1.2 Two-Connection Modes

In the two-connection case, two of the three nodes of the first PG are connected to two of the three nodes of the second PG. There are 18 unique ways to make these connections and 4 available PG nodes, to which the components (engine, two electric machines, vehicle output shaft, brakes) can be assigned. The restrictions for the assignment of the components are the same as those for the one-connection case. As a result, the total number of modes that need to be evaluated becomes $18 \times 4 \times 3 \times 4 \times 4 \times 2^2 = 13,824$.

The search algorithm that will be designed in this study will, therefore, need to

evaluate $36,000 + 13,824 = 49,824$ modes.

3.2 Derivation of Steady-State Speed and Torque Equations

A well-known and widely used "Lever Analogy" is a method to generate the speed equations of a planetary gearset configuration [12]. This method is suitable for manual derivation yet difficult for computerization. Hence, the method for conventional automatic transmissions in [16, 15], which is suitable for computerization, will be adapted to derive the speed and torque equations of HEV modes.

3.2.1 Derivation of Speed Equations

In the derivation of speed equations, the governing PG speed equations and the constraints due to the brakes and connections between PGs are placed into a matrix form. To explain this procedure, one of the modes shown in Figure 3.2 will be used as an example. In this mode, electric machine 1 and electric machine 2 are connected to the ring and carrier of the first PG, respectively. The vehicle output shaft lies also on the same node as electric machine 2. The brake at the sun gear of the first PG keeps it at zero speed. The internal combustion engine (ICE) is connected to the sun gear of the second PG. The ring and carrier of the first and second PGs are connected to each other.

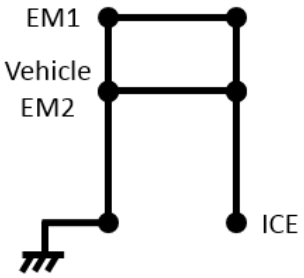

Figure 3.2: Mode whose Speed Equations will be derived.

First, the variable vector, called speed vector, which multiplies the speed matrix

from its right, is established as shown in Eq. (3.1). It consists of all six nodes of the two PGs and the speed of components, which are connected to the same node (in this example, vehicle and electric machine 2). Using this information, the speed equations are populated in the matrix shown in Eq. (3.2) as follows. The first two rows of the matrix represent the governing speed equations of two PGs. The third and fourth rows are the connection constraints, which make the speeds of ring and carrier gears of PG1 equal to the speeds of the same nodes of PG2. The fifth row shows the speed constraint imposed by the brake onto the sun gear of PG1. The last row equates the speeds of the components that are connected to the same node.

$$\Omega = \begin{bmatrix} \omega_{EM1} & \omega_{Wheels} & \omega_{S1} & \omega_{R2} & \omega_{C2} & \omega_{ICE} & \omega_{EM2} \end{bmatrix}^T \tag{3.1}$$

$$\underbrace{\left[\begin{array}{ccccccc} \alpha & -(1+\alpha) & 1 & 0 & 0 & 0 & 0 \\ 0 & 0 & 0 & \beta & -(1+\beta) & 1 & 0 \\ \hline 1 & 0 & 0 & -1 & 0 & 0 & 0 \\ 0 & 1 & 0 & 0 & -1 & 0 & 0 \\ \hline 0 & 0 & 1 & 0 & 0 & 0 & 0 \\ \hline 0 & 1 & 0 & 0 & 0 & 0 & -1 \end{array}\right]}_{Speed\ Matrix} \underbrace{\begin{bmatrix} \omega_{EM1} \\ \omega_{Wheels} \\ \omega_{S1} \\ \omega_{R2} \\ \omega_{C2} \\ \omega_{ICE} \\ \omega_{EM2} \end{bmatrix}}_{Speed\ Vector} = 0 \tag{3.2}$$

3.2.2 Derivation of Torque Equations

In the steady-state torque equations, the variable vector, called torque vector, consists of the mode elements that actively or reactively behave as a torque source (electric machines, engine, vehicle, brakes, connections and reaction forces in the PGs). In contrast to building speed equations, the torque equation matrix is established column by column, that is, the column size of the matrix is determined by the number of

components in the mode.

Each row of the matrix corresponds to one of the nodes in the mode. Thus, the row size of the matrix is always 6 for a 2-PG design. In each row, the torque sources that act to the corresponding node of that row are set to 1 or -1, depending on the direction; the remaining elements in that row become 0. According to these rules, the torque equations of the example mode become Eq. (3.3), where F_1 and F_2 are the tangential forces between gears in each PG, T_{C1} and T_{C2} are connection torques between PGs, and T_B is the reaction torque exerted by the brake.

$$
\begin{array}{c}
\\
R_1 \\
C_1 \\
S_1 \\
R_2 \\
C_2 \\
S_2
\end{array}
\overset{\overset{Torque\ Matrix}{\downarrow}}{\left[\begin{array}{cc|ccccccc}
\alpha & 0 & 0 & 0 & 1 & 0 & 1 & 0 & 0 \\
-(1+\alpha) & 0 & 0 & 1 & 0 & 1 & 0 & 1 & 0 \\
1 & 0 & 0 & 0 & 0 & 0 & 0 & 0 & 1 \\
0 & \beta & 0 & 0 & 0 & 0 & -1 & 0 & 0 \\
0 & -(1+\beta) & 0 & 0 & 0 & 0 & 0 & -1 & 0 \\
0 & 1 & 1 & 0 & 0 & 0 & 0 & 0 & 0
\end{array}\right]}
\overset{\overset{Torque\ Vector}{\downarrow}}{\left[\begin{array}{c}
F_1 \\ F_2 \\ T_{ICE} \\ T_{Wheels} \\ T_{EM1} \\ T_{EM2} \\ T_{C1} \\ T_{C2} \\ T_B
\end{array}\right]} = 0 \tag{3.3}
$$

3.3 Derivation of Dynamic Equations

In this study, dynamic equations will be used in the 0-60mph time analysis, fuel economy simulations, and mode transition control. They are derived by combining steady-state speed and torque equations with the inertia matrix as follows.

First, the derivative of the speed vector in the speed equations is augmented with the torque vector in the steady-state torque equations to obtain the variable vector

Ω of the dynamic equations. Ω of the example in Figure 3.2 becomes Eq. (3.4). The inertia matrix J is created first as a zero matrix with the size of $6 \times N$, where each row and N correspond to one of the PG nodes and the size of the speed vector, respectively. Each of the first 6 diagonal elements of the inertia matrix is populated with the sum of the inertia terms of the components connected to the corresponding PG node. The inertia matrix of the example in Figure 3.2 becomes Eq. (3.5). Finally, the dynamic equation matrix is created by placing the inertia matrix, steady-state speed and torque matrices into its upper left, lower left, and upper right corners, respectively, as shown in Eq. (3.6). The torque matrix is multiplied by -1 before this placement, as inertia and torque matrices are on the same side of the dynamic equation.

$$\Omega = [\dot{\omega}_{EM1}\, \dot{\omega}_{Wheels}\, \dot{\omega}_{S1}\, \dot{\omega}_{R2}\, \dot{\omega}_{C2}\, \dot{\omega}_{ICE}\, \dot{\omega}_{EM2}\, F_1\, F_2\, T_{ICE}\, T_{Wheels}\, T_{EM1}\, T_{EM2}\, T_{C1}\, T_{C2}\, T_B]^T \tag{3.4}$$

$$J = \begin{bmatrix} J_{EM1} + J_{R1} & 0 & 0 & 0 & 0 & 0 & 0 \\ 0 & J_{Wheels} + J_{EM2} + J_{C1} & 0 & 0 & 0 & 0 & 0 \\ 0 & 0 & J_{S1} & 0 & 0 & 0 & 0 \\ 0 & 0 & 0 & J_{R2} & 0 & 0 & 0 \\ 0 & 0 & 0 & 0 & J_{C2} & 0 & 0 \\ 0 & 0 & 0 & 0 & 0 & J_{ICE} & 0 \end{bmatrix} \tag{3.5}$$

$$\left[\begin{array}{c|c} J & -Torque\ Matrix \\ \hline Speed\ Matrix & 0 \end{array}\right] \Omega = 0 \tag{3.6}$$

3.4 Reduction of Modes

The generation and analysis of the speed and torque matrices should be repeated by the number of modes that need to be evaluated ($49,824$ times). To perform this time-consuming process more efficiently, similarities between speed and torque matrices of

the modes are explored and the following observations are made.

When the lever representation of a PG is flipped about the x-axis, the speed equation of the new PG remains the same, except that α and β are replaced with $1/\alpha$ and $1/\beta$ in the new equation, respectively. For example, consider the mode in Figure 3.3 and its speed equations in Eq. (3.7). After its PG1 (left PG) is flipped over about the x-axis, the resulting mode looks like Figure 3.4, and the properties of the new speed matrix in Eq. (3.8) are the same as those in Eq. (3.7) for the practical values of $\alpha \in [1.8\ 3.8]$ and $\beta \in [1.8\ 3.8]$ [77]. The same phenomenon is observed for the torque equations. Thus, analytical results of the first mode would be applicable to the modes, which are generated by flipping PG1 and/or PG2 of the original mode about the x-axis.

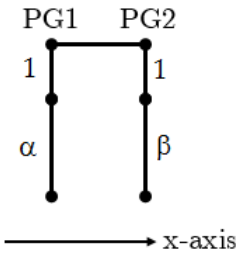

Figure 3.3: Mode before the PG1 is flipped over around the x-axis.

$$\begin{bmatrix} \alpha & -(1+\alpha) & 1 & 0 & 0 & 0 \\ 0 & 0 & 0 & \beta & -(1+\beta) & 1 \\ 1 & 0 & 0 & -1 & 0 & 0 \end{bmatrix} \begin{bmatrix} \omega_{R1} \\ \omega_{C1} \\ \omega_{S1} \\ \omega_{R2} \\ \omega_{C2} \\ \omega_{S2} \end{bmatrix} = 0 \tag{3.7}$$

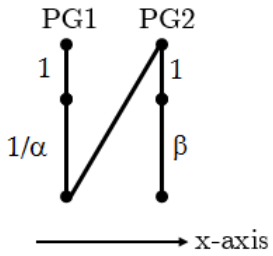

Figure 3.4: Mode after the PG1 is flipped over around the x-axis.

$$\begin{bmatrix} 1/\alpha & -(1+1/\alpha) & 1 & 0 & 0 & 0 \\ 0 & 0 & 0 & \beta & -(1+\beta) & 1 \\ 0 & 0 & 1 & -1 & 0 & 0 \end{bmatrix} \begin{bmatrix} \omega_{R1} \\ \omega_{C1} \\ \omega_{S1} \\ \omega_{R2} \\ \omega_{C2} \\ \omega_{S2} \end{bmatrix} = 0 \tag{3.8}$$

As a result of this observation, the analysis requirement for 9 and 18 ways of connecting two PGs with one and two connections is reduced to the analysis requirement for 4 and 5 ways of connecting two PGs, as seen in Figures 3.5 and 3.6.

Furthermore, although the two electric machines are numbered 1 and 2, and considered as unique components in the analysis, they are in fact the same from the point of view of feasibility analysis, because feasibility analysis results are affected by which nodes the electric machines are assigned to rather than the assignment of the specific electric machines. For example, the modes in Figure 3.7 would give the same results in the feasibility analysis. This observation reduces the number of modes for the electric machine assignment from 25 and 16 to 15 and 10 for one-connection and two-connection PG designs, respectively.

Following these mode reduction analyses, the number of modes to be investigated decreases from $9 \times 5 \times 4 \times 5 \times 5 \times 2^3 = 36,000$ and $18 \times 4 \times 3 \times 4 \times 4 \times 2^2 = 13,824$ to

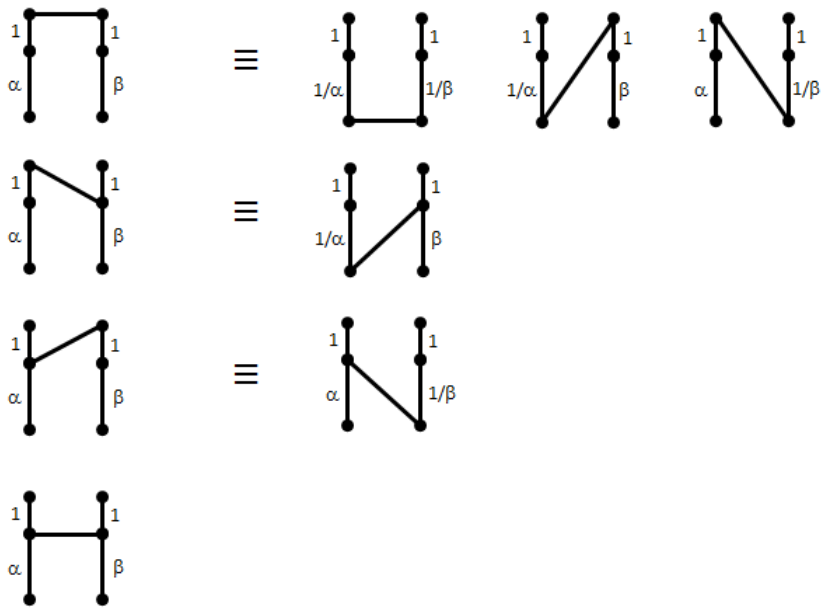

Figure 3.5: Equivalent Configurations with One Connection between Two PGs.

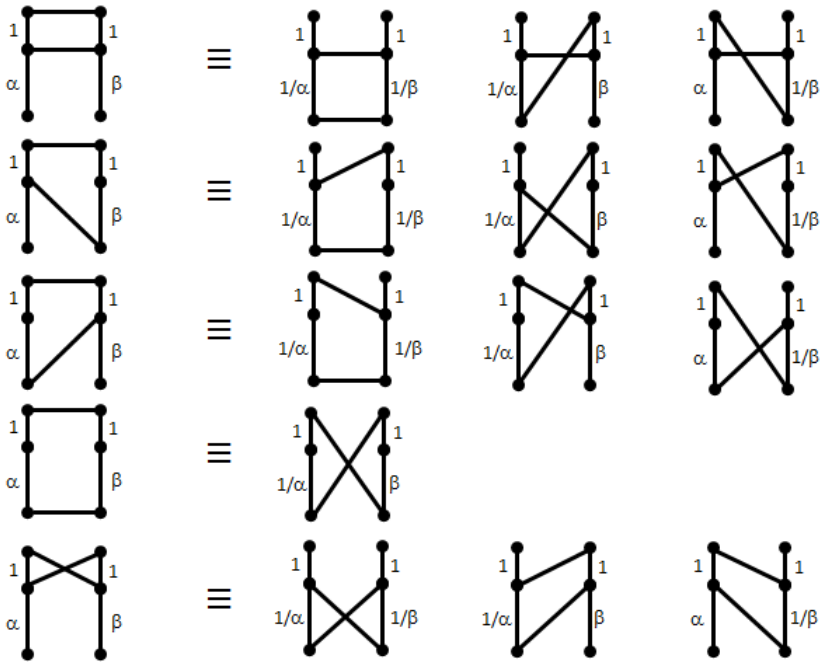

Figure 3.6: Equivalent Configurations with Two Connections between Two PGs.

$4 \times 5 \times 4 \times 15 \times 2^3 = 9,600$ and $5 \times 4 \times 3 \times 10 \times 2^2 = 2,400$ for one-connection and two-connection PG designs, respectively. Analyzing $12,000$ modes instead of $49,824$ provides an advantage in terms of analysis complexity and processing time.

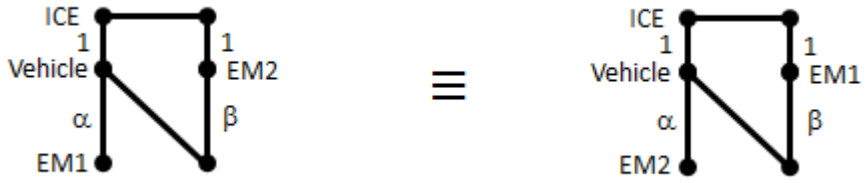

Figure 3.7: Equivalent Configurations due to the Insignificance of the Electric Machine Numbering in the Feasibility Analysis.

3.5 Mode Data Structure

Each mode's basic characteristic information is stored in a data structure whose fields include, but are not limited to, Vehicle, Engine, EM1, EM2, Brakes, Mechanical Connections, Speed and Torque Equations, Powertrain Type, and Performance related Entries. In order to store the information about component connections in the most effective way and to determine the clutch locations while combining modes to establish a design, PG nodes are numbered 1 to 6, where numbers 1 to 3 correspond to the ring, carrier, and sun gears of the first PG, respectively, and numbers 4 to 6 belong to the second PG's nodes. For example, if EM1 field in the data structure of a mode holds the string '1-5', it means that electric machine 1 is connected to the ring gear of PG1 and there is a mechanical connection between PG1's ring gear and PG2's carrier gear. In this case, the Mechanical Connection field in the data structure should hold the same information as well. The speed and torque equations are stored in the matrix format for just one combination of PG gear ratio since PG gear ratio variation is not needed in the feasibility analysis. While progressing in the design process, new fields such as powertrain type, symbolic equations, performance flags, and performance vectors are added to the mode data structure.

CHAPTER IV

Feasibility Analysis

The goal of this chapter is to describe the steps of the design process that are related to the topology of a mode. The first step is to eliminate the infeasible modes from the design space. The second step is to categorize the feasible modes according to the structure of speed and torque equations. This categorization is needed to understand the limitations of each mode and to apply proper performance evaluation algorithms.

4.1 Mode Feasibility Check

Some of the design modes in the design space are incapable of providing any torque to the wheels ($T_{Vehicle} = 0$) or having nonzero wheel speed ($\omega_{Vehicle}$=0). These modes are deemed to be infeasible and are eliminated from the design space. Steady-state torque and speed equations of each mode are evaluated to determine their feasibility.

4.1.1 Feasibility Check using Torque Equations

In this analysis, all modes are tested to determine whether any torque transmission to the wheels is possible. First, the columns of the torque matrix are reordered such that the first column of the matrix belongs to $T_{Vehicle}$ and the last three columns belong to T_{EM1}, T_{EM2}, and T_{ICE}. The Gaussian elimination method is then applied, and the resultant first row is analyzed. If the remaining elements are all zero after the first

1 in the first row, it means that $T_{Vehicle}$ is always equal to 0 and there is no torque transmission to the wheels. This is an infeasible condition for a powertrain mode and is not worth further investigation. If there are nonzero elements after the first 1 in the first row, the design mode passes the feasibility check for further analysis.

4.1.2 Feasibility Check using Speed Equations

In this analysis, all modes are tested to determine whether or not $\omega_{Vehicle}$ can take nonzero values. First, the columns of the speed equation matrix are reordered such that the first column of the matrix belongs to $\omega_{Vehicle}$ and the last three columns belong to ω_{EM1}, ω_{EM2}, and ω_{ICE}. The Gaussian elimination method is then applied and the resultant first row is analyzed. If the remaining elements after the first 1 are all zero, it means that $\omega_{Vehicle}$ is always 0 and the corresponding mode is infeasible.

4.2 Determination of Powertrain Type of Feasible Modes

After eliminating the infeasible modes from the design space, the remaining modes need to be categorized according to their powertrain type to be able to apply the suitable performance analysis techniques.

Powertrain types are determined according to the source of the propulsion (full-electric, hybrid-electric, conventional) and the dependence of engine and electric machine speeds on vehicle speed (fixed-gear, parallel, series, power-split). In the literature, they are described in terms of the characteristics of the existing designs or ad-hoc results or fixed number of PGs [78, 79, 80, 81, 35, 82]. In this study, the characteristics of all possible powertrain types that can be constructed with any number of PGs will be shown mathematically. Thus, any mode that might belong to an unknown powertrain type will not be ignored. The significance of the method introduced in this section is its applicability to the identification of all powertrain types in a set of mode candidates that can be constructed with any number of components.

The algorithm that determines the powertrain types relies on the following derivation.

Proposition IV.1. *The sum of the number of free variables (degrees of freedom) in steady-state torque and speed equations is equal to the number of power generating/consuming components in a powertrain mode.*

Proof. Assume there are m power generating/consuming components and the speed values of k components determine the rest of the speed variables via the matrix $A_{m-k\times k} = \begin{bmatrix} a_1 \dots a_k \end{bmatrix}$ where a_i's are the columns of the A matrix: Using the energy conservation law,

$$\begin{bmatrix} T_1 & \dots & T_k & T_{k+1} & \dots & T_m \end{bmatrix} \cdot \begin{bmatrix} \omega_1 \\ \vdots \\ \omega_k \\ \omega_{k+1} \\ \vdots \\ \omega_m \end{bmatrix} = 0 \qquad (4.1a)$$

$$\begin{bmatrix} T_1 & \dots & T_k & T_{k+1} & \dots & T_m \end{bmatrix} \cdot \begin{bmatrix} I_{k\times k} \\ A_{m-k\times k} \end{bmatrix} \cdot \begin{bmatrix} \omega_1 \\ \vdots \\ \omega_k \end{bmatrix} = 0 \qquad (4.1b)$$

$$\begin{bmatrix} T_1 + \begin{bmatrix} T_{k+1} & \dots & T_m \end{bmatrix} \cdot a_1 & \dots & T_k + \begin{bmatrix} T_{k+1} & \dots & T_m \end{bmatrix} \cdot a_k \end{bmatrix} \cdot \begin{bmatrix} \omega_1 \\ \vdots \\ \omega_k \end{bmatrix} = 0 \qquad (4.1c)$$

Since $\omega_1, \dots, \omega_k$ are independent variables, $T_i + \begin{bmatrix} T_{k+1} \dots T_m \end{bmatrix} \cdot a_i, i = 1, ..., k$ terms should be 0. As a result, $m-k$ variables $T_{k+1}, ..., T_m$ are independent torque variables.

□

This result is applied to the design process as follows: The columns of the speed

and torque equation matrices are reordered so that their first columns belong to the vehicle output shaft and their last three columns belong to the electric machines 1 and 2 (EM1, EM2), and the engine. After the Gaussian elimination method is applied to these matrices, the free variables are obtained. For the feasible modes, since the number of power generating/consuming components is four (Vehicle, Engine, EM1, EM2), three cases are possible, where k and n are the number of free speed and torque variables among Vehicle, Engine, EM1 and EM2, respectively:

1. $k = 1, n = 3$
2. $k = 3, n = 1$
3. $k = 2, n = 2$

Figures 4.1-4.5 show the algorithms that determine all possible powertrain types in the design space through a systematic approach. The derivation of these algorithms heavily relies on two facts. The first one is the energy conservation law the way it is used in the proof of Lemma IV.1. The second one is the property of reduced row echelon form, where each leading entry (left most nonzero entry) of a row is in a column to the right of the leading entry of the row above it. For example, if ω_{EM1} and ω_{ICE} are the free variables in the reduced row echelon form of a speed matrix, ω_{EM2} should be either 0 or $a \cdot \omega_{ICE}$ since these variables are ordered in the last three columns of the speed matrix as ω_{EM1}, ω_{EM2}, and ω_{ICE}, respectively.

4.2.1 $k = 1, n = 3$ Case

When $k = 1, n = 3$, one of the ω_{EM1}, ω_{EM2}, and ω_{ICE} is the free speed variable.

If the independent speed variable is ω_{ICE}, $\omega_{Vehicle} = a \cdot \omega_{ICE}, a \neq 0$. Since $n = 3$; T_{EM1}, T_{EM2}, and T_{ICE} are independent torque variables. $T_{Vehicle}$ can depend on either only T_{ICE} or $(T_{EM1}, T_{EM2}, T_{ICE})$. In the first case, the powertrain type is fixed-gear, because vehicle speed and vehicle torque are determined solely by the engine speed

and engine torque. In the second case, $T_{Vehicle}$ can depend on either (T_{EM1}, T_{EM2}) or (T_{EM1}, T_{EM2}, T_{ICE}). If $T_{Vehicle} = b \cdot T_{EM1} + c \cdot T_{EM2}, b \cdot c \neq 0$, T_{ICE} should be 0 due to the energy conservation law but T_{ICE} is a free variable. Therefore, this condition is impossible. If $T_{Vehicle} = b \cdot T_{EM1} + c \cdot T_{EM2} + d \cdot T_{ICE}, b \cdot c \neq 0, d \neq 0$, then $d = -\frac{1}{a}$ using the energy conversation law. As a result, the powertrain type is parallel, as shown in Figure 4.1 because vehicle speed is determined solely by engine speed and vehicle torque is the combination of electric machine and engine torque.

Similar arguments can be used if either of ω_{EM1}, ω_{EM2} is the free variable and $\omega_{Vehicle} = a \cdot \omega_{EM1/2}, a \neq 0$. In this case, the powertrain type can only be the EV type, as shown in Figure 4.1, because of the ineffectiveness of the engine on the vehicle torque or speed.

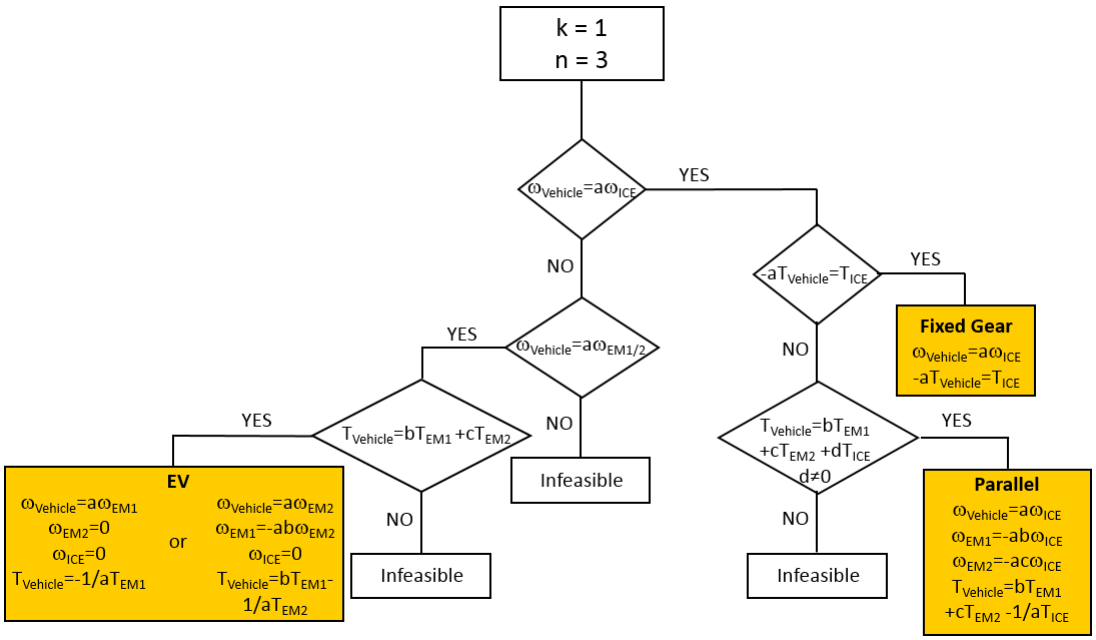

Figure 4.1: Flow Chart to determine Powertrain Type for $k = 1$, $n = 3$.

4.2.2 $k = 2, n = 2$ Case

When $k = 2, n = 2$, two of the ω_{EM1}, ω_{EM2}, and ω_{ICE} are the free speed variables.

If one of the independent speed variables is ω_{ICE} and $\omega_{Vehicle} = b \cdot \omega_{ICE}, b \neq 0$, using the same arguments in Subsection 4.2.1, powertrain type can be either fixed gear or parallel, depending on whether $T_{Vehicle}$ is determined by only T_{ICE} or T_{ICE} and $T_{EM1/2}$, as shown in Figure 4.2.

If $\omega_{Vehicle} = a \cdot \omega_{EM1} + b \cdot \omega_{ICE}, a, b \neq 0$, using the property of reduced row echelon form, where each leading entry (left most nonzero entry) of a row is in a column to the right of the leading entry of the row above it, ω_{EM2} can be either 0 or dependent on only ω_{ICE}, because ω_{EM2} is the variable before the last column ω_{ICE} in the row echelon form. If $\omega_{EM2} = 0$, using the energy conservation law, $T_{Vehicle} = -\frac{1}{b} \cdot T_{ICE}$ and $T_{EM1} = -a \cdot T_{Vehicle}$. As seen in these equations, although engine speed can be controlled independent from vehicle speed, $T_{Vehicle}$ determines both T_{ICE} and T_{EM1}. Therefore, this powertrain type resembles a power-split type in speed equations but a fixed gear type in torque equations. In this study, this powertrain type will be called Special Power-Split Type 1, as shown in Figure 4.2. If $\omega_{EM2} = c \cdot \omega_{ICE}, c \neq 0$, engine speed and torque can be determined independent from the vehicle speed and torque, whereas engine speed is proportional to EM2 speed. This powertrain type by definition is output-split type, which is one of the subcategories of power-split type.

If $\omega_{Vehicle} = a \cdot \omega_{EM2} + b \cdot \omega_{ICE}, a, b \neq 0$, using the property of reduced row echelon form, where each leading entry (left most nonzero entry) of a row is in a column to the right of the leading entry of the row above it, ω_{EM1} can take the following four forms:

1. $\omega_{EM1} = 0$: It is the same form as Special Power-Split Type 1 in Figure 4.2.

2. $\omega_{EM1} = c \cdot \omega_{EM2}$: Similar to Special Power-Split Type 1, engine speed can be controlled independent from vehicle speed, but engine torque is set by the vehicle torque. But contrary to Special Power-Split Type 1, using the energy conservation law, it can be shown that $\omega_{EM1} = c \cdot \omega_{EM2}$ and $T_{EM2} = -c \cdot T_{EM1} + \frac{a}{b} \cdot T_{ICE}$. Therefore, this powertrain type is called Special Power-Split Type 2.

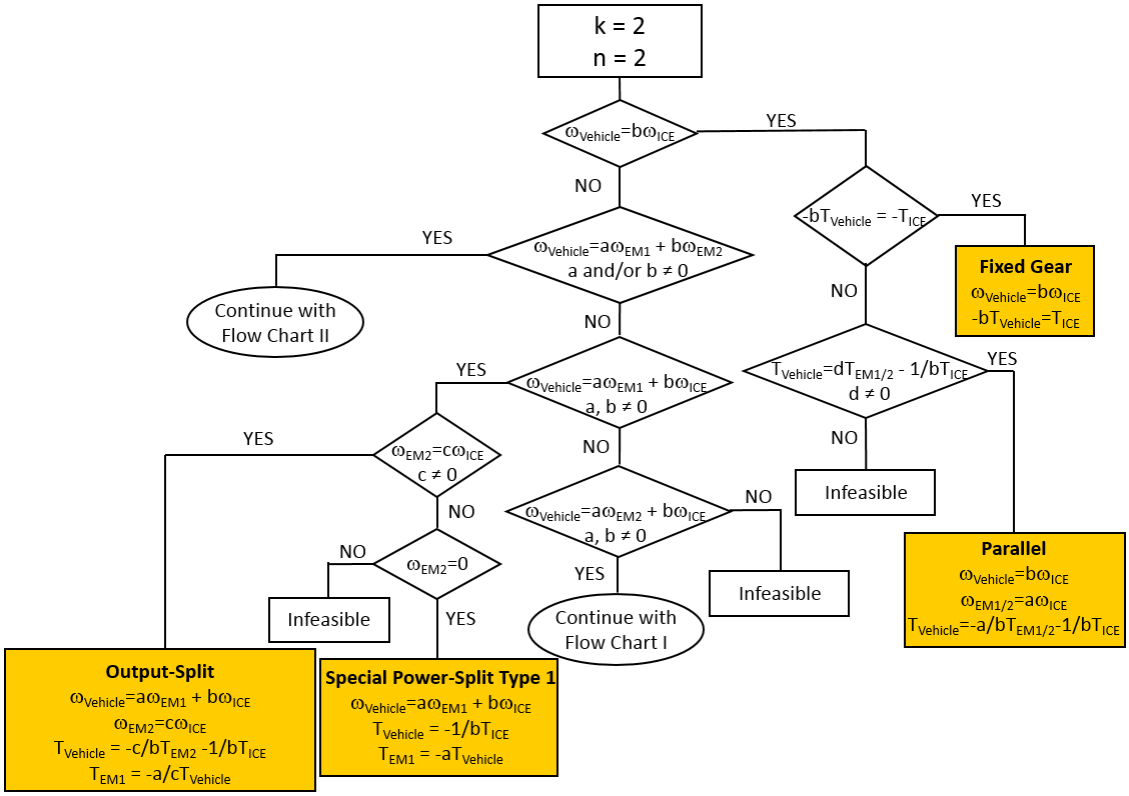

Figure 4.2: Main Flow Chart to determine Powertrain Type for $k = 2$, $n = 2$.

3. $\omega_{EM1} = c \cdot \omega_{ICE}$: Speed and torque equations depicted in Figure 4.3 match the characteristic equations of output-split powertrain type.

4. $\omega_{EM1} = c \cdot \omega_{EM2} + d \cdot \omega_{ICE}, c, d \neq 0$: Engine speed and torque can be controlled independent from vehicle speed and torque. Furthermore, the speed and torque of any electric machine are not directly proportional to vehicle or engine speed and torque. Therefore, this powertrain type by definition is compound-split type, which is one of the subcategories of power-split type.

In the case of $\omega_{Vehicle} = a \cdot \omega_{EM1} + b \cdot \omega_{EM2}, a \cdot b \neq 0$, there are three possibilities of $\omega_{Vehicle}$'s dependence on electric machines, as shown in Figure 4.4:

1. $\omega_{Vehicle} = a \cdot \omega_{EM1}$: Using the property of reduced row echelon form as before, there are three options. In the first option, ω_{ICE} is the independent variable and

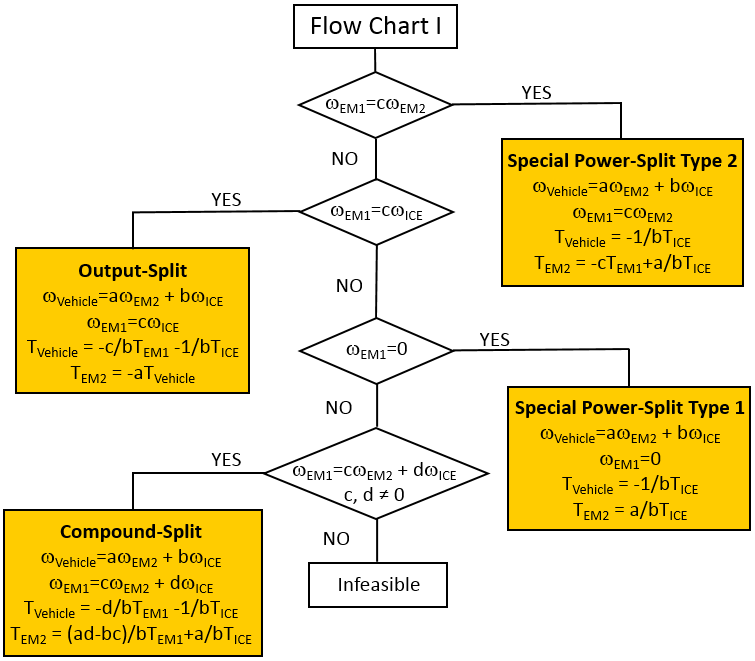

Figure 4.3: Flow Chart I to determine Powertrain Type for $k = 2$, $n = 2$.

$\omega_{EM2} = b{\cdot}\omega_{ICE}, b \neq 0$. In this case, vehicle speed and torque are proportional to the EM1 speed and torque, whereas engine speed and torque are proportional to the EM2 speed and torque. These relationships correspond to the series powertrain type. In the second option, ω_{ICE} is still the independent variable but no relationship exists between ω_{ICE} and ω_{EM2}. The only choice for T_{ICE} and ω_{EM2} is to be 0 in this case due to the energy conservation law and the reduced row echelon form. In the last option, ω_{EM2} is another free variable but it does not affect $\omega_{Vehicle}$. Following the same arguments in the second option, ω_{ICE} and T_{EM2} should be 0. As a result, the powertrain type of the last two options is EV, because vehicle speed and torque are determined solely by the EM1 speed and torque.

2. $\omega_{Vehicle} = b \cdot \omega_{EM2}$: In this case, there are three possibilities as follows:

   (a) The second free variable is ω_{ICE} and ω_{EM1} is dependent on ω_{ICE}, as $\omega_{EM1} = c \cdot \omega_{ICE}$. Using the energy conservation law, $T_{Vehicle} = -\frac{1}{b} \cdot T_{EM2}$

and $T_{ICE} = -c \cdot T_{EM1}$. These torque and speed equations correspond to the series powertrain type.

(b) ω_{EM1} is dependent solely on ω_{EM2}. In this case, ω_{ICE} is either 0 or the second free variable. If ω_{ICE} is the second free variable, T_{ICE} should be 0 due to the energy conservation law. As a result, vehicle speed and torque equations are determined by only EM1 and EM2. Hence, the powertrain type is EV.

(c) ω_{EM2} and ω_{ICE} are free variables and $\omega_{EM1} = c \cdot \omega_{EM2} + d \cdot \omega_{ICE}, c, d \neq 0$. If these speed equations are used in the energy conservation law, $T_{Vehicle} = -\frac{c}{b} \cdot T_{EM1} - \frac{1}{b} \cdot T_{EM2}$ and $T_{EM1} = -\frac{1}{d} \cdot T_{ICE}$. As seen in these equations, engine speed and torque can be controlled independent from vehicle speed and torque, whereas vehicle speed is proportional to EM2 speed. This powertrain type by definition is input-split type, which is one of the subcategories of the power-split type.

3. $\omega_{Vehicle} = a \cdot \omega_{EM1} + b \cdot \omega_{EM2}, a, b \neq 0$: Since ω_{EM1} and ω_{EM2} are free variables, ω_{ICE} should be 0 due to the property of the reduced row echelon form. As a result, vehicle speed and torque are determined by EM1 and EM2 and the powertrain type is EV.

4.2.3 $k = 3, n = 1$ Case

When $k = 3, n = 1$, ω_{EM1}, ω_{EM2}, and ω_{ICE} are free speed variables and $\omega_{Vehicle}$ can be dependent on these speed variables in four ways as shown in Figure 4.5:

1. $\omega_{Vehicle} = a \cdot \omega_{EM1} + b \cdot \omega_{EM2} + c \cdot \omega_{ICE}, a, b, c \neq 0$: Applying the energy conservation law to this speed equation shows that $T_{Vehicle}$, T_{EM1}, and T_{EM2} are directly proportional to T_{ICE}. Since this powertrain type resembles a power-split type in speed equations but a fixed gear type in torque equations, this powertrain type

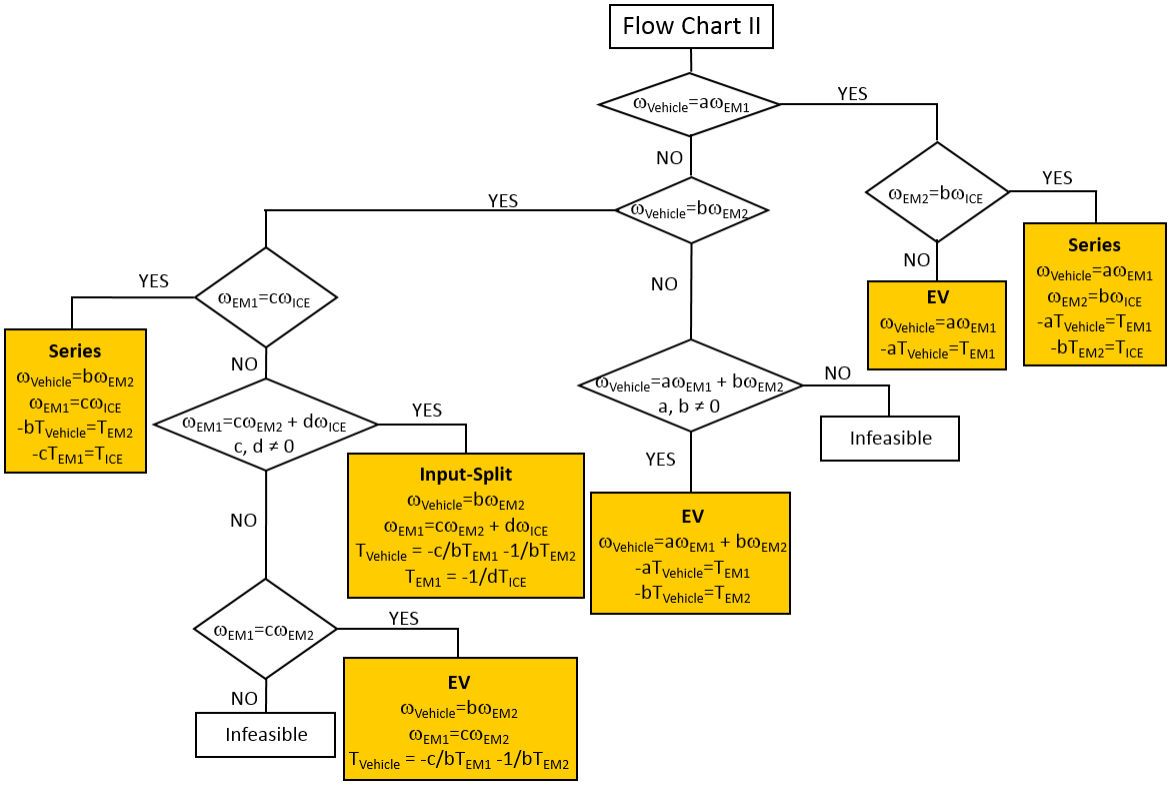

Figure 4.4: Flow Chart II to determine Powertrain Type for $k = 2$, $n = 2$.

will be called Special Power-Split Type 3. The difference between Power-Split Type 1 and Type 3 is the existence of the third speed variable in the vehicle speed equation.

2. $\omega_{Vehicle} = a \cdot \omega_{EM1} + b \cdot \omega_{EM2}, a \cdot b \neq 0$: Although $\omega_{Vehicle}$ is dependent on only two speed variables, there is a third free speed variable, ω_{ICE}. Therefore, according to Proposition IV.1, $T_{Vehicle}$ should be dependent on only one EM torque variable. According to the energy conservation law, however, $T_{Vehicle}$ cannot be dependent on T_{ICE}. As a result, since vehicle speed and torque are determined by only electric machines, this powertrain type is EV.

3. $\omega_{Vehicle} = a \cdot \omega_{EM1/2} + c \cdot \omega_{ICE}, a, c \neq 0$ where EM1/2 means either of EM1 and EM2 is in the equation: Since there are three free speed variables, there is only one free torque variable according to Proposition IV.1. Applying the energy

conservation law to the speed equation reveals that the free torque variable is T_{ICE}, and that $T_{Vehicle}$ and $T_{EM1/2}$ are proportional to T_{ICE}. As defined in Subsection 4.2.2, this powertrain type is defined as Special Power-Split Type 1.

4. $\omega_{Vehicle} = c \cdot \omega_{ICE}, c \neq 0$: Since there should be one free torque variable, $T_{Vehicle}$ should be proportional to T_{ICE}. Therefore, this powertrain type is fixed gear.

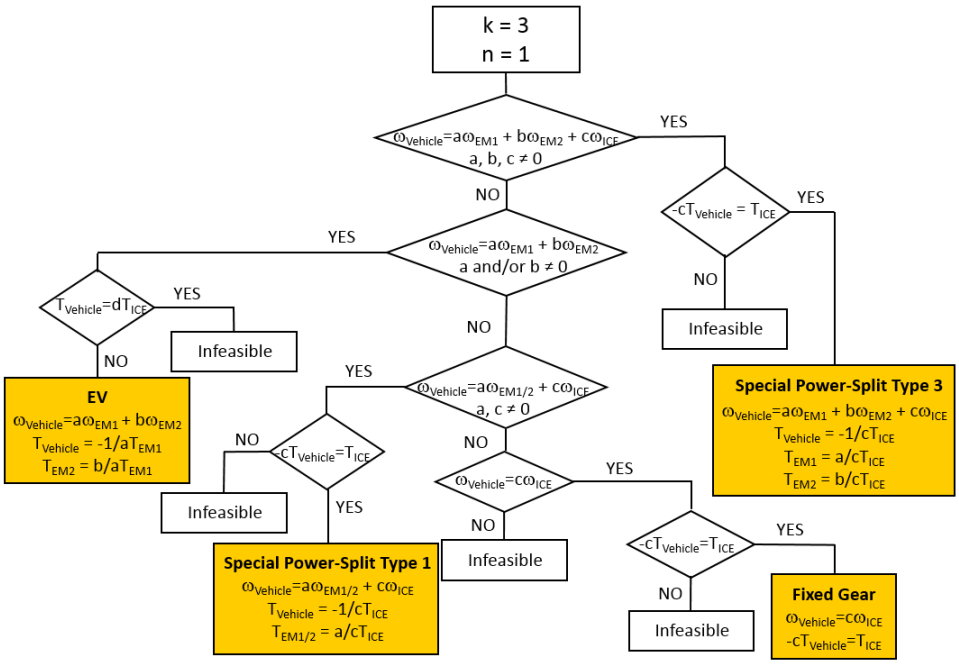

Figure 4.5: Flow Chart to determine Powertrain Type for $k = 3$, $n = 1$.

The important results these algorithms provide are as follows:

- The characteristics equations of each powertrain type are cast to a standard format, so that the analysis techniques in the design process can be automated seamlessly.

- All powertrain types achievable with the given set of components can be identified mathematically, regardless of the number of PGs. For example, a new special power-split powertrain type, where T_{ICE} is determined solely by $T_{Vehicle}$,

while $\omega_{Vehicle}$ is a function of $\omega_{EM1/2}$ and ω_{ICE}, is uncovered thanks to this method.

4.3 Results

After applying the feasibility and powertrain type determination rules, $7,996$ out of $12,000$ modes are identified as feasible. Since the analyses in this chapter are conducted on the modes that are obtained after the application of the mode reduction technique in Section 3.4, the reverse operation of this technique should be applied to the $7,996$ modes. After the mode extraction process, the number of feasible modes for the next step increases to $24,228$ and $10,152$ for 1-connection and 2-connection PG systems, respectively, as listed in Table 4.1.

Table 4.1: Feasibility and Powertrain Type Determination Analyses Results

	1-Connection	2-Connection
Total Number of Modes	36,000	13,824
Feasible Modes	24,228	10,152
Powertrain Type		
Fixed Gear	2,988	432
EV	5,364	216
Parallel	8,712	6,480
Series	2,232	432
Input-Split	1,368	864
Output-Split	1,368	864
Compound-Split	0	432
Special Power-Split	2,196	432

CHAPTER V

Forward-Speed and Backward-Speed Capability Analysis

A practical vehicle should be able to move in both forward and backward directions. Hence, it is important to analyze whether the positive engine torque in a mode contributes to the forward or reverse motion of the vehicle. In this chapter, two methods will be developed for this purpose. While the first method is suitable for an automated evaluation, the second one is applicable to a manual evaluation. In the proposed design process, the first method is applied to all feasible modes, and they are grouped under forward-speed and backward-speed capable categories.

5.1 Automated Method of Forward/Backward Speed Capability Evaluation

Like the feasibility analysis in Section 4.1, the steady-state torque matrix of the mode under investigation will be used to evaluate the fixed-gear, parallel, input-split, output-split, compound-split, and special power-split powertrain types. EV and series powertrain types are not evaluated because the torque characteristics of electric machines enable them to propel the vehicle in both directions without any performance degradation.

For the fixed-gear, parallel, and special power-split powertrain types, $T_{Vehicle}$ depends on either only T_{ICE} or T_{EM1}, T_{EM2}, and T_{ICE}. Hence, the columns of the torque matrix are reordered such that the first column of the matrix corresponds to $T_{Vehicle}$ and the last three columns belong to T_{EM1}, T_{EM2}, and T_{ICE}. Then, the Gaussian elimination is performed to obtain the dependence of $T_{Vehicle}$ on the T_{ICE} term.

Since the degrees of freedom in the torque equations are two for the input-split, output-split, and compound-split powertrain types, a slightly modified version of the method in the previous paragraph is utilized. In this case, the columns of the torque matrix are reordered such that the first two and the last two columns of the matrix belong to $T_{Vehicle}$, T_{EM1} and T_{ICE}, T_{EM2}, respectively. Then, the Gaussian elimination is performed to obtain the dependence of $T_{Vehicle}$ and T_{EM1} on T_{ICE} and T_{EM2} in Eq. (5.1). The same procedure is reapplied such that the first two and the last two columns of the torque matrix belong to $T_{Vehicle}$, T_{EM2} and T_{ICE}, T_{EM1}, respectively. After the application of the Gaussian elimination to this matrix, the dependence of $T_{Vehicle}$ and T_{EM2} on T_{ICE} and T_{EM1} as in Eq. (5.2) is obtained. $T_{Vehicle}$ in the torque matrices is the reaction torque of the PG node to which the vehicle output shaft is connected. Thus, $T_{Vehicle}$ should be negative to overcome the road load for the forward motion. Contrary to forward speed operation, $T_{Vehicle}$ should be positive for backward motion.

$$\begin{bmatrix} T_{Vehicle} \\ T_{EM1} \end{bmatrix} = \begin{bmatrix} h_{11} & h_{12} \\ h_{21} & h_{22} \end{bmatrix} \begin{bmatrix} T_{ICE} \\ T_{EM2} \end{bmatrix} \tag{5.1}$$

$$\begin{bmatrix} T_{Vehicle} \\ T_{EM2} \end{bmatrix} = \begin{bmatrix} \tilde{h}_{11} & \tilde{h}_{12} \\ \tilde{h}_{21} & \tilde{h}_{22} \end{bmatrix} \begin{bmatrix} T_{ICE} \\ T_{EM1} \end{bmatrix} \tag{5.2}$$

In the next step, the signs of h_{11} in Eq. (5.1) and $\tilde{h}_{11}$ in Eq. (5.2) are evaluated. If both h_{11} and $\tilde{h}_{11}$ are negative, the contribution of the positive engine torque to

$T_{Vehicle}$ is always negative. Hence, positive engine torque helps the vehicle to move forward. The reverse speed operation of this mode can be achieved only through the operation of electric machines while the engine is turned off.

If both h_{11} and $\tilde{h}_{11}$ are positive, the contribution of the positive engine torque to $T_{Vehicle}$ is always positive. Hence, positive engine torque helps the vehicle to move backwards. The forward speed operation of this mode can be achieved only through the operation of electric machines while the engine is turned off.

There might be some cases, where h_{11} and $\tilde{h}_{11}$ have opposite signs, as the mode in Figure 5.1. As seen in Eqs. (5.3)-(5.4), $h_{11} = -\frac{(1+\alpha)(1+\beta)}{\alpha\beta}$ and $\tilde{h}_{11} = \frac{1+\beta}{\alpha}$ have opposite signs for $\forall \alpha, \beta \in [1.8, 3.8]$. In this case, whether the contribution of positive engine torque to $T_{Vehicle}$ is positive or negative depends on other factors such as vehicle speed and electric machines' maximum torque. Thus, in these cases, the maximum acceleration calculation method, which is formulated in the next chapter using linear programming concepts, must be used.

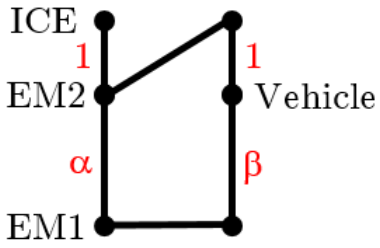

Figure 5.1: An Example Mode with Opposite-Sign h_{11} and $\tilde{h}_{11}$ Terms

$$\begin{bmatrix} T_{Vehicle} \\ T_{EM1} \end{bmatrix} = \begin{bmatrix} -\frac{(1+\alpha)(1+\beta)}{\alpha\beta} & -\frac{1+\beta}{\beta} \\ \frac{1+\alpha+\beta}{\alpha\beta} & \frac{1}{\beta} \end{bmatrix} \begin{bmatrix} T_{ICE} \\ T_{EM2} \end{bmatrix} \tag{5.3}$$

$$\begin{bmatrix} T_{Vehicle} \\ T_{EM2} \end{bmatrix} = \begin{bmatrix} \frac{1+\beta}{\alpha} & -(1+\beta) \\ -\frac{1+\alpha+\beta}{\alpha} & \beta \end{bmatrix} \begin{bmatrix} T_{ICE} \\ T_{EM1} \end{bmatrix} \tag{5.4}$$

5.2 Effect of PG Gear Ratio

Contrary to the feasibility and powertrain mode determination algorithms, forward/backward speed capability is dependent on the PG gear ratio. This section describes how the forward/backward speed capability checks for varying PG gear ratios can be performed on thousands of feasible modes in a computationally efficient manner.

The effect of PG gear ratio on the forward/backward speed capability can be evaluated by analyzing the dependence of the sign of h_{11} and $\tilde{h}_{11}$ coefficients in Eqs. (5.1)-(5.2) on the PG gear ratio using the following proposition.

Proposition V.1. *If $T_{Vehicle}$'s dependence on T_{EM1}, T_{EM2}, and T_{ICE} is generalized in steady-state as: $T_{Vehicle} = h_{11}(\alpha,\beta)\cdot T_{ICE} + h_{12}(\alpha,\beta)\cdot T_{EM1} + h_{13}(\alpha,\beta)\cdot T_{EM2}$, where $T_{Vehicle}$, T_{ICE}, T_{EM1}, and T_{EM2} are the vehicle output shaft, engine, electric machine 1, and electric machine 2 torque variables, respectively, and α and β are the ratio of ring gear tooth number over sun gear tooth number of the first and second PGs, then, $h_{11}(\alpha,\beta)$ is a monotonic function of α and β, $\alpha,\beta \in [1.8\ 3.8]$.*

Proof. The connections in a 2-PG mode can occur in five different ways, as shown in Figure 5.2, where contrary to the PG representation in this study, each node on the PG can be any node from the set of ring, carrier, and sun gears. x_1, x_2, and x_3 can be any component from the set of EM1, EM2, and brakes or their combinations. Thus, the torque equations of the first and second PGs can be written in a generic way using the terms ψ_1-ψ_6 to represent the PG gear ratio related coefficients. Hence, ψ_1, ψ_2 and ψ_3 can take any one of the $\{1+\alpha, -\alpha, -1\}$ as long as $\psi_1 \neq \psi_2 \neq \psi_3$. Similarly, ψ_4, ψ_5 and ψ_6 can take any one of the $\{1+\beta, -\beta, -1\}$ as long as $\psi_4 \neq \psi_5 \neq \psi_6$.

Steady-state torque equations are derived for all five unique configurations in Figure 5.2 using the method described in Section 3.2. Then, the relationship between $T_{Vehicle}$ and T_{ICE} is analyzed by rearranging the equations such that $T_{Vehicle}$ is a function of T_{ICE}. Tables 5.1-5.2 show the results of these operations. As seen from

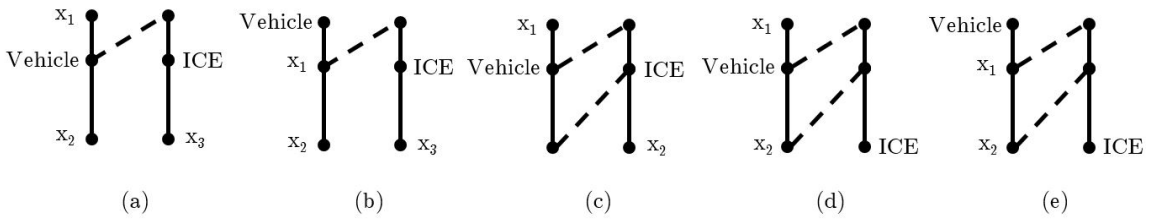

Figure 5.2: Five Unique Ways Vehicle and Engine can be assigned to the nodes of 2 PGs.

these tables, the coefficients of T_{ICE} can take the following unique forms:

- $\frac{\psi_4(\beta)}{\psi_5(\beta)}$ or $\frac{\psi_4(\beta)}{\psi_6(\beta)}$ or $\frac{\psi_2(\alpha)}{\psi_3(\alpha)}$
- $-\frac{\psi_1(\alpha)\cdot\psi_4(\beta)}{\psi_2(\alpha)\cdot\psi_5(\beta)}$ or $-\frac{\psi_1(\alpha)\cdot\psi_4(\beta)}{\psi_2(\alpha)\cdot\psi_6(\beta)}$ or $-\frac{\psi_1(\alpha)\cdot\psi_5(\beta)}{\psi_3(\alpha)\cdot\psi_6(\beta)}$
- $\frac{\psi_3(\alpha)\cdot\psi_4(\beta)-\psi_2(\alpha)\cdot\psi_5(\beta)}{\psi_3(\alpha)\cdot\psi_6(\beta)}$

In all cases above, since $\psi_i(\alpha) \in \{1+\alpha, -\alpha, -1\}, i = 1,2,3$ and $\psi_i(\beta) \in \{1+\beta, -\beta, -1\}, i = 4,5,6$, the numerators and denominators of the coefficients are an affine function of α if β is kept constant or vice versa. Since the ratio of two affine functions is monotonic, all coefficients are a monotonic function of α as well. The same argument is valid for β. As a result, T_{ICE} coefficients are monotonic functions of α and β for all possible configurations of engine and vehicle in a 2-PG mode.

Table 5.1: $T_{Vehicle}$ Equations as Functions of T_{ICE}, T_{x1}

Generic Configurations	$T_{Vehicle} = f(T_{ICE}, T_{x1})$
(a)	$T_{Vehicle} = \frac{\psi_2(\alpha)}{\psi_1(\alpha)} \cdot T_{x1} + \frac{\psi_4(\beta)}{\psi_5(\beta)} \cdot T_{ICE}$
(b)	$T_{Vehicle} = \frac{\psi_1(\alpha)}{\psi_2(\alpha)} \cdot T_{x1} - \frac{\psi_1(\alpha)\cdot\psi_4(\beta)}{\psi_2(\alpha)\cdot\psi_5(\beta)} \cdot T_{ICE}$
(c)	$T_{Vehicle} = \frac{\psi_2(\alpha)\cdot\psi_5(\beta)-\psi_3(\alpha)\cdot\psi_4(\beta)}{\psi_1(\alpha)\cdot\psi_5(\beta)} \cdot T_{x1} + \frac{\psi_4(\beta)}{\psi_5(\beta)} \cdot T_{ICE}$
(d)	$T_{Vehicle} = \frac{\psi_2(\alpha)}{\psi_1(\alpha)} \cdot T_{x1} + \frac{\psi_4(\beta)}{\psi_6(\beta)} \cdot T_{ICE}$
(e)	$T_{Vehicle} = \frac{\psi_1(\alpha)}{\psi_2(\alpha)} \cdot T_{x1} - \frac{\psi_1(\alpha)\cdot\psi_4(\beta)}{\psi_2(\alpha)\cdot\psi_6(\beta)} \cdot T_{ICE}$

□

Using the result of Proposition V.1, the forward/backward speed capability of a mode with engine on can be evaluated for varying PG gear ratios by simply check-

Table 5.2: $T_{Vehicle}$ Equations as Functions of T_{ICE}, T_{x2}

Generic Configurations	$T_{Vehicle} = f(T_{ICE}, T_{x2})$
(a)	$T_{Vehicle} = \frac{\psi_2(\alpha)}{\psi_3(\alpha)} \cdot T_{x2} + \frac{\psi_4(\beta)}{\psi_5(\beta)} \cdot T_{ICE}$
(b)	$T_{Vehicle} = \frac{\psi_3(\alpha)}{\psi_1(\alpha)} \cdot T_{x2}$
(c)	$T_{Vehicle} = \frac{\psi_3(\alpha)\cdot\psi_4(\beta) - \psi_2(\alpha)\cdot\psi_5(\beta)}{\psi_3(\alpha)\cdot\psi_6(\beta)} \cdot T_{x2} + \frac{\psi_2(\alpha)}{\psi_3(\alpha)} \cdot T_{ICE}$
(d)	$T_{Vehicle} = \frac{\psi_2(\alpha)}{\psi_3(\alpha)} \cdot T_{x2} + \frac{\psi_3(\alpha)\cdot\psi_4(\beta) - \psi_2(\alpha)\cdot\psi_5(\beta)}{\psi_3(\alpha)\cdot\psi_6(\beta)} \cdot T_{ICE}$
(e)	$T_{Vehicle} = \frac{\psi_1(\alpha)}{\psi_3(\alpha)} \cdot T_{x2} - \frac{\psi_1(\alpha)\cdot\psi_5(\beta)}{\psi_3(\alpha)\cdot\psi_6(\beta)} \cdot T_{ICE}$

ing the combinations of α and β limits: $(\alpha_{max}, \beta_{max})$, $(\alpha_{max}, \beta_{min})$, $(\alpha_{min}, \beta_{max})$, $(\alpha_{min}, \beta_{min})$, instead of assessing the T_{ICE} coefficient for all PG gear ratio combinations. If all four combinations have the same sign for the T_{ICE} coefficient, then the mode does not change any behavior with respect to the PG gear ratio and it belongs to either the forward-speed capable or backward-speed capable category. If there is any sign difference among the four combinations, it means that the backward-speed capability of this mode changes with the changing PG gear ratios and the mode falls in both categories.

5.3 Manual Process of Forward/Backward Vehicle Speed Capability Evaluation

The following algorithm is developed using the mathematical relationships in the torque matrix, whose derivation is explained in Chapter III.

- Determine all paths from the engine node to the vehicle node.
- Start the path from the engine node with a positive sign.
- On the path, when it is moved from the ring or sun node to the carrier node, reverse the sign.
- On the path, when it is moved from the ring(sun) node to the sun(ring) node, do not change the sign.

- Reverse the sign after the transition from one PG to another on the path, unless the originating node or the ending node in the transition is the engine or vehicle node.
- Once the path reaches the vehicle node, check the latest sign. If it is negative(positive), then the vehicle can be propelled in the forward(reverse) direction with positive engine torque.
- Repeat this process for all available paths between the engine node and vehicle node.
- If the ending sign is negative in all paths, the vehicle cannot be propelled in the reverse direction while the engine is on.

The reasoning behind these rules and how they can be applied will be explained through the following four examples:

Example 1:

The first example mode is shown in Figure 5.3, where the engine and vehicle are on the same PG. There is only one path between the engine and vehicle. Starting with a positive sign at the ring gear (engine), the sign would change to negative when it reaches the carrier. Since the ending sign is negative, positive engine torque would propel the vehicle in the forward direction.

The reason for the change in sign when it is moved from the ring or sun gear to the carrier is as follows: The torque equations at the ring gear and carrier are $T_{ICE} + T_{C1} = -\alpha F_1$ and $T_{Vehicle} = (1+\alpha)F_1$, respectively, where T_{C1} is the torque at the connection between the left and right PGs, α is the gear ratio between ring and sun gears of the left PG, and F_1 is the tangential force between the sun gear and pinion gear. Replacing F_1 with $\frac{T_{Vehicle}}{1+\alpha}$, $T_{Vehicle} = -\frac{1+\alpha}{\alpha}T_{ICE} - \frac{1+\alpha}{\alpha}T_{C1}$ is obtained. As seen in this equation, the coefficient in front of the T_{ICE} is always negative.

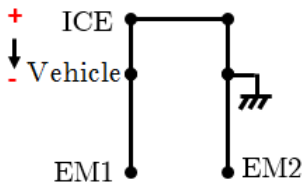

Figure 5.3: Example 1: The engine can only drive the vehicle forwards.

Example 2:

The second example mode is shown in Figure 5.4, where the engine and vehicle are on different PGs. There is only one path between the engine and vehicle. Since the engine is on the node to which the second PG is connected, moving from the ring node of the first PG to the carrier of the second PG does not change the sign. The path between the engine and vehicle moves from the carrier to the ring gear of the second PG. Hence, the sign changes to negative. Since the sign ends up being negative at the vehicle node, positive engine torque would propel the vehicle in the forward direction. The reason the sign does not change when it is moved from the engine node on the first gear to the second gear is as follows: The torque equations at the ring gear of the first PG and carrier of the second PG are $T_{ICE}+T_{C1}=-\alpha F_1$ and $-T_{C1}=(1+\beta)F_2$, respectively, where T_{C1} is the torque at the connection between the left and right PGs. Replacing T_{C1} with $-(1+\beta)F_2$, $T_{ICE}=-\alpha F_1+(1+\beta)F_2$ is obtained. As seen in this equation, there is a positive correlation between T_{ICE} and F_2 and replacing F_2 with T_{ICE} would not change the sign relationships between T_{ICE} and $T_{Vehicle}=-\beta F_2$.

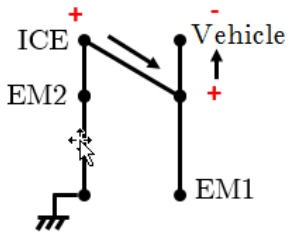

Figure 5.4: Example 2: The engine can only drive the vehicle forwards.

Example 3:

The third example mode is shown in Figure 5.5, where the engine and vehicle are on different PGs. There are two paths between the engine and vehicle. The first path reaches the vehicle node from the engine node through EM_2 and the ring gear of the right PG. Starting with a positive sign at the engine node, the sign changes to negative when the torque is transmitted to the carrier of the left PG on this path. Another sign change occurs when it is moved from the carrier to the ring gear of the right PG. Moving from the ring gear of the right PG to its carrier requires another sign change. The sign at the carrier to which the vehicle is connected becomes negative. The second path reaches the vehicle node from the engine node through EM_1 and the sun gear of the right PG. Starting with a positive sign at the engine node, the sign remains the same when torque is transmitted to the sun gear of the left PG on this path. A sign change occurs when it is moved from the sun gear of the left PG to the sun gear of the right PG. Moving from the sun gear to the carrier requires another sign change. The sign at the carrier to which the vehicle is connected now becomes positive. Since the two paths have different signs at the vehicle node, whether positive engine torque propels the vehicle in the forward or reverse direction cannot be determined at this stage. Making this decision requires the maximum acceleration analysis, explained in the next chapter.

The reason the sign changes when it is moved from the left PG to the right PG and the engine is not connected to any of the connected nodes is as follows: The torque equations at the sun gears of the left and right PGs are $T_{EM1} + T_{C2} = -F_1$ and $-T_{C2} = -F_2$, respectively, where T_{C2} is the torque at the second connection between the left and right PGs. Replacing T_{C2} with F_2, $T_{EM1} + F_2 = -F_1$ is obtained. As seen in this equation, there is a negative correlation between F_1 and F_2. Thus, the sign changes when the torque is transmitted from the left PG to the right one.

Example 4:

The fourth example mode is shown in Figure 5.6, where the engine and vehicle are on

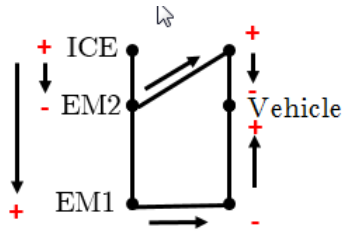

Figure 5.5: Example 3: The engine can drive the vehicle both forwards and backwards.

different PGs. There are two paths between the engine and vehicle. The first path reaches from the engine node to the vehicle node through the ring gear of the right PG. Starting with a positive sign at the engine node, the sign remains positive when the torque is transmitted to the ring gear of the right PG on this path. The sign changes to negative when the torque is transmitted from the ring gear of the right PG to the carrier to which the vehicle is connected. The second path reaches from the engine node to the vehicle node through the carrier of the left PG and the sun gear of the right PG. Starting with a positive sign at the engine node, the sign changes to negative when the torque is transmitted to the carrier of the left PG. Another sign change occurs when there is a transition from the carrier gear to the sun gear of the right PG. Moving from the sun gear to the carrier of the right PG requires another sign change. As a result, the final sign at the vehicle node becomes negative. Since two paths have resulted in negative signs at the vehicle node, positive engine torque propels the vehicle in the forward direction only.

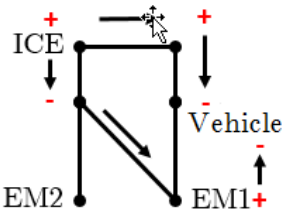

Figure 5.6: Example 4: The engine can only drive the vehicle forwards.

5.4 Analysis Results

The automated forward and backward speed capability algorithms described in Section 5.1 are applied to the feasible $34,380$ modes for four combinations of α and β. Table 5.3 summarizes the analysis results. The reason for the high number of forward- and backward speed capable modes is the inclusion of all EV and series modes in this group. In fact, the number of modes where T_{ICE} coefficient changes its sign due to the PG gear ratio variation is 552. Moreover, the forward and backward speed capability of 120 compound-split modes cannot be determined, since h_{11} and $\tilde{h}_{11}$ coefficients in Section 5.1 have different signs. Therefore, these modes are also grouped under the category of forward- and backward speed capable modes.

Table 5.3: Forward- and Backward Speed Capable Modes

	Forward Speed	Backward Speed	Forward and Backward Speed
Total Number of Modes	17,396	9,412	8,916
Powertrain Type			
Fixed Gear	2,260	1,184	24
EV	0	0	5,580
Parallel	10,140	5,412	360
Series	0	0	2,664
Input-Split	1,464	816	48
Output-Split	1,464	816	48
Compound-Split	368	232	168
Special Power-Split	1,700	952	24

CHAPTER VI

Performance Analysis

In this chapter, the performance criteria and the algorithms derived to analyze each mode against these criteria are explained.

In the HEV powertrain design literature, performance criteria other than 0-60mph time have been overlooked due to either lack of practical automotive experience or algorithm simplification. Thus, the results of the design processes may not be of any practical value. Moreover, 0-60mph time is calculated under assumptions that degrade the accuracy of the results. In this study, not only analyses related to the performance criteria necessary for designing a marketable vehicle are introduced but also an accurate 0-60mph time calculation method applicable to varying PG gear ratios.

The performance criteria have been determined based on the SAE J2807 Standard [83] and general design requirements in the automotive industry. The requirements in the SAE J2807 Standard are tightened in this study because the standard gives the minimum requirements that a light-duty truck should meet and the vehicles with conventional powertrains in the marketplace easily exceed them. These performance criteria set for a vehicle at its Gross Combination Weight Rating (GCWR) are categorized into three groups, shown in detail in Table 6.1. The difference between gradeability and long-hauling capability is the fact that in the evaluation of long-hauling

capability, maximum output torque of the HEV powertrain is calculated under the assumption of charge sustaining operation, whereas in gradeability, the only constraint is the limits of the components in the design. Forward-speed capable modes are eval-

Table 6.1: Performance Criteria

Gradeability	**Long-Hauling Capability**	x-y **mph Time**
15% at 6mph	8% at 25mph	0-60mph Time $\leq$ 20s
12% at 12mph	6% at 40mph	0-30mph Time $\leq$ 10s
0% at 113mph	4% at 50mph	40-60mph Time $\leq$ 10s
	2% at 75mph	

uated against the criteria in Table 6.1; the modes for the backward-speed capable group are assessed against the gradeability criteria in Table 6.2. In addition to these gradeability criteria, the engine should also be at least at its idle speed (600rpm) below -8 mph so that it can produce positive torque.

Table 6.2: Backward-Speed Performance Criteria

Backward-Speed Gradeability
15% at 0mph
15% at -6mph
0% at -10mph

In the following sections, how each mode is evaluated against these performance criteria will be explained in detail.

6.1 Performance Evaluation for varying PG Gear Ratios

Feasibility and powertrain type analyses can be performed for just one set of PG ratios because the structure of the equations is sufficient for drawing conclusions. Similarly, four PG ratio combinations are needed to complete forward- and backward speed capability checks of feasible modes. However, the performance analyses in the design process require the evaluation of the feasible modes for each PG gear ratio combination since the value of the PG gear ratio has a significant effect on the analysis

outcomes. Due to the computational complexity of introducing PG ratios into the design process, the literature either assumes a constant PG ratio or works with a smaller design space.

The standard way of doing PG gear ratio evaluation is to calculate speed and torque equations for each PG gear ratio combination iteratively. The cost of this implementation results in high computational inefficiency. Considering the need to evaluate thousands of modes, this approach is not practical. In this study, a different approach is developed as follows:

1. Using Symbolic Toolbox of Matlab, two symbolic variables α and β are created.

2. Steady-state torque and speed matrices are constructed by using the method in Section 3.2. PG gear ratios exist symbolically in these matrices. However, the matrix form is not suitable for evaluating the modes with varying PG gear ratios.

3. The Gaussian elimination method is applied to these matrices as described in Section 4.2 to calculate speed and torque equations in a compact symbolic form that consists of only torque and speed variables of the engine, vehicle, and electric machines. These symbolic equations are then converted into a text string.

4. PG gear ratios are discretized with 0.1 increments in the physically feasible range of $[1.8, 3.8]$, and all PG gear ratio combinations in the vector form are applied as inputs to the symbolic equations in the string format using Matlab's "eval" command.

This method allows all mode performance analyses for all PG gear ratio combinations to be conducted extremely fast thanks to the vector arithmetic operations.

6.2 Long-Hauling Performance Analysis

In this study, long-hauling performance of a powertrain is defined as its capability of moving a fully loaded vehicle at a constant speed over a long distance. Because the battery state of charge in EV powertrain types is not sufficient for long distance trips, they are excluded from this analysis. Moreover, other HEV powertrain types should operate at charge sustaining mode so as not to deplete the battery. This section will explain how the long-hauling performance of each powertrain type is calculated for each PG gear ratio combination.

6.2.1 Fixed Gear, Series, and Parallel Powertrain Types

The degrees of freedom in speed equations are one in fixed gear, series, and parallel powertrain types. Hence, in fixed gear and parallel powertrain types, engine speed is easily calculated from the vehicle speed using ω_{ICE} coefficient a in $\omega_{Vehicle} = a \cdot \omega_{ICE}$. Using speed vs. maximum torque curve of the engine, maximum engine torque T_{ICEmax} and $T_{Vehiclemin} = -\frac{1}{a} \cdot T_{ICEmax}$ are obtained. In a parallel powertrain type, it is assumed that electric machines supply zero torque so as not to deplete the battery. Similarly, in a series powertrain type, the electric machine speed at the given $\omega_{Vehicle}$ is first calculated, then the maximum electric machine torque and $T_{Vehiclemin}$. Since the mathematical operations involved are just multiplications and table lookups, each operation can handle variables in vector form. Each element of a vector variable corresponds to that variable's value for a specific PG gear ratio combination.

6.2.2 Compound-Split, Input-Split, and Output-Split Powertrain Types

Besides regenerative braking and torque assist, the main task of electric machines in a power-split based hybrid powertrain is to provide eCVT operation, where the engine can run at its highest system efficiency point independent from the vehicle speed when assisted by the electric machines. In the long-hauling performance analysis of

power-split powertrain types, it is assumed that the powertrain operates in the eCVT mode and the efficiency of electric machines is 100% so that there is no energy transfer from/to the battery.

The derivation of the electric machine power in the eCVT operation begins with the generic ω_{EM1}, ω_{EM2}, T_{EM1}, and T_{EM2} equations of a power-split powertrain type, which are derived from the steady-state speed and torque equations, where f_{1-4} and g_{1-4} are PG gear ratio dependent coefficients.

$$\frac{\omega_{EM1}}{\omega_{ICE}} = f_1 + g_1 \cdot \frac{\omega_{Vehicle}}{\omega_{ICE}} \tag{6.1a}$$

$$\frac{\omega_{EM2}}{\omega_{ICE}} = f_2 + g_2 \cdot \frac{\omega_{Vehicle}}{\omega_{ICE}} \tag{6.1b}$$

$$\frac{T_{EM1}}{T_{ICE}} = f_3 + g_3 \cdot \frac{T_{Vehicle}}{T_{ICE}} \tag{6.1c}$$

$$\frac{T_{EM2}}{T_{ICE}} = f_4 + g_4 \cdot \frac{T_{Vehicle}}{T_{ICE}} \tag{6.1d}$$

For the eCVT operation with 0 battery power and lossless electric machines,

$$P_{EM1} = -P_{EM2} \tag{6.2a}$$

$$\frac{T_{EM1} \cdot \omega_{EM1}}{T_{ICE} \cdot \omega_{ICE}} = -\frac{T_{EM2} \cdot \omega_{EM2}}{T_{ICE} \cdot \omega_{ICE}} \tag{6.2b}$$

Using the energy conservation principle,

$$T_{Vehicle} \cdot \omega_{Vehicle} = -T_{ICE} \cdot \omega_{ICE} \tag{6.3}$$

After some algebraic manipulations with Eqs. (6.1a) through (6.3), the following equation is obtained:

$$f_1 \cdot f_3 - g_1 \cdot g_3 + f_3 \cdot g_1 \cdot \frac{\omega_{Vehicle}}{\omega_{ICE}} - f_1 \cdot g_3 \frac{\omega_{ICE}}{\omega_{Vehicle}} = -f_2 \cdot f_4 + g_2 \cdot g_4 - f_4 \cdot g_2 \cdot \frac{\omega_{Vehicle}}{\omega_{ICE}} + f_2 \cdot g_4 \cdot \frac{\omega_{ICE}}{\omega_{Vehicle}} \tag{6.4}$$

Since Eq. (6.4) should hold for all values of $\omega_{Vehicle}$ and ω_{ICE},

$$f_1 \cdot f_3 - g_1 \cdot g_3 = -f_2 \cdot f_4 + g_2 \cdot g_4 \tag{6.5a}$$

$$f_3 \cdot g_1 = -f_4 \cdot g_2 \tag{6.5b}$$

$$f_1 \cdot g_3 = -f_2 \cdot g_4 \tag{6.5c}$$

Using the results derived above, the electric machine power equation is calculated as:

$$\frac{P_{EM1}}{P_{ICE}} = \frac{T_{EM1} \cdot \omega_{EM1}}{T_{ICE} \cdot \omega_{ICE}} = \frac{a \cdot x^2 + b \cdot x + c}{x} \tag{6.6}$$

where

$$x = \frac{\omega_{Vehicle}}{\omega_{ICE}} \tag{6.7}$$

$$a = f_3 \cdot g_1 = -f_4 \cdot g_2 \tag{6.8}$$

$$b = f_1 \cdot f_3 - g_1 \cdot g_3 = -f_2 \cdot f_4 + g_2 \cdot g_4 \tag{6.9}$$

$$c = -f_1 \cdot g_3 = f_2 \cdot g_4 \tag{6.10}$$

a, b, and c terms in Eqs. (6.8)-(6.10) can be simplified with the following proposition.

Proposition VI.1. *Suppose the speed and torque equations of a mode with any number of PGs are represented as:*

$$\begin{bmatrix} \omega_{EM1} \\ \omega_{EM2} \end{bmatrix} = \begin{bmatrix} f_1(\alpha,\beta) & g_1(\alpha,\beta) \\ f_2(\alpha,\beta) & g_2(\alpha,\beta) \end{bmatrix} \begin{bmatrix} \omega_{ICE} \\ \omega_{Vehicle} \end{bmatrix}$$

$$\begin{bmatrix} T_{ICE} \\ T_{Vehicle} \end{bmatrix} = \begin{bmatrix} f_3(\alpha,\beta) & g_3(\alpha,\beta) \\ f_4(\alpha,\beta) & g_4(\alpha,\beta) \end{bmatrix} \begin{bmatrix} T_{EM1} \\ T_{EM2} \end{bmatrix}$$

Then,

$$\begin{bmatrix} f_3(\alpha,\beta) & g_3(\alpha,\beta) \\ f_4(\alpha,\beta) & g_4(\alpha,\beta) \end{bmatrix} = - \begin{bmatrix} f_1(\alpha,\beta) & g_1(\alpha,\beta) \\ f_2(\alpha,\beta) & g_2(\alpha,\beta) \end{bmatrix}^T = \begin{bmatrix} -f_1(\alpha,\beta) & -f_2(\alpha,\beta) \\ -g_1(\alpha,\beta) & -g_2(\alpha,\beta) \end{bmatrix}$$

Proof. Using energy conservation law,

$T_{EM1} \cdot \omega_{EM1} + T_{EM2} \cdot \omega_{EM2} + T_{ICE} \cdot \omega_{ICE} + T_{Vehicle} \cdot \omega_{Vehicle} = 0$

Replacing ω_{EM1} and ω_{EM2} with $f_1(\alpha,\beta) \cdot \omega_{ICE} + g_1(\alpha,\beta) \cdot \omega_{Vehicle}$ and $f_2(\alpha,\beta) \cdot \omega_{ICE} + g_2(\alpha,\beta) \cdot \omega_{Vehicle}$,

$\omega_{ICE} \cdot (f_1 \cdot T_{EM1} + f_2 \cdot T_{EM2} + T_{ICE}) + \omega_{Vehicle} \cdot (g_1 \cdot T_{EM1} + g_2 \cdot T_{EM2} + T_{Vehicle}) = 0$

Since the equation above should be 0 for $\forall \omega_{ICE}, \omega_{Vehicle} \in \mathbf{R}$,

$f_1 \cdot T_{EM1} + f_2 \cdot T_{EM2} + T_{ICE} = 0$

$g_1 \cdot T_{EM1} + g_2 \cdot T_{EM2} + T_{Vehicle} = 0$

As a result,

$$\begin{bmatrix} T_{ICE} \\ T_{Vehicle} \end{bmatrix} = \begin{bmatrix} -f_1(\alpha,\beta) & -f_2(\alpha,\beta) \\ -g_1(\alpha,\beta) & -g_2(\alpha,\beta) \end{bmatrix} \begin{bmatrix} T_{EM1} \\ T_{EM2} \end{bmatrix}$$

□

Applying the result of the Proposition VI.1 to the Eqs. (6.1c)-(6.1d), f_3, f_4, g_3, and g_4 can be represented as:

$$\begin{bmatrix} T_{EM1} \\ T_{EM2} \end{bmatrix} = \begin{bmatrix} f_3 & g_3 \\ f_4 & g_4 \end{bmatrix} \begin{bmatrix} T_{ICE} \\ T_{Vehicle} \end{bmatrix} = \frac{1}{f_1 \cdot g_2 - f_2 \cdot g_1} \begin{bmatrix} -g_2 & f_2 \\ g_1 & -f_1 \end{bmatrix} \begin{bmatrix} T_{ICE} \\ T_{Vehicle} \end{bmatrix} \tag{6.11}$$

6.2.2.1 Input-Split Powertrain Types

For an input-split powertrain type, $f_2 = 0$. Thus, Eq. (6.11) becomes

$$\begin{bmatrix} T_{EM1} \\ T_{EM2} \end{bmatrix} = \begin{bmatrix} f_3 & g_3 \\ f_4 & g_4 \end{bmatrix} \begin{bmatrix} T_{ICE} \\ T_{Vehicle} \end{bmatrix} = \begin{bmatrix} -\frac{1}{f_1} & 0 \\ \frac{g_1}{f_1 \cdot g_2} & -\frac{1}{g_2} \end{bmatrix} \begin{bmatrix} T_{ICE} \\ T_{Vehicle} \end{bmatrix} \tag{6.12}$$

Representing f_3, g_3 terms in Eqs. (6.8)-(6.10) in terms of f_1, g_1, and g_2 according to the Eq. (6.12) yields,

$$a = -\frac{g_1}{f_1} \tag{6.13}$$

$$b = -f_1 \cdot \frac{1}{f_1} - g_1 \cdot 0 = -1 \tag{6.14}$$

$$\frac{P_{EM1}}{P_{ICE}} = -\frac{g_1}{f_1} \cdot x - 1 \tag{6.15}$$

$\frac{P_{EM1}}{P_{ICE}}$ curve is plotted in Figure 6.1 for positive and negative $-\frac{g_1}{f_1}$'s. As seen in the figure, if $-\frac{g_1}{f_1}$ is positive, P_{EM1} requirement is less and the mechanical point $-\frac{f_1}{g_1}$ becomes positive. However, if mechanical point is negative i.e. $-\frac{g_1}{f_1} < 0$, P_{EM1} requirement is much more. Therefore, in an input-split mode, the slope of the curve $-\frac{g_1}{f_1}$ should be positive and small for high long-hauling performance with limited electric machine power.

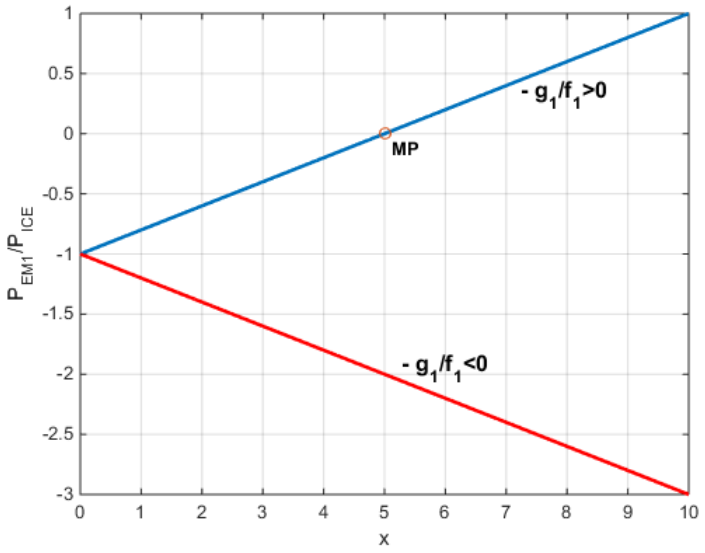

Figure 6.1: P_{EM1}/P_{ICE} with respect to $\frac{\omega_{Vehicle}}{\omega_{ICE}}$ for Input-Split Powertrain Types.

6.2.2.2 Output-Split Powertrain Types

For an output-split powertrain type, $g_2 = 0$. Thus, Eq. (6.11) becomes

$$\begin{bmatrix} T_{EM1} \\ T_{EM2} \end{bmatrix} = \begin{bmatrix} f_3 & g_3 \\ f_4 & g_4 \end{bmatrix} \begin{bmatrix} T_{ICE} \\ T_{Vehicle} \end{bmatrix} = \begin{bmatrix} 0 & -\frac{1}{g_1} \\ -\frac{1}{f_2} & \frac{f_1}{f_2 \cdot g_1} \end{bmatrix} \begin{bmatrix} T_{ICE} \\ T_{Vehicle} \end{bmatrix} \tag{6.16}$$

Representing f_3, g_3 terms in Eqs. (6.8)-(6.10) in terms of f_1, f_2, and g_1 according to the Eq. (6.16) yields,

$$b = -f_1 \cdot 0 + g_1 \cdot \frac{1}{g_1} = 1 \tag{6.17}$$

$$c = \frac{f_1}{g_1} \tag{6.18}$$

$$\frac{P_{EM1}}{P_{ICE}} = 1 + \frac{f_1}{g_1} \cdot \frac{1}{x} \tag{6.19}$$

$\frac{P_{EM1}}{P_{ICE}}$ curve is plotted in Figure 6.2 for positive and negative $\frac{f_1}{g_1}$'s. As seen in the figure, if $\frac{f_1}{g_1}$ is negative, P_{EM1} requirement is less and the mechanical point $-\frac{f_1}{g_1}$ becomes positive. However, if mechanical point is negative i.e. $-\frac{g_1}{f_1} < 0$, P_{EM1} requirement is much more because the power ratio curve always stays above the horizontal line at $y = 1$. Hence, in an output-split mode, the coefficient of x, $\frac{f_1}{g_1}$, should be negative for high long-hauling performance with limited electric machine power.

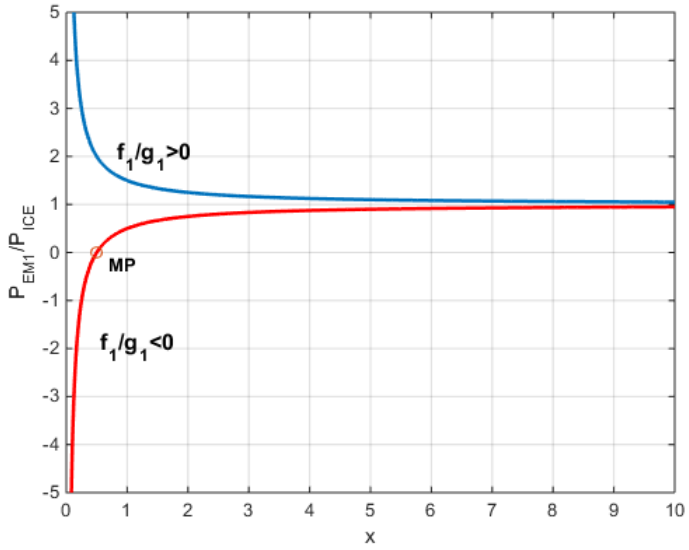

Figure 6.2: P_{EM1}/P_{ICE} with respect to $\frac{\omega_{Vehicle}}{\omega_{ICE}}$ for Output-Split Powertrain Types.

6.2.2.3 Compound-Split Powertrain Types

For a compound-split powertrain type, using Eq. (6.11), $\frac{P_{EM1}}{P_{ICE}}$ becomes

$$x = \frac{\omega_{Wheels}}{\omega_{ICE}} \tag{6.20}$$

$$\frac{P_{EM1}}{P_{ICE}} = \frac{ax^2 + bx + c}{x} \tag{6.21}$$

$$a = \frac{1}{-\frac{f_1}{g_1} + \frac{f_2}{g_2}} \tag{6.22}$$

$$b = \frac{1}{\frac{g_1 f_2}{f_1 g_2} - 1} + \frac{1}{-\frac{f_1 g_2}{g_1 f_2} + 1} \tag{6.23}$$

$$c = \frac{1}{\frac{g_1}{f_1} - \frac{g_2}{f_2}} \tag{6.24}$$

Compound-split powertrain type has two mechanical points, $MP_1 = -\frac{f_1}{g_1}$ and $MP_2 = -\frac{f_2}{g_2}$. There are three possibilities for the mechanical point pairs: $MP1 > 0$, $MP2 > 0$ or $MP1 < 0$, $MP2 < 0$ or $MP1 < 0$, $MP2 > 0$. $\frac{P_{EM1}}{P_{ICE}}$ curve is plotted in Figure 6.3 for these MP pairs. As seen in the figure, P_{EM1} requirement is the least when both mechanical points are positive. Hence, in an compound-split mode,

$\frac{f_1}{g_1}$ and $\frac{f_2}{g_2}$ should be negative for high long-hauling performance with limited electric machine power.

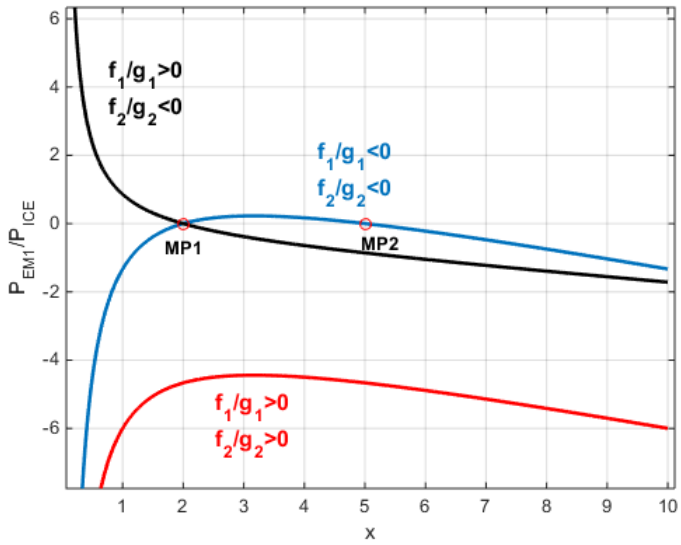

Figure 6.3: P_{EM1}/P_{ICE} with respect to $\frac{\omega_{Vehicle}}{\omega_{ICE}}$ for Compound-Split Powertrain Types.

6.2.2.4 Implementation of Long-Hauling Capability Analysis for Input-Split, Output-Split, and Compound-Split Types

In Subsections 6.2.2.1-6.2.2.3, the formulas are derived to calculate the required electric machine power for a given desired vehicle output power. In this subsection, the implementation of these formulas in the long-hauling analysis is explained.

First, the coefficients of the power ratio formulas are calculated for all PG gear ratio combinations in vector form. The long-hauling requirements are specified for constant vehicle speeds. But in the power ratio formulas, $x = \frac{\omega_{Vehicle}}{\omega_{ICE}}$ is required. Therefore, x should be calculated for a set of engine speed points between ω_{ICEmin} and ω_{ICEmax}. For each x point, the corresponding power ratio $\frac{P_{EM1}}{P_{ICE}}$ is calculated for all PG gear ratio combinations. In the long-hauling requirement, $P_{Vehiclereq} = T_{Vehiclereq} \cdot \omega_{Vehicle}$ is also known. Since the vehicle is propelled with 0 net electrical power, that is, $P_{Vehiclereq} = -P_{ICEreq}$, P_{EM1req} is easily obtained from the power ratio.

Furthermore, for each engine speed point, corresponding ω_{EM1} is calculated using Eq. (6.1a). Utilizing the maximum torque curve of the electric machine with respect to the electric machine speed, P_{EM1max} for the given ω_{EM1} is calculated. Notice that all these variables are in vector form to cover PG gear ratio combinations. P_{EM1max} is compared to P_{EM1req}. PG gear ratios, which realize $P_{EM1max} \geq P_{EM1req}$, are recorded as long-hauling capable ratios. This entire operation is repeated for all engine speed points, and the engine speed point that provides the highest number of PG gear ratios with the condition of $P_{EM1max} \geq P_{EM1req}$ is recorded with the long-hauling capable gear ratios.

6.2.3 Special Power-Split Powertrain Types

As shown in Chapter IV, special power-split powertrain types fall into three categories based on their speed and torque equations. In this section, how the long-hauling analysis is conducted for each of these categories will be described.

6.2.3.1 Special Power-Split Type I

In a special power-split type I, one of the electric machines is either at 0 speed or 0 torque. The relationships among the remaining actuators are as follows:

$$\omega_{Vehicle} = a \cdot \omega_{EM1} + b \cdot \omega_{ICE} \tag{6.25}$$

$$T_{EM1} = -a \cdot T_{Vehicle} \tag{6.26}$$

$$T_{ICE} = -b \cdot T_{Vehicle} \tag{6.27}$$

For 0 battery power operation during long-hauling, ω_{EM1} should be set to 0 since EM2 does not generate/use any power, and T_{EM1} is determined directly by $T_{Vehicle}$ as seen in Eq. (6.26). The first step of the long-hauling analysis is to calculate ω_{ICE} using Eq. (6.25), where $\omega_{Vehicle}$ is constant and $\omega_{EM1} = 0$. The second step is to

calculate $T_{Vehicle}$ twice, once through T_{EM1max} or T_{EM1min} at $\omega_{EM1} = 0$ in Eq. (6.26), and the other through T_{ICEmax} at the known ω_{ICE} in Eq. (6.27). Since $T_{Vehicle}$ is a negative number, the maximum of two $T_{Vehicle}$ values is the minimum attainable $T_{Vehicle}$ during long-hauling at a given vehicle speed. If $T_{Vehicle}$ exceeds the limit, then the corresponding mode can meet the long-hauling requirement.

6.2.3.2 Special Power-Split Type II

In a special power-split type II, the speed and torque relationships among the actuators are as follows:

$$\omega_{Vehicle} = a \cdot \omega_{EM2} + b \cdot \omega_{ICE} \tag{6.28}$$

$$\omega_{EM1} = c \cdot \omega_{EM2} \tag{6.29}$$

$$T_{EM2} = -c \cdot T_{EM1} + \frac{a}{b} \cdot T_{ICE} \tag{6.30}$$

$$T_{ICE} = -b \cdot T_{Vehicle} \tag{6.31}$$

Using the condition $P_{EM1} = -P_{EM2}$ during long-hauling, and Eq. (6.29), the relationship between T_{EM1} and T_{EM2} is found to be $T_{EM2} = -c \cdot T_{EM1}$. Placing this equation into Eq. (6.30) shows that 0 battery power operation can be achieved when $T_{ICE} = 0$ and $T_{Vehicle} = 0$. Therefore, this powertrain type cannot possess any long-hauling capability without battery power.

6.2.3.3 Special Power-Split Type III

In a special power-split type III, the speed and torque relationships among the actuators are as follows:

$$\omega_{Vehicle} = a \cdot \omega_{EM1} + b \cdot \omega_{EM2} + c \cdot \omega_{ICE} \tag{6.32}$$

$$T_{EM1} = -a \cdot T_{Vehicle} \tag{6.33}$$

$$T_{EM2} = -b \cdot T_{Vehicle} \tag{6.34}$$

$$T_{ICE} = -c \cdot T_{Vehicle} \tag{6.35}$$

Using the condition $P_{EM1} = -P_{EM2}$ during long-hauling, and Eqs. (6.33)-(6.34), the relationship between ω_{EM1} and ω_{EM2} is found to be $-a \cdot \omega_{EM1} = b \cdot \omega_{EM2}$. Placing this equation into Eq. (6.32), the relationship between $\omega_{Vehicle}$ and ω_{ICE} is obtained as $\omega_{Vehicle} = c \cdot \omega_{ICE}$.

The first step of the long-hauling analysis is to calculate ω_{ICE} using the relationship $\omega_{Vehicle} = c \cdot \omega_{ICE}$. The second step is to calculate T_{ICEmax} at that engine speed. In the third step, T_{EM1} and T_{EM2} are calculated using Eqs. (6.33)-(6.35). If T_{EM1} or T_{EM2} exceeds their max or min limits, T_{ICEmax} is reduced until they are within torque limits. In the final step, $T_{Vehicle}$ that corresponds to the adjusted T_{ICEmax} is compared to the long-hauling requirement.

6.3 Long-Hauling Performance Analysis for Varying PG Gear Ratios

The long-hauling analysis methods explained for all powertrain types in Subsections 6.2.2-6.2.3 should be implemented for all PG gear ratio combinations. Instead of a "for loop," where one PG gear ratio combination is evaluated in each iteration, the coefficients of the speed and torque equations f_1, f_2, g_1, g_2 are calculated in vector

form using the method in Section 6.1. Each element in these vectors corresponds to a PG gear ratio combination. Due to the vector form of these coefficients, $T_{Vehicle}$, T_{ICE}, T_{EM1}, and T_{EM2} variables that are calculated with the help of these coefficients are also in vector form.

Since there are two PGs and the practical PG gear ratio range is $[1.8, 3.8]$, the size of each vector becomes 441 for a gear ratio resolution of 0.1. To record the long-hauling capability of a mode for each PG gear ratio combination, a 441×4 matrix, where each column corresponds to a long-hauling performance criterion, is generated as shown in Figure 6.4. For the long-hauling performance requirement, if an element of the $|T_{Vehicle}|$ vector is greater than the minimum requirement, that mode with the corresponding PG gear ratio is capable of delivering the expected long-hauling performance, and the corresponding cell of the long-hauling performance matrix is filled out with 1. If a column in that matrix is all zeros, the mode cannot meet the long-hauling requirement for any PG gear ratio combination. Furthermore, logical OR is performed along each column to identify whether a mode can meet the requirement of that column with at least one PG gear ratio combination.

	α, β	25 mph	40 mph	50 mph	75 mph
	1 $\alpha = 1.8, \beta = 1.8$	0/1	0/1	0/1	0/1
OR ↓	...	...	...	...	...
	441 $\alpha = 3.8, \beta = 3.8$	0/1	0/1	0/1	0/1
	Capability Vector	0/1	0/1	0/1	0/1

Figure 6.4: Long-Hauling Performance Matrix and Capability Vector.

6.4 Gradeability Analysis

In the gradeability evaluation, the minimum vehicle output torque (vehicle torque is negative) that a mode can deliver within the limits of its components needs to be calculated. Similar to the long-hauling analysis, this calculation is simple for

fixed gear, parallel, series, and EV powertrain types with one degree of freedom in speed equations. The difficulty arises for powertrain types with more than one degree of freedom, where the speed of both the engine and electric machines needs to be optimized for maximum acceleration. Therefore, in the literature, this calculation is performed by either unjustified assumptions [32] or brute force [33], which is not computationally feasible when PG gear ratio is a design variable. In this section, how the minimum vehicle output torque is calculated in a computationally efficient way for varying PG gear ratios will be explained.

6.4.1 Fixed Gear, Series, Parallel, and EV Powertrain Types

The degree of freedom in speed equations is one in fixed gear, series, parallel, and some EV powertrain types. In the fixed gear, two electric machines are not considered, whereas in the EV and series types, the engine is not taken into account. In the parallel type, both electric machine- and engine torque are involved in minimizing $T_{Vehicle}$. In all cases, engine speed and/or electric machine speed are easily calculated from the vehicle speed using ω_{ICE} and ω_{EMi} coefficients a, b_i in $\omega_{Vehicle} = a \cdot \omega_{ICE}$ and $\omega_{Vehicle} = b_i \cdot \omega_{EMi}, i = 1, 2$, respectively.

In fixed gear and parallel types, the maximum engine torque that can be delivered at a given engine speed is obtained using the maximum torque curve of the engine. Similarly, in the parallel, series, and EV types, T_{EMmaxi} and T_{EMmini} are calculated from the speed vs. maximum/minimum torque curves of the electric machines. In the final step, $T_{Vehiclemin}$ is calculated by inserting T_{ICEmax}, and/or $T_{EMimax/min}$ into the torque equation for $T_{Vehicle}$. Since the modes under investigation are forward-speed capable ones, the coefficient of T_{ICE} term is always negative and, hence, T_{ICEmax} should be used. For the electric machines, the usage of T_{EMimax} and T_{EMimin} depends on the sign of the coefficient of T_{EMi} in the $T_{Vehicle}$ equation.

Some EV types have two degrees of freedom in speed equations, that is, $\omega_{Vehicle} =$

$a \cdot \omega_{EM1} + b \cdot \omega_{EM2}$. Therefore, the $T_{Vehiclemin}$ calculation requires a more sophisticated method, which will be described in the next section.

6.4.2 Power-Split Powertrain Types

The degrees of freedom in speed equations are two or three for power-split powertrain types. Therefore, the simple technique explained in Subsection 6.4.1 for the powertrain types with one degree of freedom is not applicable to assess gradeability. In this subsection, $T_{Vehiclemin}$ calculation technique based on linear programming will be explained.

6.4.2.1 Application of Linear Programming Technique to Gradeability Analysis

Linear programming can be applied to the problem of minimizing $T_{Vehicle}$ for powertrain types with more than one degree of freedom in speed equations by formulating the speed and torque relationships between components as the combination of linear segments.

The variables in the linear program are ω_{EM1}, ω_{EM2}, ω_{ICE}, $\omega_{Vehicle}$, T_{EM1}, T_{EM2}, T_{ICE}, and $T_{Vehicle}$. The upper and lower limits of the speed variables ω_{EM1}, ω_{EM2}, $\omega_{Vehicle}$, and ω_{ICE} in Eqs. (6.36a)-(6.36d) are constants. In this study, $\omega_{EM1-2min}$, $\omega_{EM1-2max}$, $\omega_{Vehiclemin}$, $\omega_{Vehiclemax}$, ω_{ICEmin}, ω_{ICEmax} are chosen as $-8000rpm$, $8000rpm$, 0, $113mph$, 0 and $5000rpm$, respectively. However, the maximum/minimum torque of an electric machine and the maximum torque of an engine depend on their respective speed values. Thus, their maximum/minimum torque curves with respect to their speed should be formulated such that the linear programming techniques can be used

to calculate minimum vehicle torque $T_{Vehiclemin}$.

$$-\omega_{EM1max} \leq \omega_{EM1} \leq \omega_{EM1max} \tag{6.36a}$$

$$-\omega_{EM2max} \leq \omega_{EM2} \leq \omega_{EM2max} \tag{6.36b}$$

$$\omega_{ICEmin} \leq \omega_{ICE} \leq \omega_{ICEmax} \tag{6.36c}$$

$$0 \leq \omega_{Vehicle} \leq \omega_{Vehiclemax} \tag{6.36d}$$

Engine:

The maximum torque of an internal combustion engine increases as the speed begins to rise from its minimum speed. At a speed point, the peak of maximum torque is reached and the maximum torque starts dropping as the speed increases further. Since the maximum torque tests are conducted at a limited number of speed points, a maximum torque curve can be formulated as a combination of linear segments. Furthermore, the slope generally decreases at each subsequent linear segment. This characteristic enables the maximum torque curve of an engine to be approximated as a concave function of engine speed. Moreover, the minimum engine torque while the engine is on can be approximated as 0.

The maximum torque curve of the engine used in this study is shown as a blue line in Figure 6.5. It is a typical maximum torque vs. engine speed plot of a gasoline engine. The original curve is approximated by three line segments ($a_i\omega_{ICE} + b_i$, $i = 1, 2, 3$) concatenated to each other and shown as the red lines in the same figure. Since the approximation of the original curve is a concave function of the engine speed, the upper and lower limits of the engine torque can be represented as:

$$0 \leq T_{ICE}(\omega_{ICE}) \leq \min_i(a_i\omega_{ICE} + b_i) \quad i = 1, 2, 3 \tag{6.37}$$

where

$a_1 = 0.929,\ b_1 = 273$

$a_2 = 0.263,\ b_2 = 386$

$a_3 = -0.295,\ b_3 = 623$

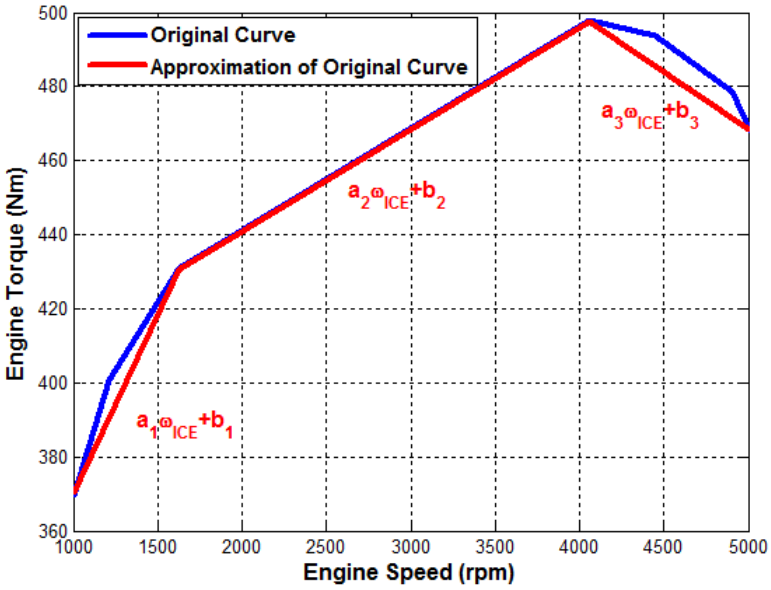

Figure 6.5: Maximum Engine Torque Curve.

Electric Machines:

In hybrid electric vehicles, either induction or permanent magnet type electric machines are used, depending on the requirements of the application (e.g., performance, cost, efficiency, durability, power level). The maximum torque of a permanent magnet or induction electric machine is constant in the low speed range. As the speed exceeds a critical point, the machine enters the constant power region and the maximum torque begins to decrease as the speed increases. In contrast to engines, electric machines can also produce negative torque. The minimum torque curve of an electric machine is generally the reflection of its maximum torque curve about the speed axis (x-axis).

The maximum and minimum torque curves of the electric machines used in this

study are shown as the blue lines in Figure 6.6. Although the maximum(minimum) torque curve is not a concave(convex) function of the machine speed, it can be approximated as a concave(convex) function by concatenating three line segments ($\tilde{a}_i\omega_{EM}+\tilde{b}_i$, $i = 1, 2, 3$ for the maximum torque curve and $\bar{a}_i\omega_{EM} + \bar{b}_i$, $i = 1, 2, 3$ for the minimum torque curve) shown as the red lines in Figure 6.6. This is a legitimate approximation since electric machines can exceed their limits temporarily as long as overheating is prevented. With this approximation, the electric machine torque limits can be represented as:

$$\max_i(\bar{a}_i\omega_{EM1} + \bar{b}_i) \leq T_{EM1}(\omega_{EM1}) \leq \min_i(\tilde{a}_i\omega_{EM1} + \tilde{b}_i) \quad i = 1, 2, 3 \tag{6.38a}$$

$$\max_i(\bar{a}_i\omega_{EM2} + \bar{b}_i) \leq T_{EM2}(\omega_{EM2}) \leq \min_i(\tilde{a}_i\omega_{EM2} + \tilde{b}_i) \quad i = 1, 2, 3 \tag{6.38b}$$

The coefficients $\bar{a}_i$, $\bar{b}_i$, $\tilde{a}_i$ and $\tilde{b}_i$ $i = 1, 2, 3$ in Eqs. (6.38a)-(6.38b) are calculated for the maximum/minimum torque curves in Figure 6.6 as:

$\bar{a}_1 = -0.228,\ \bar{b}_1 = -263$

$\bar{a}_2 = 0,\ \bar{b}_2 = -191$

$\bar{a}_3 = 0.228,\ \bar{b}_3 = -263$

$\tilde{a}_1 = 0.228,\ \tilde{b}_1 = 263$

$\tilde{a}_2 = 0,\ \tilde{b}_2 = 191$

$\tilde{a}_3 = -0.228,\ \tilde{b}_3 = 263$

In addition to the speed limits of electric machines, engine, and vehicle in Eqs. (6.36a)-(6.36d), their speed dependencies are also integrated into the linear program. The speed equations of a power-split powertrain type with two degrees of freedom are shown in Eqs. (6.39a)-(6.39b), while the speed equation of a powertrain type with

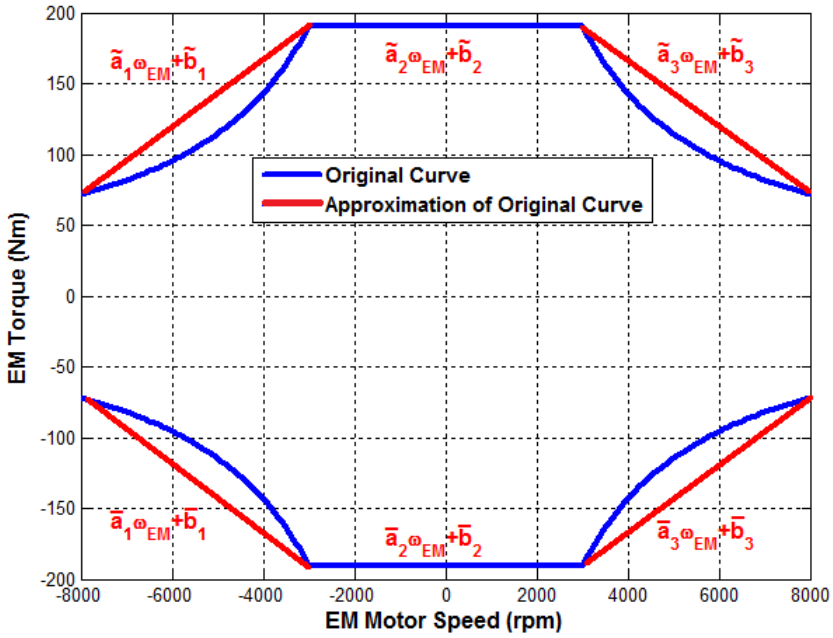

Figure 6.6: Maximum and Minimum Electric Machine Torque Curves.

three degrees of freedom can be found in Eq. 6.40.

$$\omega_{EM1} - f_1(\alpha,\beta)\omega_{ICE} - g_1(\alpha,\beta)\omega_{Vehicle} = 0 \tag{6.39a}$$

$$\omega_{EM2} - f_2(\alpha,\beta)\omega_{ICE} - g_2(\alpha,\beta)\omega_{Vehicle} = 0 \tag{6.39b}$$

$$\omega_{Vehicle} - f_1(\alpha,\beta)\omega_{ICE} - g_1(\alpha,\beta)\omega_{EM1} - h_1(\alpha,\beta)\omega_{EM2} = 0 \tag{6.40}$$

Eqs. (6.41a)-(6.41b) and Eqs. (6.42a)-(6.42c) are used in the linear program as constraints in torque variables for two- and three degrees of freedom powertrain types, respectively.

$$T_{ICE} + f_1(\alpha,\beta)T_{EM1} + f_2(\alpha,\beta)T_{EM2} = 0 \tag{6.41a}$$

$$T_{Vehicle} + g_1(\alpha,\beta)T_{EM1} + g_2(\alpha,\beta)T_{EM2} = 0 \tag{6.41b}$$

$$T_{ICE} + f_1(\alpha, \beta) T_{Vehicle} = 0 \tag{6.42a}$$

$$T_{EM1} + g_1(\alpha, \beta) T_{Vehicle} = 0 \tag{6.42b}$$

$$T_{EM2} + h_1(\alpha, \beta) T_{Vehicle} = 0 \tag{6.42c}$$

In the linear program, $\omega_{Vehicle}$ is set to the vehicle speed at which the vehicle begins its acceleration. In formulating the maximum acceleration calculation, $T_{Vehicle}$ is the reaction torque of the PG node to which the output shaft is connected, as shown in Figure 6.7. Arrows facing to the right represent positive torque. Maximum acceleration is achieved if $T_{Vehicle}$ is minimized. Thus, the objective of the linear program is to minimize $T_{Vehicle}$ within the speed and torque constraints of the components in the system. In the formulation, it is assumed that the component speeds have settled at the speed solutions of the linear program at the start of acceleration and the torque solutions of the linear program are applied to the actuators at these speed points.

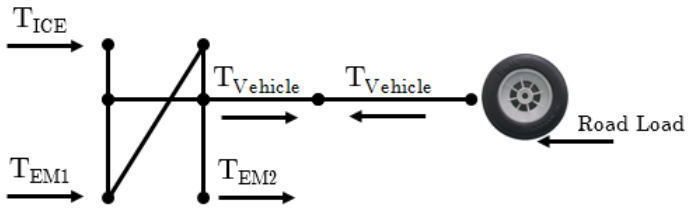

Figure 6.7: Maximum Acceleration Formulation.

LP solver in Matlab can find the solution of the linear program configured in this section. Hundreds of power-split modes in the design space and 441 PG gear ratio combinations for each mode require calling that LP solver hundreds of thousands times. Hence, this method is not practical given the slow execution of the solver. This drawback becomes much more severe in the $0 - 60$mph time calculation, where the LP solver needs to be called tens of millions of times. To overcome this problem, computationally efficient LP solvers specific to each powertrain type with more than one degree of freedom in speed equations are developed such that they are suitable

for vector operations to accommodate PG gear variations.

The following proposition helps in developing a computationally efficient LP solver.

Proposition VI.2. *In the minimization of $T_{Vehicle}$, for the power-split powertrain types with two degrees of freedom and positive mechanical points, the limiting factor is either T_{ICEmax} or $-sgn(f_i)T_{EMimax} = sgn(g_i)T_{EMimax}, \quad i = 1, 2$, where T_{ICEmax} and T_{EMimax} are maximum torque of the engine and electric machine i at the speed solutions of minimum $T_{Vehicle}$ and*

$\omega_{EM1} = f_1\omega_{ICE} + g_1\omega_{Vehicle}$

$\omega_{EM2} = f_2\omega_{ICE} + g_2\omega_{Vehicle}$

Proof. As shown in Section 6.2, the mechanical points should be positive for the power-split powertrain types.

$$-\frac{f_1}{g_1} > 0 \tag{6.43a}$$

$$-\frac{f_2}{g_2} > 0 \tag{6.43b}$$

The optimization goal is

$$minimize(-g_1T_{EM1} - g_2T_{EM2}) \tag{6.44}$$

$$s.t.$$

$$T_{ICEmin} = 0 \leq -f_1T_{EM1} - f_2T_{EM2} \leq T_{ICEmax} \tag{6.45}$$

Due to the sign constraints of the positive mechanical points, four possibilities exist for the signs of f_1, f_2, g_1 and g_2 as shown in Table 6.3. For each possibility, T_{EM1} and T_{EM2} should be maximized or minimized in order to minimize $-g_1T_{EM1} - g_2T_{EM2}$. For example, in the first row of Table 6.3, f_1 and f_2 are positive while g_1 and g_2 are negative. In order to minimize $-g_1T_{EM1} - g_2T_{EM2}$, both T_{EM1} and T_{EM2} should be minimized. Since T_{EM1} and T_{EM2} can generate negative torque values, their minimum

is negative. However, negative T_{EM1} and T_{EM1} have positive contribution to the $-f_1T_{EM1}$ and $-f_2T_{EM2}$. As observed in the table, the signs of T_{EMi}'s should be $-sgn(f_i) = sgn(g_i), \quad i = 1, 2$ in order to minimize $T_{Vehicle} = -g_1T_{EM1} - g_2T_{EM2}$. $T_{ICE} = -f_1T_{EM1} - f_2T_{EM2}$, however, is always positive in this case regardless of the signs of f_1, g_1, f_2, and g_2. As a result, the limiting factor in the minimization of $T_{Vehicle}$ is either $-sgn(f_i)T_{EMimax} = sgn(g_i)T_{EMimax}$ or T_{ICEmax}, whichever comes first.

Table 6.3: Sign Combinations and Assignments for Maximum Acceleration

f_1	g_1	f_2	g_2	T_{EM1}	T_{EM2}	$-f_1T_{EM1}$	$-f_2T_{EM2}$
+	-	+	-	-	-	+	+
+	-	-	+	-	+	+	+
-	+	+	-	+	-	+	+
-	+	-	+	+	+	+	+

□

In the proposed solver, the optimum solution is found by leveraging the fact that the LP solution is always associated with a corner point (where two lines intersect) of the solution space [84]. Moreover, the speed and torque equations and the solution algorithms are constructed such that all mathematical operations can be performed in vector form without the use of any "for" loop. In the following subsections, the solver algorithms will be described for each powertrain type with more than one degree of freedom in speed equations.

6.4.2.2 LP Solver for Input-Split Powertrain Type

The speed and torque equations of an input-split powertrain type have been derived in Section 4.2 as:

$$\omega_{Vehicle} = f_1 \cdot \omega_{EM2} \tag{6.46a}$$

$$\omega_{EM1} = f_2 \cdot \omega_{EM2} + g_2 \cdot \omega_{ICE} \tag{6.46b}$$

$$T_{Vehicle} = -\frac{1}{f_1} \cdot T_{EM2} + \frac{f_2}{f_1 \cdot g_2} \cdot T_{ICE} \tag{6.46c}$$

$$T_{EM1} = -\frac{1}{g_2} \cdot T_{ICE} \tag{6.46d}$$

Since vehicle torque is minimized for a given vehicle speed, ω_{EM2} is constant and $\omega_{EM1} = \frac{f_2}{f_1} \cdot \omega_{Vehicle} + g_2 \cdot \omega_{ICE}$.

The first set of corner points as possible solution candidates are the speed points, where their maximum/minimum torque curves change their slope. Assume these corner points for EM1, EM2, and ICE are $\omega_{EM1,i}, i = 1, \ldots, m$; $\omega_{EM2,j}, j = 1, \ldots, m$; and $\omega_{ICE,k}, k = 1, \ldots, n$, respectively. Using Eq. (6.46b), the first set of EM1 corner points can be represented in terms of ω_{ICE} as $\omega_{ICE,EM1,i}, i = 1, \ldots, m$ since ω_{EM2} is constant. Similarly, EM1 speed points $\omega_{EM1,ICE,k}, k = 1, \ldots, n$ that correspond to the first set of ICE corner points $\omega_{ICE,k}$ are calculated using Eq. (6.46b). The corner points that are out of bounds, that is, $\omega_{ICE,EM1,i} < \omega_{ICEmin}, \omega_{ICE,EM1,i} > \omega_{ICEmax}, \omega_{EM1,ICE,k} < \omega_{EM1min}, \omega_{EM1,ICE,k} > \omega_{EM1max}$ are eliminated from the solution set. Then, the set of corner points is established in the ω_{ICE} domain as

$$\begin{aligned}\Omega_{ICE,corner} =& \{\{\omega_{ICE,k}, k = 1, \ldots, n\} \cup \{\omega_{ICE,EM1,i}, i = 1, \ldots, m\} | \\ & \omega_{ICEmin} \leq \omega_{ICE,k} \leq \omega_{ICEmax} \wedge \omega_{ICEmin} \leq \omega_{ICE,EM1,i} \leq \omega_{ICEmax}\}\end{aligned} \tag{6.47}$$

The elements of $\Omega_{ICE,corner}$, $\omega_{ICE,k}$ and $\omega_{ICE,EM1,i}$, are shown as blue and red circles

in Figure 6.8, respectively. Then, T_{EM1max} and T_{ICEmax}, which correspond to the

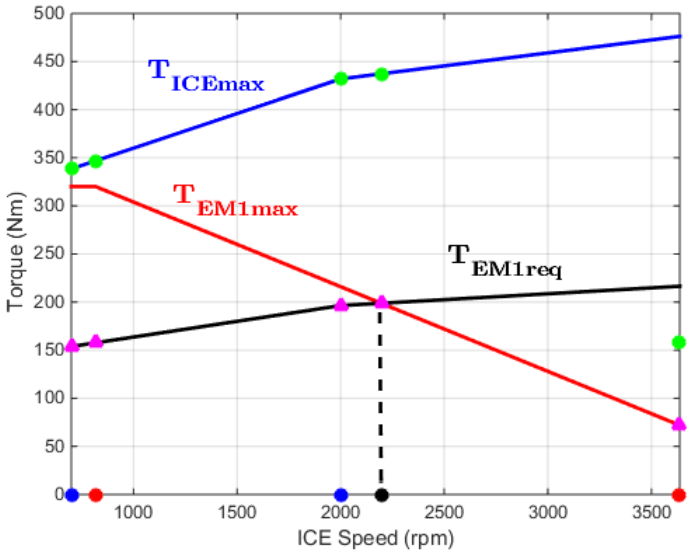

Figure 6.8: ω_{ICE} and ω_{EM} Corner Points.

elements of $\Omega_{ICE,corner}$, are calculated using Eqs. (6.37) and (6.38a). T_{ICEmax} imposes the value of T_{EM1} in Eq. (6.46d), which is defined as T_{EM1req} shown as a black line in Figure 6.8.

Another corner point exists when the T_{EM1req} curve intersects with the T_{EM1max} curve, represented as a black dot in Figure 6.8. This corner point is obtained by solving the following linear equation for each linear segment between the consecutive elements of $\Omega_{ICE,corner}$:

$$T_{EM1max} \cdot sgn(-\frac{1}{g_2}) = -\frac{1}{g_2} \cdot T_{ICEmax} \tag{6.48a}$$

$$\min_i(\tilde{a}_i\omega_{ICE,intersect} + \tilde{b}_i) \cdot sgn(-\frac{1}{g_2}) = -\frac{1}{g_2} \cdot \min_i(a_i\omega_{ICE,intersect} + b_i), \quad i = 1, \ldots, size(\Omega_{ICE,corner}) \tag{6.48b}$$

In the final step, $T_{Vehicle}$ is minimized at $\Omega_{ICE,corner} \cup \omega_{ICE,intersect}$ using Eq. (6.46c). In the minimization process, since ω_{EM2} is constant, T_{EM2} is set to $T_{EM2max} \cdot sgn(-\frac{1}{f_1})$.

Furthermore, T_{ICE} takes either T_{ICEmax} or $T_{EM1max} \cdot sgn(-\frac{1}{g_2}) \cdot \frac{-g_2}{f_1}$. T_{ICE} and T_{EM1} points that minimize $T_{Vehicle}$ at every corner point are shown in Figure 6.8 as green circles and magenta triangles, respectively. The corner point that gives the lowest $T_{Vehicle}$ is the optimum speed solution, and the corresponding $T_{Vehicle}$ becomes the torque solution $T_{Vehiclemin}$.

Since the proposed solver consists of simple algebraic operations, and these operations are implemented with vector inputs to accommodate PG gear ratio variations, it executes 150 times faster than Matlab's native LP solver, and analyses that require a high number of $T_{Vehicle}$ minimizations become feasible.

6.4.2.3 LP Solver for Output-Split Powertrain Type

The speed and torque equations of an output-split powertrain type have been derived in Section 4.2 as:

$$\omega_{Vehicle} = f_1 \cdot \omega_{EM1} + g_1 \cdot \omega_{ICE} \tag{6.49a}$$

$$\omega_{EM2} = g_2 \cdot \omega_{ICE} \tag{6.49b}$$

$$T_{Vehicle} = -\frac{g_2}{g_1} \cdot T_{EM2} - \frac{1}{g_1} \cdot T_{ICE} \tag{6.49c}$$

$$T_{EM1} = -f_1 \cdot T_{Vehicle} \tag{6.49d}$$

First of all, similar to the technique explained in Subsection 6.4.2.2, the speed corner points, where all maximum torque curves change their slope, are determined in the ω_{ICE} domain using Eqs. (6.49a) and (6.49b). As seen in Eqs. (6.49b)-(6.49d), ω_{EM2} is directly proportional to ω_{ICE}, and both $T_{Vehicle}$ and T_{EM1} are determined by T_{EM2} and T_{ICE}. Hence, a dummy component $\tilde{T}_{ICE}$, which is a combination of T_{EM2} and

T_{ICE}, can be generated using the following equations:

$$\tilde{T}_{ICE} = g_2 \cdot T_{EM2} + T_{ICE} \tag{6.50a}$$

$$\tilde{T}_{ICEmax} = sgn(g_2) \cdot g_2 \cdot T_{EM2max} + T_{ICEmax} \tag{6.50b}$$

$$\tilde{T}_{ICEmax} = sgn(g_2) \cdot g_2 \cdot \min_i(\tilde{a}_i \cdot g_2 \cdot \omega_{ICE} + \tilde{b}_i) \cdot + \min_i(a_i \omega_{ICE} + b_i) \tag{6.50c}$$

After this formulation, the problem becomes the minimization of $T_{Vehicle}$ such that

$$T_{Vehicle} = -\frac{1}{g_1} \cdot \tilde{T}_{ICE} \tag{6.51a}$$

$$T_{EM1} = \frac{f_1}{g_1} \cdot \tilde{T}_{ICE} \tag{6.51b}$$

T_{EM1max} and $\tilde{T}_{ICEmax}$ are evaluated at each speed corner point using torque equations (6.51a)-(6.51b). Two possibilities exist as follows:

- The limiting factor is T_{EM1max}: $T_{Vehiclemin} = sgn(-f_1) \cdot -\frac{1}{f_1} \cdot T_{EM1max}$ and $\tilde{T}_{ICE} = \frac{g_1}{f_1} \cdot T_{EM1max}$.
- The limiting factor is $\tilde{T}_{ICEmax}$: $T_{Vehiclemin} = -\frac{1}{g_1} \cdot \tilde{T}_{ICEmax}$ and $T_{EM1} = \frac{f_1}{g_1} \cdot \tilde{T}_{ICEmax}$.

In addition to these points and their corresponding $T_{Vehicle}$'s, another corner point named $\omega_{ICE,intersect}$ exists, which makes $T_{EM1max} = \frac{f_1}{g_1} \cdot \tilde{T}_{ICEmax}$. This corner point is calculated using the same technique explained in Subsection 6.4.2.2. Finally, the corner point that gives the lowest $T_{Vehicle}$ is the optimum speed solution, and the corresponding $T_{Vehicle}$ becomes $T_{Vehiclemin}$.

6.4.2.4 LP Solver for Compound-Split Powertrain Type

The speed and torque equations of a compound-split powertrain type have been derived in Section 4.2 as:

$$\omega_{Vehicle} = f_1 \cdot \omega_{EM2} + g_1 \cdot \omega_{ICE} \tag{6.52a}$$

$$\omega_{EM1} = f_2 \cdot \omega_{EM2} + g_2 \cdot \omega_{ICE} \tag{6.52b}$$

$$T_{Vehicle} = -\frac{g_2}{g_1} \cdot T_{EM1} - \frac{1}{g_1} \cdot T_{ICE} \tag{6.52c}$$

$$T_{EM2} = \frac{f_1 \cdot g_2 - g_1 \cdot f_2}{g_1} \cdot T_{EM1} + \frac{f_1}{g_1} \cdot T_{ICE} \tag{6.52d}$$

The first set of corner points as possible solution candidates are the speed points, where their maximum/minimum torque curves change their slope. Assume these corner points for EM1, EM2, and ICE are $\omega_{EM1,i}, i = 1, \ldots, m$; $\omega_{EM2,j}, j = 1, \ldots, m$; and $\omega_{ICE,k}, k = 1, \ldots, n$, respectively. Using Eqs. (6.52a)-(6.52b), all corner points are represented in terms of ω_{ICE} as:

$$\omega_{ICE,EM1,i} = \frac{f_1 \cdot \omega_{EM1,i} - f_2 \cdot \omega_{Vehicle}}{g_2 \cdot f_1 - g_1 \cdot f_2} \quad i = 1, \ldots, m \tag{6.53a}$$

$$\omega_{ICE,EM2,j} = \frac{\omega_{Vehicle} - f_1 \cdot \omega_{EM2,j}}{g_1} \quad j = 1, \ldots, m \tag{6.53b}$$

The corner points that are out of bounds are eliminated from the solution set. Moreover, if EM1 and EM2 speed points that are calculated from $\omega_{ICE,k}$ and $\omega_{Vehicle}$ are out of bounds, the corresponding $\omega_{ICE,k}$ is also eliminated. Then the set of corner points is established in the ω_{ICE} domain as

$$\begin{aligned}\Omega_{ICE,corner} =& \{\{\omega_{ICE,k}, k = 1, \ldots, n\} \cup \{\omega_{ICE,EM1,i}, i = 1, \ldots, m\} \cup \\ & \{\omega_{ICE,EM2,j}, j = 1, \ldots, m\} | \omega_{ICEmin} \leq \omega_{ICE,k} \leq \omega_{ICEmax} \wedge \\ & \omega_{ICEmin} \leq \omega_{ICE,EM1,i} \leq \omega_{ICEmax} \wedge \omega_{ICEmin} \leq \omega_{ICE,EM2,j} \leq \omega_{ICEmax}\}\end{aligned} \tag{6.54}$$

For the optimum solution, two possibilities exist:

1. One of the elements in $\Omega_{ICE,corner}$, where two of the T_{EM1}, T_{EM2}, and T_{ICE} are at their limit points.

2. $\omega_{ICE,intersect}$, where $T_{EM2max/min} = \frac{f_1 \cdot g_2 - g_1 \cdot f_2}{g_1} \cdot T_{EM1max/min} + \frac{f_1}{g_1} \cdot T_{ICEmax}$

For the first case, T_{EM1max}, T_{EM2max}, and T_{ICEmax} at the elements of $\Omega_{ICE,corner}$ are calculated using their maximum torque linear equations specified in Eqs. (6.37) and (6.38a). As shown in the Proposition VI.2, T_{ICE} becomes either T_{ICEmax} or the value that is restricted by $T_{EM1max/min}$ or $T_{EM2max/min}$. Five possibilities exist for the solution candidates at each corner point:

1. T_{ICEmax}, T_{EM1max} and T_{EM2} is determined by Eq. (6.52d).

2. T_{ICEmax}, T_{EM1min} and T_{EM2} is determined by Eq. (6.52d).

3. T_{ICEmax}, T_{EM2max} and T_{EM1} is determined by Eq. (6.52d).

4. T_{ICEmax}, T_{EM2min} and T_{EM1} is determined by Eq. (6.52d).

5. $sgn(\frac{g_1 \cdot f_2 - f_1 \cdot g_2}{f_1}) \cdot T_{EM1max}$, $sgn(\frac{g_1}{f_1}) \cdot T_{EM2max}$ and T_{ICE} is determined by Eq. (6.52d).

For each of these five possibilities, $T_{Vehicle}$ is calculated and their minimum is taken as the solution candidate as $T_{Vehiclemin,1}$. For the second case, the speed points where $T_{EM1max/min}$, $T_{EM2max/min}$ and T_{ICEmax} intersect are calculated as another corner point. The following four linear equations are solved to identify the intersection points:

1. $\min\limits_k(\tilde{a}_k\omega_{ICE} + \tilde{b}_k) = \frac{f_1 \cdot g_2 - g_1 \cdot f_2}{g_1} \cdot \min\limits_j(\tilde{a}_j\omega_{ICE} + \tilde{b}_j) + \frac{f_1}{g_1} \cdot \min\limits_i(a_i\omega_{ICE} + b_i) \ \ \forall i, j, k$

2. $-1 \cdot \min\limits_k(\tilde{a}_k\omega_{ICE} + \tilde{b}_k) = \frac{f_1 \cdot g_2 - g_1 \cdot f_2}{g_1} \cdot \min\limits_j(\tilde{a}_j\omega_{ICE} + \tilde{b}_j) + \frac{f_1}{g_1} \cdot \min\limits_i(a_i\omega_{ICE} + b_i) \ \ \forall i, j, k$

3. $\min\limits_k(\tilde{a}_k\omega_{ICE} + \tilde{b}_k) = -1 \cdot \frac{f_1 \cdot g_2 - g_1 \cdot f_2}{g_1} \cdot \min\limits_j(\tilde{a}_j\omega_{ICE} + \tilde{b}_j) + \frac{f_1}{g_1} \cdot \min\limits_i(a_i\omega_{ICE} + b_i) \ \ \forall i, j, k$

4. $-1 \cdot \min_k(\tilde{a}_k \omega_{ICE} + \tilde{b}_k) = -1 \cdot \frac{f_1 \cdot g_2 - g_1 \cdot f_2}{g_1} \cdot \min_j(\tilde{a}_j \omega_{ICE} + \tilde{b}_j) + \frac{f_1}{g_1} \cdot \min_i(a_i \omega_{ICE} + b_i) \quad \forall i, j, k$

If there are any solutions for the intersection points, the minimum of their corresponding $T_{Vehicle}$'s is chosen as the $T_{Vehiclemin,intersect}$. The minimum of $T_{Vehiclemin,1}$ and $T_{Vehiclemin,intersect}$ becomes the global minimum vehicle torque $T_{Vehiclemin}$.

6.4.2.5 LP Solver for Special Power-Split Powertrain Type I

The speed and torque equations of a special power-split powertrain type I have been derived in Section 4.2 as:

$$\omega_{Vehicle} = f_1 \cdot \omega_{EM1} + g_1 \cdot \omega_{ICE} \tag{6.55a}$$

$$\omega_{EM2} = 0 \tag{6.55b}$$

$$T_{Vehicle} = -\frac{1}{g_1} \cdot T_{ICE} \tag{6.55c}$$

$$T_{EM1} = \frac{f_1}{g_1} \cdot T_{ICE} \tag{6.55d}$$

Similar to the other power-split powertrain types, the first set of corner points as possible solution candidates are the speed points, where their maximum/minimum torque curves change their slope. Assume these corner points for EM1 and ICE are $\omega_{EM1,i}, i = 1, \ldots, m$ and $\omega_{ICE,k}, k = 1, \ldots, n$, respectively. Using Eq. (6.55a), all corner points are represented in terms of ω_{ICE} as:

$$\omega_{ICE,EM1,i} = \frac{1}{g_1} \cdot (\omega_{Vehicle} - f_1 \cdot \omega_{EM1,i}) \quad i = 1, \ldots, m \tag{6.56}$$

The corner points that are out of bounds are eliminated from the solution set. Moreover, if EM1 speed points that are calculated from $\omega_{ICE,k}$ and $\omega_{Vehicle}$ are out of bounds, the corresponding $\omega_{ICE,k}$ is also eliminated. Then the set of corner points is

established in the ω_{ICE} domain as

$$\Omega_{ICE,corner} = \{\{\omega_{ICE,k}, k = 1, \ldots, n\} \cup \{\omega_{ICE,EM1,i}, i = 1, \ldots, m\} | \\ \omega_{ICEmin} \leq \omega_{ICE,k} \leq \omega_{ICEmax} \wedge \omega_{ICEmin} \leq \omega_{ICE,EM1,i} \leq \omega_{ICEmax}\} \tag{6.57}$$

For the optimum solution, two possibilities exist:

1. One of the elements in $\Omega_{ICE,corner}$, where either T_{ICE}=T_{ICEmax} or T_{EM1}=$sgn(\, f_1) \cdot T_{EM1max}$.

2. The $\omega_{ICE,intersect}$, where $sgn(\, f_1) \cdot T_{EM1max} = \frac{f_1}{g_1} \cdot T_{ICEmax}$.

For the first case, the required engine torque T_{ICEreq} from $sgn(\, f_1) \cdot T_{EM1max}$ and the required EM1 torque $sgn(\, f_1) \cdot T_{EM1max}$, and T_{EM1req} from T_{ICEmax} are calculated using Eq. (6.55d). The minimum of the two $T_{Vehicle}$ calculations is recorded as the optimum solution candidate, $T_{Vehiclemin,1}$. For the second case, an exploration is made to determine whether $\omega_{ICE,intersect}$ exists for the condition of $sgn(\, f_1) \cdot T_{EM1max} = \frac{f_1}{g_1} \cdot T_{ICEmax}$ by solving the linear equations of

$$sgn(\, f_1) \cdot \min_j(\tilde{a}_j \omega_{ICE} + \tilde{b}_j) = \frac{f_1}{g_1} \cdot \min_i(a_i \omega_{ICE} + b_i) \;\; \forall i, j \tag{6.58}$$

If there are any solutions for the intersection points, the minimum of their corresponding $T_{Vehicle}$'s is chosen as the $T_{Vehiclemin,intersect}$. The minimum of $T_{Vehiclemin,1}$ and $T_{Vehiclemin,intersect}$ becomes the global minimum vehicle torque $T_{Vehiclemin}$.

6.4.2.6 LP Solver for Special Power-Split Powertrain Type II

The speed and torque equations of a special power-split powertrain type II have been derived in Section 4.2 as:

$$\omega_{Vehicle} = f_1 \cdot \omega_{EM2} + g_1 \cdot \omega_{ICE} \tag{6.59a}$$

$$\omega_{EM1} = f_2 \cdot \omega_{EM2} \tag{6.59b}$$

$$T_{Vehicle} = -\frac{1}{g_1} \cdot T_{ICE} \tag{6.59c}$$

$$T_{EM2} = -f_2 \cdot T_{EM1} + \frac{f_1}{g_1} \cdot T_{ICE} \tag{6.59d}$$

The solution for this powertrain type is accomplished the same way as is the special power-split type I by defining a dummy component $\tilde{T}_{EM2}$ with the following torque equation:

$$\tilde{T}_{EM1} = T_{EM2} + f_2 \cdot T_{EM1} \tag{6.60}$$

After this conversion, the same steps explained in Subsection 6.4.2.5 are executed, where T_{EM1} is replaced by $\tilde{T}_{EM1}$.

6.4.2.7 LP Solver for Special Power-Split Powertrain Type III

The speed and torque equations of a special power-split powertrain type III have been derived in Section 4.2 as:

$$\omega_{Vehicle} = f_1 \cdot \omega_{EM1} + g_1 \cdot \omega_{EM2} + h_1 \cdot \omega_{ICE} \tag{6.61a}$$

$$T_{Vehicle} = -\frac{1}{h_1} \cdot T_{ICE} \tag{6.61b}$$

$$T_{EM1} = \frac{f_1}{h_1} \cdot T_{ICE} \tag{6.61c}$$

$$T_{EM2} = \frac{g_1}{h_1} \cdot T_{ICE} \tag{6.61d}$$

The first set of corner points as possible solution candidates are the speed points, where their maximum/minimum torque curves change their slope. Assume these corner points for EM1, EM2, and ICE are $\omega_{EM1,i}, i = 1, \ldots, m$; $\omega_{EM2,j}, j = 1, \ldots, m$; and $\omega_{ICE,k}, k = 1, \ldots, n$, respectively. All these corner points are represented in terms of ω_{EM1}, ω_{EM2}, and ω_{ICE} as:

$$\omega_{EM1,ICE,EM2,j,k} = \frac{1}{f_1} \cdot (\omega_{Vehicle} - g_1 \cdot \omega_{EM2,j} - h_1 \cdot \omega_{ICE,k}) \quad \forall j, k \tag{6.62a}$$

$$\omega_{EM2,ICE,EM1,i,k} = \frac{1}{g_1} \cdot (\omega_{Vehicle} - f_1 \cdot \omega_{EM1,i} - h_1 \cdot \omega_{ICE,k}) \quad \forall i, k \tag{6.62b}$$

$$\omega_{ICE,EM1,EM2,i,j} = \frac{1}{h_1} \cdot (\omega_{Vehicle} - f_1 \cdot \omega_{EM1,i} - g_1 \cdot \omega_{EM2,j}) \quad \forall i, j \tag{6.62c}$$

The corner points that are out of bounds are eliminated from the solution set and T_{EM1max}, T_{EM2max}, and T_{ICEmax} are evaluated at the remaining corner points. T_{ICEmax} is reduced if T_{EM1} or T_{EM2} is the limiting variable using the torque Eqs. (6.61c) and (6.61d). $T_{Vehicle}$ calculated using Eq. (6.61b) is recorded as $T_{Vehiclemin,1}$. Since the degrees of freedom in speed equations are three, there are four more cases, each of which identifies a new set of corner points:

1. $\omega_{ICE,intersect,1}$ and $\omega_{EM1,intersect,1}$, where $sgn(\frac{f_1}{h_1}) \cdot T_{EM1max} = \frac{f_1}{h_1} \cdot T_{ICEmax}$.

2. $\omega_{ICE,intersect,2}$ and $\omega_{EM2,intersect,2}$, where $sgn(\frac{g_1}{h_1}) \cdot T_{EM2max} = \frac{g_1}{h_1} \cdot T_{ICEmax}$.

3. $\omega_{EM1,intersect,3}$ and $\omega_{EM2,intersect,3}$, where $sgn(\frac{f_1}{h_1}) \cdot g_1 \cdot T_{EM1max} = sgn(\frac{g_1}{h_1}) \cdot f_1 \cdot T_{EM2max}$.

4. $\omega_{ICE,intersect,4}$, $\omega_{EM1,intersect,4}$, and $\omega_{EM2,intersect,4}$, where $sgn(\frac{f_1}{h_1}) \cdot T_{EM1max} = \frac{f_1}{h_1} \cdot T_{ICEmax}$ and $sgn(\frac{g_1}{h_1}) \cdot T_{EM2max} = \frac{g_1}{h_1} \cdot T_{ICEmax}$.

If there are any solutions for the intersection points, the minimum of their corresponding $T_{Vehicle}$'s is chosen as the $T_{Vehiclemin,intersect}$. The minimum of $T_{Vehiclemin,1}$ and $T_{Vehiclemin,intersect}$ becomes the global minimum vehicle torque $T_{Vehiclemin}$.

6.5 Gradeability Performance Analysis for Varying PG Gear Ratios

The gradeability analysis methods explained for all powertrain types in Subsections 6.4.2.2-6.4.2.7 should be implemented for all PG gear ratio combinations. The operations in the introduced LP solver algorithms are performed in vector form without the use of any "for" loop, where each element in the vectors corresponds to a PG gear ratio combination.

Since there are two PGs and the practical PG gear ratio range is $[1.8, 3.8]$, the size of each vector becomes 441 for a gear ratio resolution of 0.1. To record the gradeability capability of a mode for each PG gear ratio combination, a 441×3 matrix, where each column corresponds to one of the three gradeability criteria, is generated as shown in Figure 6.9. For a gradeability requirement, if an element of the $|T_{Vehicle}|$ vector is greater than the minimum requirement, that mode with the corresponding PG gear ratio is capable of delivering the expected gradeability performance, and the corresponding cell of the gradeability performance matrix is filled out with 1. If a column in that matrix is all zeros, the mode cannot meet the gradeability requirement for any PG gear ratio combination. Furthermore, logical OR is performed along each column to identify whether a mode can meet the requirement of that column with at least one PG gear ratio combination.

	α, β	6 mph	12 mph	113 mph
1	$\alpha = 1.8, \beta = 1.8$	0/1	0/1	0/1
OR ↓	...	...	...	...
441	$\alpha = 3.8, \beta = 3.8$	0/1	0/1	0/1
	Capability Vector	0/1	0/1	0/1

Figure 6.9: Gradeability Performance Matrix and Capability Vector.

6.6 x-y mph Time Analysis

Like the gradeability analysis, x-y mph time calculation is straight forward for the powertrain types with one degree of freedom in speed equations. Hence, in this section, the algorithm developed to assess the powertrain types with more than one degree of freedom will be explained.

Gradeability analysis for the powertrain types with more than one degree of freedom is done under the assumption that the engine and electric machines are at steady state before the vehicle begins to accelerate, because this assumption is valid for the evaluation of gradeability. In this section, the time to reach from x mph to y mph speed will be evaluated by leveraging the results derived in the previous section, and by introducing the one time-step predictive control concept.

6.6.1 One Time-Step Predictive Control

The one time-step predictive control concept assumes that the vehicle starts its acceleration at x mph, while the speeds of the engine and electric machines are at steady state. The inertias of the ring-, carrier-, and sun gears of the PGs and two electric machines can be ignored, as they are much smaller than the vehicle and engine inertias. Furthermore, the electric machine torque commands can be set much faster than the commands to other components due to modern power electronics control techniques.

The desired steady-state engine speed, torque commands to both the engine and electric machines for maximum acceleration (i.e., minimum $T_{Vehicle}$) at x mph are calculated using the linear programming formulation described in Subsection 6.4.2.1. In this calculation, the feasible engine torque region is set between $T_{ICEmax} - \Delta T_{ICEmax}$ and $T_{ICEmin} + \Delta T_{ICEmax} = \Delta T_{ICEmax}$. In these equations, ΔT_{ICEmax} is the reserve torque needed to bring the engine speed to the desired level at the next time step. ΔT_{ICEmax} can be calculated by $J_{ICE}\Delta\omega_{ICEmax}$, where J_{ICE} is the engine inertia and

$\Delta\omega_{ICEmax}$ is the maximum difference between optimum engine speed setpoints at two consecutive time steps. Assuming $\Delta\omega_{ICEmax}$ does not exceed $500rpm$ and using $J_{ICE} = 0.16kgm^2$ for the engine used in this dissertation, ΔT_{ICEmax} can be set to $8Nm$, which is just 1.7% of the peak engine torque.

The algorithm works in the following order:

- Start at $k\Delta t = 0$ and $\omega_{Vehicle\_k} = 0$, where Δt is the duration of each time step.
- Solve the linear program that minimizes $T_{Vehicle\_k}$ by using T_{ICEmax} curve reduced by ΔT_{ICEmax}. The solution of the linear program becomes ω_{ICE_k}, T_{EM1_k}, T_{EM2_k}. T_{EM1_k} and T_{EM2_k} determine the reaction torques at the nodes to which the engine and vehicle output shaft are connected (T_{ICE_k}, $T_{Vehicle\_k}$).
- Using the road load model and $T_{Vehicle\_k}$, predict the vehicle speed $\omega_{Vehicle\_k+1}$ at the start of the next time step $(k+1)$.
- Solve the linear program for this predicted vehicle speed $\omega_{Vehicle\_k+1}$ to determine minimum $T_{Vehicle\_k+1}$. The solution gives the desired ω_{ICE_k+1} at the end of the current time step k.
- Calculate the engine torque command for time $k\Delta t$, T_{ICEcmd_k}, that would bring ω_{ICE_k} to ω_{ICE_k+1} during time step k using $T_{ICEcmd\_k} - T_{ICE\_k}$ equal to $J_{ICE}(\omega_{ICE\_k+1} - \omega_{ICE\_k})$. Reinitialize the algorithm with a larger ΔT_{ICEmax} until T_{ICEcmd_k} is inside the T_{ICEmax} curve.
- If T_{ICEcmd_k} is inside the T_{ICEmax} curve, apply this torque command to the engine and increment k by 1 and repeat the previous steps between the time steps k and $k+1$.
- Once the vehicle speed reaches y mph, stop the process and calculate the total acceleration time. If y mph is exceeded in the last time step, Δt should be

shortened in the last step to Δt_f so as to make $\omega_{Vehicle\_k} = y$. The total acceleration time t_{x_y}, therefore, becomes $(k-1)\Delta t + \Delta t_f$.

Figure 6.11 shows the described algorithm in flow chart format, where J_V is vehicle inertia.

ΔT_{ICEmax} in the algorithm can be calculated by running the same algorithm with $\Delta T_{ICEmax} = 0$ and without controlling whether the T_{ICEcmd_k} exceeds the T_{ICEmax}. Due to the larger available torque for acceleration, this run gives larger vehicle speed increments and larger engine speed increments between consecutive time steps. The maximum engine speed increment $\Delta\omega_{ICEmax}$ in this simulation can be used in the calculation of ΔT_{ICEmax} as in Eq. (6.63). ΔT_{ICEmax} calculated this way guarantees that T_{ICEcmd_k} stays inside the T_{ICEmax} since ΔT_{ICEmax} was calculated in the best acceleration case.

$$\Delta T_{ICEmax} = J_{ICE}\Delta\omega_{ICEmax} \tag{6.63}$$

6.7 x-y mph Time Analysis for Varying PG Gear Ratios

x-y mph time calculation algorithm is executed at every 10mph interval between 0 and 60mph for all powertrain types and all PG gear ratio combinations. The results are recorded in a matrix for each mode, as shown in Figure 6.10.

	α, β	0-10mph	10-20mph	20-30mph	30-40mph	40-50mph	50-60mph
1	$\alpha = 1.8, \beta = 1.8$	$t_{0\text{-}10,1}$	$t_{10-20,1}$	$t_{20-30,1}$	$t_{30-40,1}$	$t_{40-50,1}$	$t_{50-60,1}$
	...	...	...	...	...	...	...
441	$\alpha = 3.8, \beta = 3.8$	$t_{0\text{-}10,441}$	$t_{10\text{-}20,441}$	$t_{20\text{-}30,441}$	$t_{30\text{-}40,441}$	$t_{40\text{-}50,441}$	$t_{50\text{-}60,441}$

Figure 6.10: x-y mph Time Matrix.

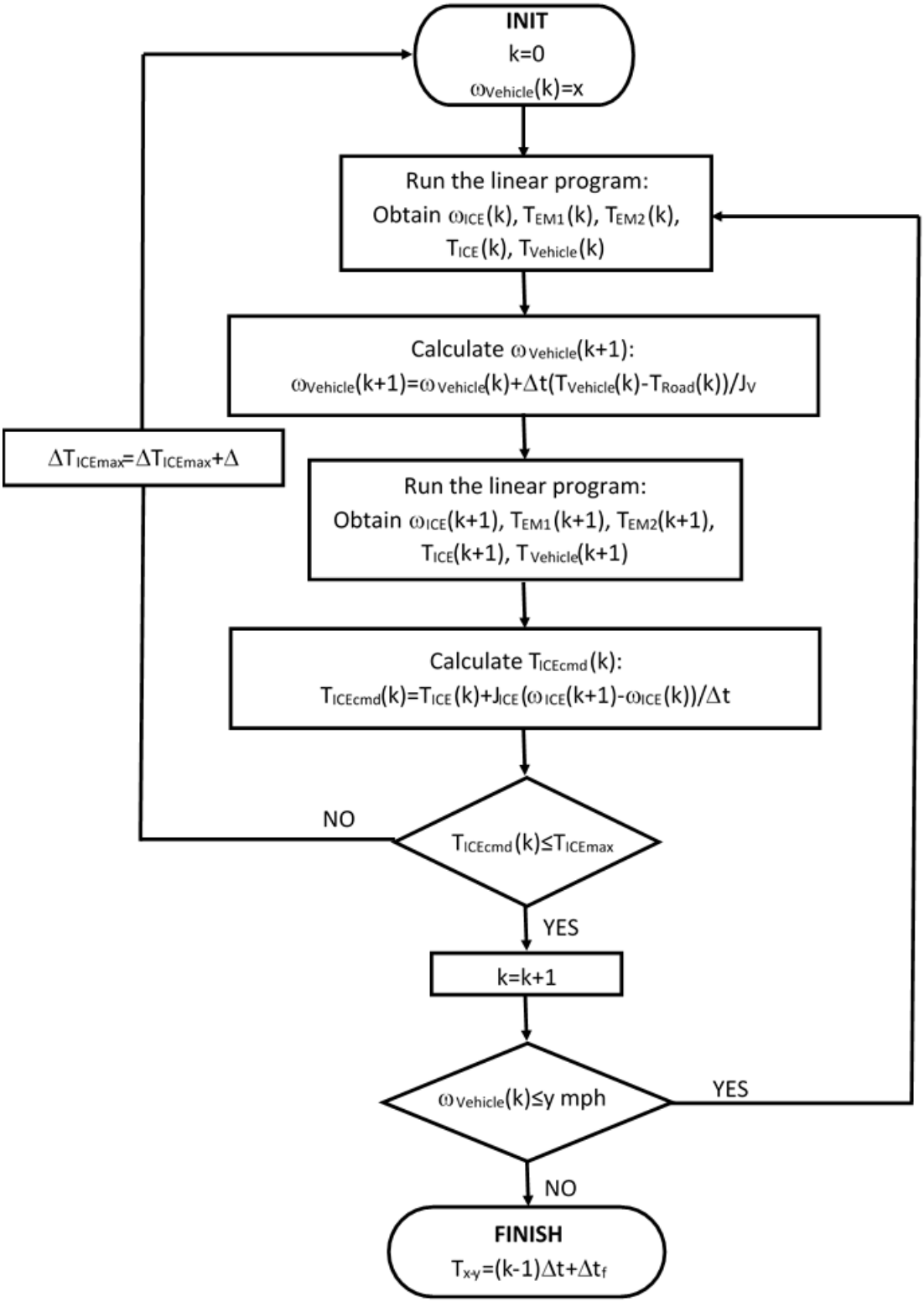

Figure 6.11: x-y mph Time Evaluation Algorithm

CHAPTER VII

Generation and Evaluation of Competent Designs

In this chapter, how the modes are combined to generate competent designs is first described. These designs are then benchmarked in terms of fuel economy for each feasible PG gear ratio combination in order to finalize the list of fuel efficient designs with superior performance. Last, the final list is analyzed to deduce some conclusions about superior designs.

7.1 Generation of Single- and Two-Mode Competent Designs

After the performance capability of all feasible modes as described in the Chapter VI is evaluated, the modes that can meet all performance criteria can be identified. These modes constitute competent single-mode designs. If two modes can meet all performance criteria collectively, then the designs with these modes are called competent two-mode designs.

7.1.1 Identification of Single-Mode Competent Designs

During the performance evaluation of modes, the gradeability matrix, long-hauling matrix, and x-y mph time matrix are generated for each mode, as shown in Figures 6.4, 6.9, and 6.10, where each row and column correspond to a PG gear ratio combination, and a specific performance criterion, respectively, and the value of 1 in

a cell means the mode can meet the performance criterion. In order to identify the modes and their corresponding PG gear ratios that can meet all performance criteria, logical AND operation is applied along each row of the gradeability, long-hauling, and $x-y$ mph time matrices in Figure 7.1. The result of this operation for each mode is gradeability-, long-hauling-, and x-y mph time vectors. Element-wise logical AND operation on these vectors in Figure 7.2 gives the final competency vector, where the value of 1 in any of its rows means that the mode is competent for the PG ratios corresponding to that row.

After running these operations, three modes, all of which are input-split power-train type are identified, which can meet all performance criteria.

Column-wise AND of Gradeability Matrix	$\Rightarrow$	Gradeability Vector
Column-wise AND of Long-Hauling Matrix	$\Rightarrow$	Long-Hauling Vector
Column-wise AND of $x-y$ mph Time Matrix	$\Rightarrow$	$x-y$ mph Time Vector

Figure 7.1: Generating Performance Vectors of Single Modes.

Gradeability Vector	AND	Long-Hauling Vector	AND	$x-y$ mph Time Vector

$=$	Competency Vector	
	$\alpha = 1.8, \beta = 1.8$	0/1
	...	...
	$\alpha = 3.8, \beta = 3.8$	0/1

Figure 7.2: Generating the Competency Vector of Single Modes.

7.1.2 Generation of Two-Mode Competent Designs

Two-mode combinations that can meet all performance criteria collectively are identified in two steps. In the first step, the modes are categorized into groups that are determined based on the PG node assignments of actuators. The purpose of creating the group structure is to eliminate symmetric modes and to reduce the number of two-mode combinations. In the second step, two-mode combinations that can meet all performance criteria under the clutch number constraint are explored.

7.1.2.1 Mode Grouping

The modes in the design space are grouped according to the PG node assignments of the vehicle, engine, EM1, and EM2 components in order to analyze mode transition feasibility through clutches. Since there are six PG nodes in a two-PG design, and vehicle and engine are not on the same node, $6 \times 5 \times 6 \times 6 = 1,080$ groups are possible. As explained in Chapter III, PG nodes are numbered 1 to 6, where 1 to 3 numbers correspond to the ring, carrier, and sun gears of the first PG, respectively, and numbers 4 to 6 belong to the second PG. Furthermore, each component entry in the data structure created to hold mode information contains the PG node to which it is connected. The group number is created as a 4-digit number in the heximal number system as $(Vehicle\_Node - 1)|(ICE\_Node - 1)|(EM1\_Node - 1)|(EM2\_Node - 1)$, since the maximum value of a four-digit heximal number (1295) is closest to $1,080$. It should be noted that a mode is assigned to more than one group if a component in the mode is connected to a PG node that has a mechanical connection with another PG node.

The advantage of such a numbering system in mode grouping is to be able to identify the symmetric topology of a mode, and to skip the analysis of the mode with a higher group number because two symmetric modes show exactly the same performance. Moreover, if the group number generated by interchanging EM1 and EM2 node assignments is greater than the original group number, the analysis of the mode with the higher number is skipped, since EM numbering is just a convention and interchanging the EM numbers would not change the performance of a mode. This approach eliminates the need to analyze at least half of the mode groups that are functionally represented in other lower-number groups, and thus accelerates the processing time.

Competent two-mode combinations are sought in each group for the following two reasons. First, the transition of a mode in one group to a mode in another group

requires at least two clutches. Considering the clutch number constraint to be three in the design approach, group transitions do not provide sufficient flexibility. The second reason is to reduce the number of two-mode combinations. The idea is to focus first on designs constructed with modes in the same group. If the number of competent designs is not sufficient with this approach, the mode combinations in different groups can then be taken into account.

7.1.2.2 Clutch Assignments

All two-mode combinations in each group are analyzed as to whether they meet the performance criteria collectively, and how many clutches are needed to make the transition between two modes. The required clutches are identified by comparing each component's PG node assignment in two modes as follows:

1. Since the competent mode-pair search is conducted in each group, the PG node assignments of the vehicle, engine, EM1, and EM2 in both modes should have at least one common PG node. If the PG node assignments of a component in the first and second modes are $PG\ Node\ 1 - PG\ Node\ 2$ and $PG\ Node\ 1$, respectively, then an off-going clutch is needed to make the transition from the first mode to the second one. If the PG node assignments are $PG\ Node\ 1$ in the first mode and $PGNode\ 1 - PG\ Node\ 2$ in the second mode, an on-coming clutch is needed to achieve the transition.

2. If the first mode has a brake at a specific PG node and the second mode does not have a brake at that specific PG node, an off-going clutch is needed to achieve the transition from the first mode to the second one. In the opposite scenario, an on-coming clutch is needed.

3. If the connection between two PG nodes in the first mode does not have any components on it and that connection does not exist in the second mode, an

off-going clutch is needed to make the transition from the first mode to the second one. In the opposite scenario, an on-coming clutch is needed.

7.1.2.3 Identification of Two-Mode Competent Designs

The performance capability of any two-mode combination is assessed using their grade-ability-, long-hauling-, and $x - y$ mph time matrices similar to the method in Section 7.1.1. The difference in the two-mode case is the implementation of the element-wise logical OR operation to the gradeability-, long-hauling-, and x-y mph time matrices of two modes as shown in Figure 7.3. Following this step, the same operations shown in Figures 7.1-7.2 are applied to the resultant performance matrices to obtain the competency vector of the mode pair, where the value of 1 in any of its rows means that the mode pair is capable of meeting the performance requirement for the PG ratios corresponding to that row. If the number of clutches to achieve the transition between those modes is less than or equal to the clutch number limit, that mode pair is declared as the competent two-mode design.

Mode 1		Mode 2		
Gradeability Matrix 1	OR	Gradeability Matrix 2	=	Gradeability Matrix
Long-Hauling Matrix 1	OR	Long-Hauling Matrix 2	=	Long-Hauling Matrix
x-y mph Time Matrix 1	OR	x-y mph Time Matrix 2	=	x-y mph Time Matrix

Figure 7.3: Combining the Performance Matrices of Two Modes.

7.1.2.4 Identification of Auxiliary Modes

In the process of identifying competent two-mode designs, the clutches that are required to make the mode transition possible are also determined. When more than one clutch is required for the transition, only two combinations of clutch states realize two competent modes. However, other feasible modes can exist in the design for the remaining combinations of clutch states. These modes are called auxiliary modes,

since they are by-products of the competent two-mode design process and do not contribute to meeting performance requirements. In this stage of the design process, the feasibility, speed and torque equations, and powertrain type of these auxiliary modes are explored using the analysis techniques in this study so that their contribution to the performance and fuel economy can be taken into account.

7.2 Addition of the Backward-Speed Capable Mode

Similar to the forward-speed capable modes, the performance of all backward-speed capable modes is evaluated against the criteria set in Table 6.2 for all PG gear ratio combinations. The competent backward-speed capable modes are then assigned to their groups as to be selected to complement the existing competent single- and two-mode designs.

A single-mode competent design does not have any backward-speed capable mode since it consists of only one forward-speed capable mode. To accommodate the backward-speed capability in these designs, all competent backward-speed capable modes in their group are searched iteratively. If a backward-speed capable mode has a common feasible PG gear ratio combination with the competent design, and the number of clutches that is required to achieve the transition between these modes is less than or equal to the clutch number limit, the backward-speed capable mode is mated with the competent mode and the required clutches are added to the mode to establish the complete design. At the end of this process, not any competent single-mode design that can be mated with a backward-speed capable mode is identified.

For the competent two-mode designs, two alternatives exist to provide the backward-speed capability. First, all auxiliary modes of a design are analyzed in terms of backward-speed capability. If an auxiliary mode with backward-speed capability is available, the competent two-mode design is complete. If there is no auxiliary mode with backward-speed capability and the number of clutches is less than the limit, all

backward-speed capable modes in the group of the competent design are searched iteratively to explore any backward-speed capable mode with a common PG gear ratio combination to which the transition is possible without exceeding the clutch number limit. At the end of this process, 43 competent designs, shown in Figure 7.4, are identified. In this figure, blue lines are fixed connections between two PGs, while black and red clutches are needed to achieve mode transitions between two competent modes. The purple clutch is needed in some of the designs when none of the auxiliary modes provides the backward-speed capability and a backward-speed capable mode should be augmented to the design.

7.3 Fuel Economy Evaluation

Performance and fuel economy are two main pillars of the design process. The focus has thus far been on the performance pillar to eliminate as many modes and designs as possible from the design space so that computationally heavy fuel economy simulations can be completed within reasonable amount of time. In this section, all competent designs are evaluated in terms of the fuel economy improvement potential for each feasible PG gear ratio combination in order to obtain a final list of designs with both superior performance and fuel economy.

The ideal method for fuel economy analysis is dynamic programming (DP), since it guarantees global optimality over the problem horizon. However, DP suffers from a heavy computation load in light of the number of independent state variables in each mode and the multi-mode characteristics of each design. In the literature, several near-optimal fuel economy analysis methods have been introduced [50, 58]. In this study, one of these methods, called power-weighted efficiency analysis for rapid sizing (PEARS), is used with some improvements. Since the PEARS method is covered in [85], its details are not presented here.

The PEARS method first calculates the best power-weighted efficiency of each

mode in the design for both EV and HEV operations at every vehicle speed and load point of the selected drive cycle. A DP algorithm over the time horizon of the drive cycle is then executed to select a mode at every instant of the drive cycle with the goal of maximizing fuel economy. In this study, the following improvements are made to this method:

1. In PEARS, special power-split powertrain types are ignored during the analysis. In this study, the PEARS algorithm is extended to include all special power-split powertrain types.

2. In the original PEARS method, just three engine speed points are evaluated in determining the most efficient EV operating point of a mode. In this study, all engine speed points between 0 and ω_{ICEmax} at 100 rpm increments are taken into account, since higher engine speed resolution lets the method obtain an operating point close to the optimal one with resultant better fuel economy.

3. PEARS evaluates just the most efficient EV and HEV operating points of each mode in determining the mode at each simulation time step during the DP stage. However, control command choices, that is, control bandwidth gets limited for some designs with few numbers of modes and, hence, the algorithm cannot find a solution. In this study, in addition to the EV and HEV operations, a third operating point, battery charging HEV, is added to the mode selection DP. With this modification, the bandwidth of the control inputs is increased for the mode selection DP, and the possibility of no solution is prevented for the designs with a limited number of modes.

Using the modified PEARS, all competent designs are assessed in the Urban Dynamometer Driving Schedule (UDDS) and Highway Fuel Economy Test (HWFET) drive cycles for all of their feasible PG gear ratio combinations. Battery SOC is allowed to vary between 55% and 65% during simulations. Moreover, the battery SOC

at the end of each cycle is kept the same as the SOC at the beginning of the cycle by penalizing the control actions that lead to an SOC mismatch. The weighted average of cycle results (55% UDDS and 45% HWFET) is calculated, and the PG gear ratio combination that gives the highest fuel economy is selected for comparison. 22 out of 43 designs represented in Figure 7.4 with a red star are able to pass the 30mpg threshold. The highest fuel economy achieved among the competent designs is 31.5mpg. The fuel economy of the same vehicle with a 6-speed automatic transmission instead of a hybrid electric powertrain is also simulated for a benchmark and is calculated to be 22.6mpg. As a result, the maximum fuel economy improvement thanks to a hybrid electric powertrain is 39%.

Ten HEV designs shown in Figures 7.5-7.6 with their individual feasible modes are chosen out of 22 competent designs based on the uniqueness of their topology in order to illustrate the benchmark of their performance and fuel economy. These 10 designs are classified into two groups in terms of the powertrain types of their competent modes. In the first group with four designs, the competent modes are parallel and input-split powertrain types; the second group consists of six designs, whose competent modes are parallel and output-split powertrain types. The performance and fuel economy benchmark results are represented in Figures 7.7-7.8 and Table 7.1. As seen from the results in Table 7.1, the designs with a competent input-split mode perform better in fuel economy simulations than those with a competent output-split mode. Moreover, although all competent designs exceed the performance of the conventional powertrain in some respects, there is no competent hybrid design that is superior in all criteria. The conventional powertrain can compete against the competent HEV modes through torque multiplication of its torque converter and high gear ratios at low vehicle speed.

The following observations are made from the analysis of all competent designs:

1. 43 competent designs are categorized according to the powertrain types of their

Table 7.1: Fuel Economy Results of Ten Competent Designs and Conventional Powertrain

Design No	UDDS (mpg)	HWFET (mpg)	Combined (mpg)
Design 43	36.8	26.7	31.5
Design 37	36.5	26.7	31.4
Design 4	36.5	26.7	31.3
Design 5	35.5	26.3	30.7
Design 2	35.6	25.7	30.3
Design 40	35.7	25.3	30.1
Design 1	35.2	25.5	30.0
Design 36	34.7	25.4	29.8
Design 23	33.8	26.1	29.8
Design 34	34.7	25.3	29.8
Conventional	26.5	19.5	22.6

two competent modes in Table 7.2. As seen in that table, most of the designs consist of parallel and input-split or parallel and output-split competent mode pairs. When these designs are analyzed in detail, the competent parallel mode can be seen to meet the gradeability requirement at launch and low vehicle speed, while the competent input-split or output-split mode provides high performance at medium and high vehicle speed.

Table 7.2: 43 Competent Designs according to the Powertrain Type of Competent Two Modes

Powertrain Types of Competent Two Modes	Number of Designs
Parallel + Output-Split	24
Parallel + Input-Split	13
Input-Split + Output-Split	1
Fixed Gear + Input-Split	1
Special Power-Split + Output-Split	1
Parallel + Compound-Split	1
Parallel + Special Power-Split	1
Fixed Gear + Parallel	1

2. Although Table 7.2 shows a diverse set of powertrain types for competent mode pairs, only 10 designs with parallel+output-split competent mode pairs and 12 designs with parallel+input-split mode pairs can reach the 30mpg threshold.

Furthermore, fully 10 of the 12 designs with parallel+input-split competent mode pairs are able to exceed 31mpg, whereas only 2 of the 10 designs with parallel+output-split competent mode pairs can exceed the same threshold. These results show that when performance and fuel economy benefits are taken into account together, parallel+input-split competent mode pairs have a clear superiority over parallel+output-split mode pairs.

3. When the topology of all competent output-split and input-split modes in Table 7.2 are investigated, input-split modes show nine unique topologies, whereas output-split modes show only six, although the number of competent output-split modes is higher. Furthermore, if backward-speed capability requirements had not existed, two designs with a single input-split mode would have met all performance requirements. These results reveal that input-split modes are superior in terms of not only fuel economy but also performance. The observation deduced from the design process results about the superior performance of input-split modes over output-split modes is supported by the following derivations.

   For an input-split powertrain type, speed equations, optimization objective for maximum acceleration, and torque constraints can be written as in Eqs. (7.1)-(7.4).

$$\omega_{EM1} = f_1 \cdot \omega_{ICE} + g_1 \cdot \omega_{Vehicle} \tag{7.1}$$

$$\omega_{EM2} = g_2 \cdot \omega_{Vehicle} \tag{7.2}$$

$$minimize(T_{Vehicle}) = minimize(-g_1 \cdot T_{EM1} - g_2 \cdot T_{EM2}) \tag{7.3}$$

$$s.t.$$

$$T_{ICE} = -f_1 \cdot T_{EM1} \leq T_{ICEmax} \tag{7.4}$$

T_{EM1} and T_{EM2} can be considered the resources used to minimize the cost of $T_{Vehicle}$ within the constraints of T_{ICEmax}. As seen in these equations, T_{EM2} is a free resource, since T_{EM2} can be set to $sgn(g_2) \cdot T_{EM2max}$ at a given ω_{EM2} without being restricted by T_{ICEmax}. In an input-split powertrain type, the contribution of $EM2$ to the vehicle torque is $-|g_2| \cdot T_{EM2max}$. T_{EM1} also contributes to the vehicle torque as long as $-f_1 \cdot T_{EM1} \leq T_{ICEmax}$. As a result, it is expected that an input-split powertrain type with high $|g_2|$ has superior maximum acceleration performance.

For an output-split powertrain type, speed equations, optimization objective for maximum acceleration, and torque constraints are shown in Eqs. (7.5)-(7.8).

$$\omega_{EM1} = f_1 \cdot \omega_{ICE} + g_1 \cdot \omega_{Vehicle} \tag{7.5}$$

$$\omega_{EM2} = f_2 \cdot \omega_{ICE} \tag{7.6}$$

$$minimize(T_{Vehicle}) = minimize(-g_1 T_{EM1}) \tag{7.7}$$

$$s.t.$$

$$T_{ICE} = -f_1 \cdot T_{EM1} - f_2 \cdot T_{EM2} \leq T_{ICEmax} \tag{7.8}$$

As seen in these equations, T_{EM2} does not have any torque contribution to the vehicle. The only resource that can contribute to the vehicle torque is T_{EM1}. T_{EM1} may not reach its limit $sgn(g_1)T_{EM1max}$ due to the T_{ICEmax} constraint. In this case, T_{EM2} is used to relax the T_{ICEmax} constraint as $-f_1 \cdot T_{EM1} \leq T_{ICEmax} + |f_2| \cdot T_{EM2max}$. The limiting factor for minimum $T_{Vehicle}$ becomes $sgn(g_1) \cdot T_{EM1max}$ this time.

According to these derivations, an output-split powertrain type is disadvantageous in minimizing $T_{Vehicle}$ compared to an input-split powertrain type since an input-split type can use both T_{EM1} and T_{EM2} for the minimization task, whereas an output-split type has the single resource T_{EM1}.

4. The competent designs in Figure 7.4 are compared to the competent HEV designs identified in previous studies for just one PG gear ratio combination using less stringent performance criteria [75, 85, 86]. The designs in Figure 7.4 are not the same as the ones in the previous studies except Designs 35 and 37. The first reason of this difference is stricter performance requirements in this dissertation. The designs in the previous studies cannot meet all those performance criteria with the chosen PG gear ratio. Moreover, since previous studies use only one PG gear ratio combination, the competent designs explored in this dissertation may not perform well at that gear ratio combination. Last but not least, the previous studies do not explore designs where electric machines share the same PG node with the vehicle or engine. When we look at the designs in this study, we observe that most of the competent designs have this type of configuration. Hence, some of the competent designs were not even in the design space of the previous studies.

5. Poor fuel economy performance of a competent mode with a fixed gear powertrain type is expected since $T_{Vehicle}$ and $\omega_{Vehicle}$ determines T_{ICE} and ω_{ICE} and no degrees of freedom exist to optimize the operating point of the engine for a drive cycle simulation.

6. Few competent modes with a special power-split powertrain type exist in the design results. However, their fuel economy cannot compete with the results of modes with input-split or output-split types. The main reason for this observation is the steady-state torque equation of a special power-split type, where $T_{Vehicle} = f_1 \cdot T_{ICE}$, while ω_{ICE} can be set independent from $\omega_{Vehicle}$. According to this equation, f_1 should be as high as possible for a superior gradeability performance. However, drive cycles used in the fuel economy simulations do not require very large $T_{Vehicle}$. Hence, T_{ICE} stays at its low range during fuel

economy simulations and the degrees of freedom in ω_{ICE} are not sufficient for setting the engine at an efficient operating point. Figure 7.9 shows the operating points of the running engine on its fuel map as red dots, while a special power-split mode is active during the UDDS simulation. As seen in the figure, changing ω_{ICE} does not help the operating points to move to the high efficient region. This analysis shows that a high performing and fuel efficient design can be created with a competent special power-split mode if it is complemented with another fuel efficient mode.

7. Each design possesses modes with a diverse set of powertrain types ranging from EV to series, parallel, and all types of power-split. These auxiliary modes contribute to the fuel economy results, while the performance is delivered by just two competent modes.

8. The effect of PG gear ratio on performance is significant due to its existence in the coefficients of torque equations, as shown in Eq. (3.3). Fuel economy simulations for varying PG gear ratios reveal that a PG gear ratio can change the fuel economy of a design between 0.2mpg and 1mpg, depending on the feasible PG ratio range. These results show that any design process that ignores PG gear ratio is not complete. Furthermore, leveraging this result, a strategic fuel economy simulation can be conducted particularly for a large design space. In that approach, fuel economy simulation for just one feasible PG gear ratio combination of all competent designs is first performed. 1mpg is added to the results assuming the selected PG gear ratio gives the worst fuel economy among all combinations for a particular design. The designs with poor fuel economy results are eliminated from the design space, and fuel economy simulations for all feasible PG gear ratios of the remaining designs are conducted for benchmarks. This approach saves significant computation time, since the most time

consuming task in the design process is the fuel economy simulation.

9. The most restricting design criterion is the backward-speed capability when the engine is on. Previous studies either ignore this criterion completely or look only at the sign of the coefficient of T_{ICE} in the $\dot{\omega}_{Vehicle}$ dynamic equation. In fact, a competent design should have superior backward-speed gradeability, and the engine speed should be above its idle speed at low backward speed so that it can produce positive torque. The design process in this study takes into account all these criteria, with the result that many competent designs are eliminated since their backward-speed modes cannot meet these requirements. Only parallel modes or series modes in competent designs can meet the backward-speed capability requirement. Few designs with parallel backward-speed capable modes are eliminated because the engine speed is below idle speed at low backward speed. If a launch clutch were added between the engine and PG node, 25 more designs would become competent.

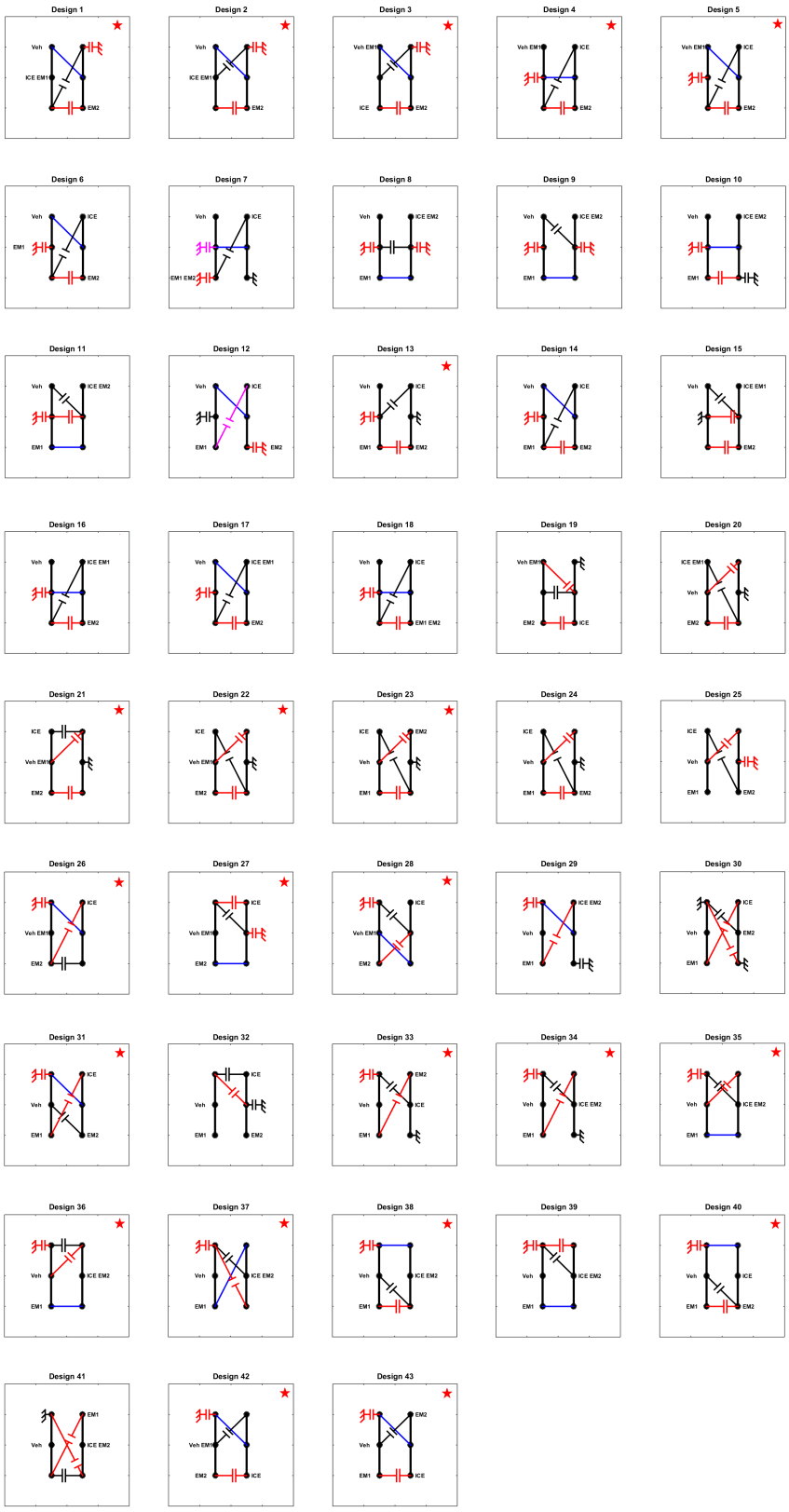

Figure 7.4: Backward-Speed Capable Competent Two-Mode Designs.

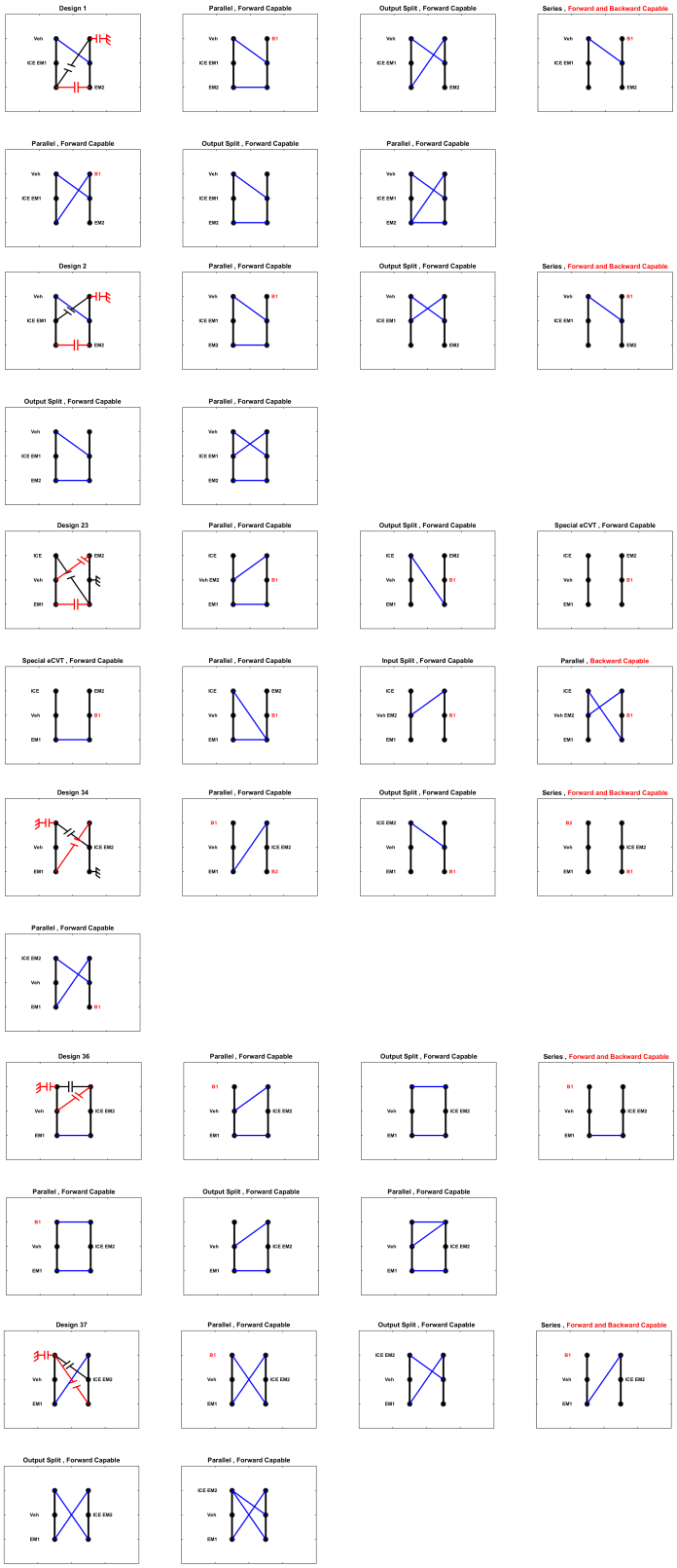

Figure 7.5: Designs with an Output-Split Competent Mode of the Selected 10 Designs.

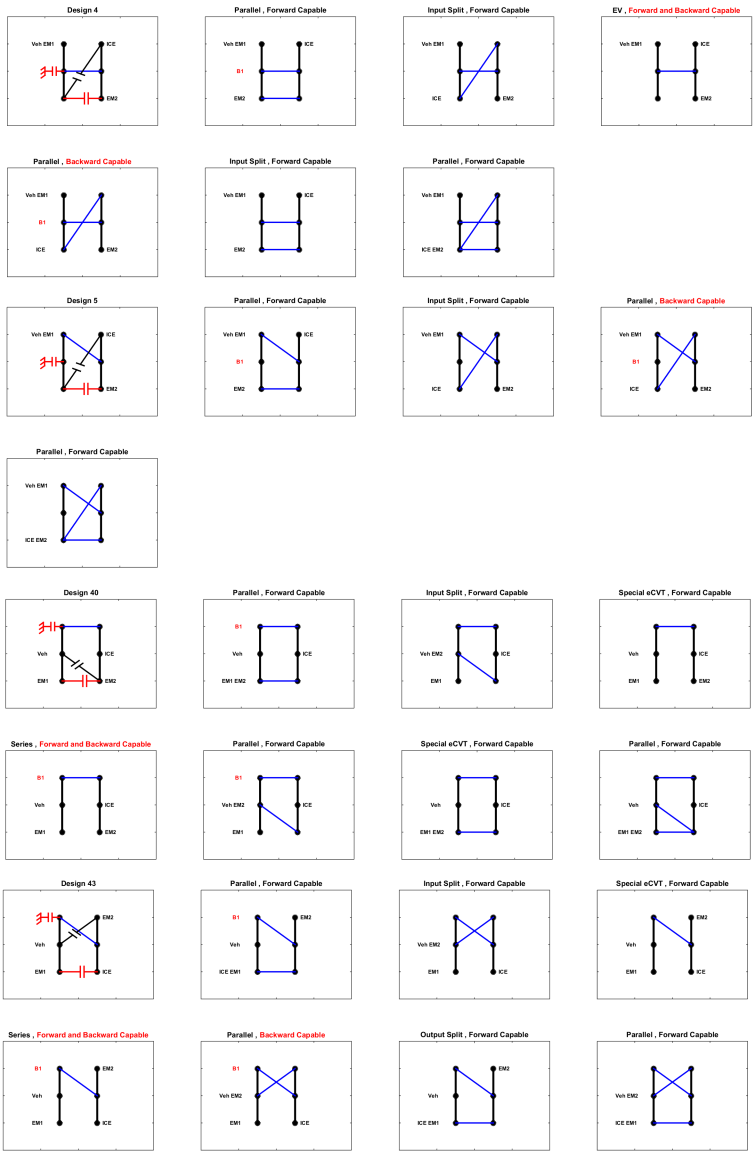

Figure 7.6: Designs with an Input-Split Competent Mode of the Selected 10 Designs.

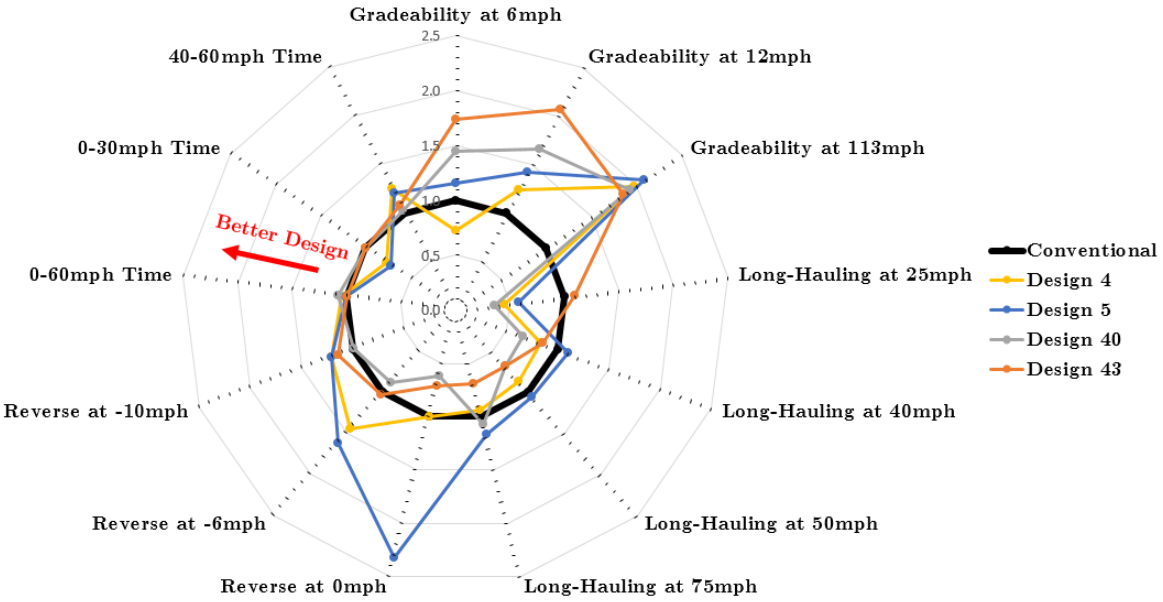

Figure 7.7: Comparison of Four Designs with competent Parallel and Input-Split Modes to a Conventional Powertrain.

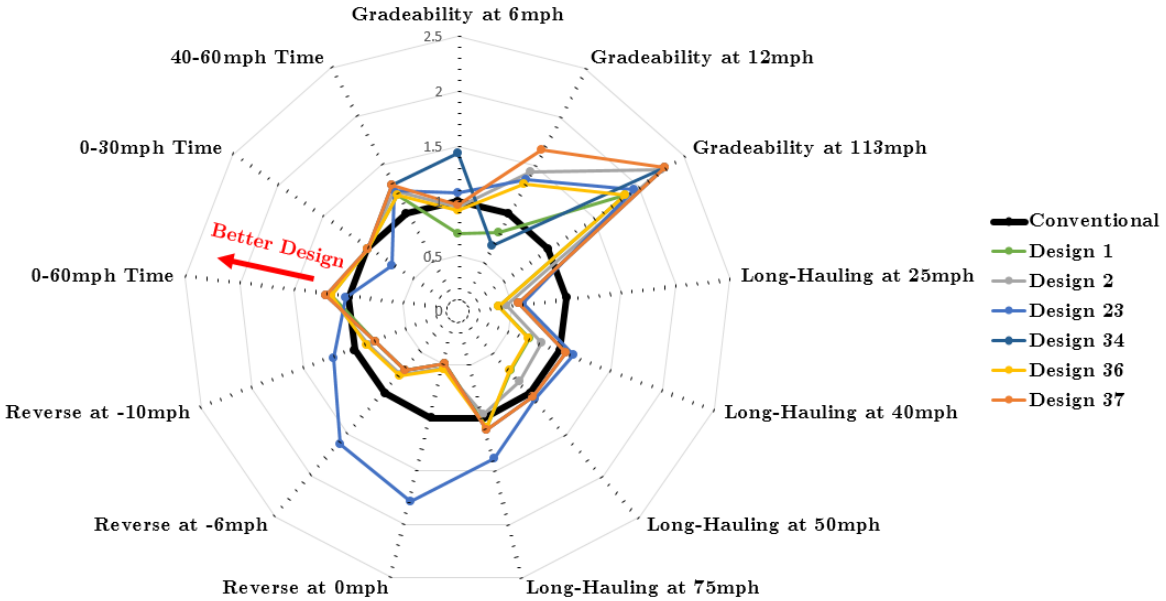

Figure 7.8: Comparison of Six Designs with competent Parallel and Output-Split Modes to a Conventional Powertrain.

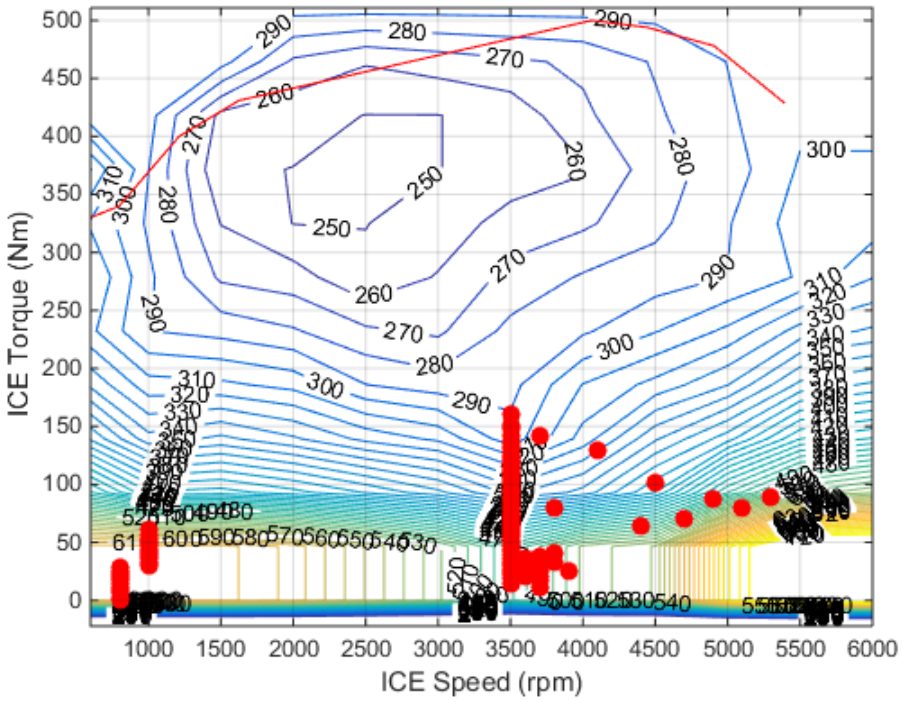

Figure 7.9: Running Engine Operating Points (Red Dots) of a Special Power-Split Mode during the UDDS Drive Cycle.

CHAPTER VIII

Mode Transition Analysis and Control

In all fuel economy evaluation algorithms (dynamic programming, PEARS, ECMS etc.), the mode that gives the lowest cost is determined at each time instant of the drive cycle. Hence, the result of the fuel economy simulations is the sequence of modes, each of which has its own operating points independent of the other time points. In these algorithms, the feasibility and cost of the mode transition between consecutive time instants are not taken into account. In this chapter, the algorithms are developed which facilitate the analysis of mode transition feasibility and calculate the control commands achieving the feasible mode transitions without deteriorating drivability. In addition, these algorithms are integrated into the PEARS software to enable automated mode transition analysis and control, and to evaluate the effect of mode transition on the fuel economy results.

8.1 Hierarchical HEV Powertrain Mode Shift Control

Before going into details, the mode shift problem must be analyzed from a higher perspective in order to tackle its right dimension. A mode shift event can be categorized into three levels in terms of controls, as shown in Figure 8.1. At the high level, the control algorithm only makes the decision to shift the current mode to another mode. The shift request can be due to several reasons. At the current driving condition,

the shift to a new mode may maximize the target criteria, for example, performance or fuel economy or the current mode can no longer deliver the required performance under current conditions. The period of decision making at this level should be at the scale of seconds to allow some time to perform the desired mode shift and to not cause undesired shift busyness. It should not be too long either, however, in order to maximize the target criteria. In this study, the execution period at this level is taken as 1s, since the vehicle speed data in the drive cycles is sampled at this rate. The outputs of the control algorithm at this stage are the desired mode and the operating points of each component at this new mode.

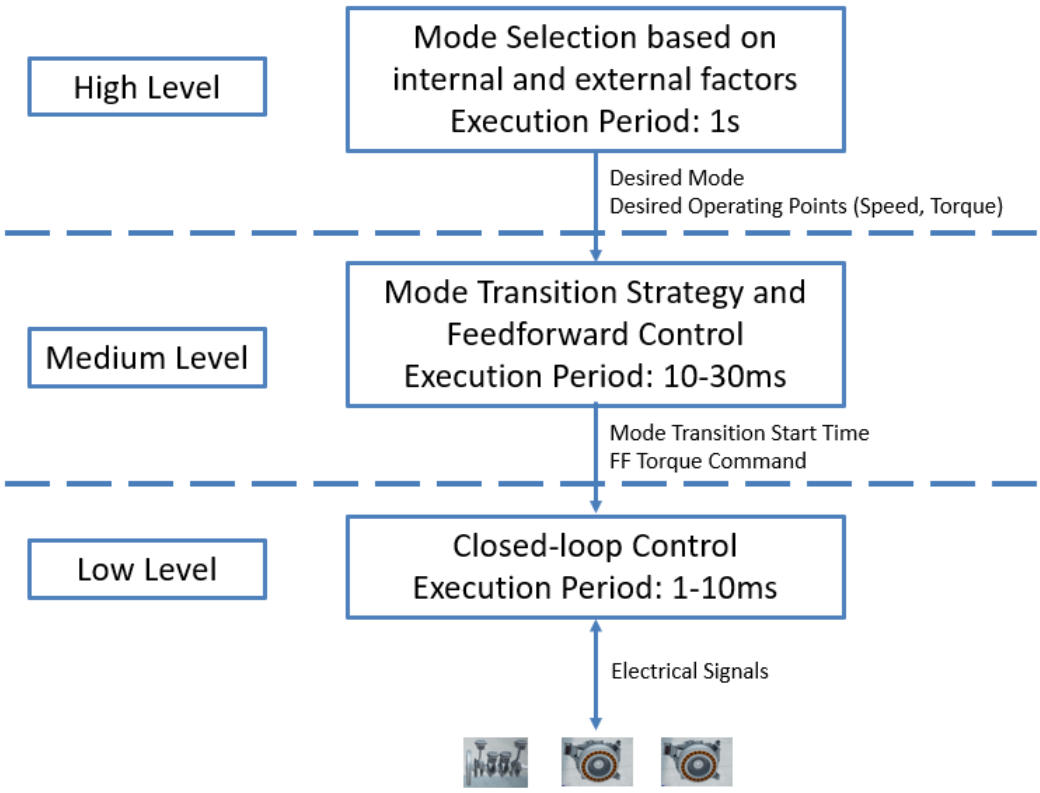

Figure 8.1: Mode Shift Control Hierarchy.

The control algorithm at the medium level of the hierarchy first analyzes the feasibility of the new mode transition because the current operating points of the actuators may not allow the transition to the new operating points at the new mode

due to drivability constraints or component limitations. If the mode shift is feasible, the algorithm determines the control strategy that achieves the shift by assuming that the mathematical model of the system is perfectly known. The execution period at this level is tens of milliseconds in order to achieve the mode transition as quickly as possible while staying within the actuator limits. The control commands are the target torque that each actuator should deliver. The control at this level can be considered feedforward control, since the perfectly known mathematical model is assumed and the control commands can be determined through the model inversion. The goal in this study is to solve the mode transition analysis and control problems at this stage.

The purpose of the control at the low level is to make sure that the torque commands of the medium level are delivered by the actuators using the closed-loop control techniques. At this level, the execution period is on a scale of milliseconds. The outputs of the control algorithms are the physical signals that directly control the actuators, for example, current, spark angle and duration, fuel quantity, throttle angle. This study does not deal with the control algorithm development at the low level.

8.1.1 Transition from High Level to Medium Level

In this subsection, how the high level control is integrated with the medium level control will be explained. Figure 8.2 shows the torque and speed signals during two execution periods of high level mode shift control without the medium level control. High level control runs at the beginning of each time period and decides which mode should be active during that period. Once the active mode is selected, the actuator torque values remain constant until the next execution of the algorithm. Due to the system's dynamic equations, the constant torque values result in a change to the component speeds. However, high level control assumes that the speed signals remain constant during the period and uses the average speed values of the actuators,

as shown as the red dots on the speed traces in Figure 8.2. Once the new execution period begins, the new torque and speed values are determined by the high level control, where step changes of these variables are assumed. This framework is used by all fuel economy evaluation algorithms, including dynamic programming, PEARS, and ECMS.

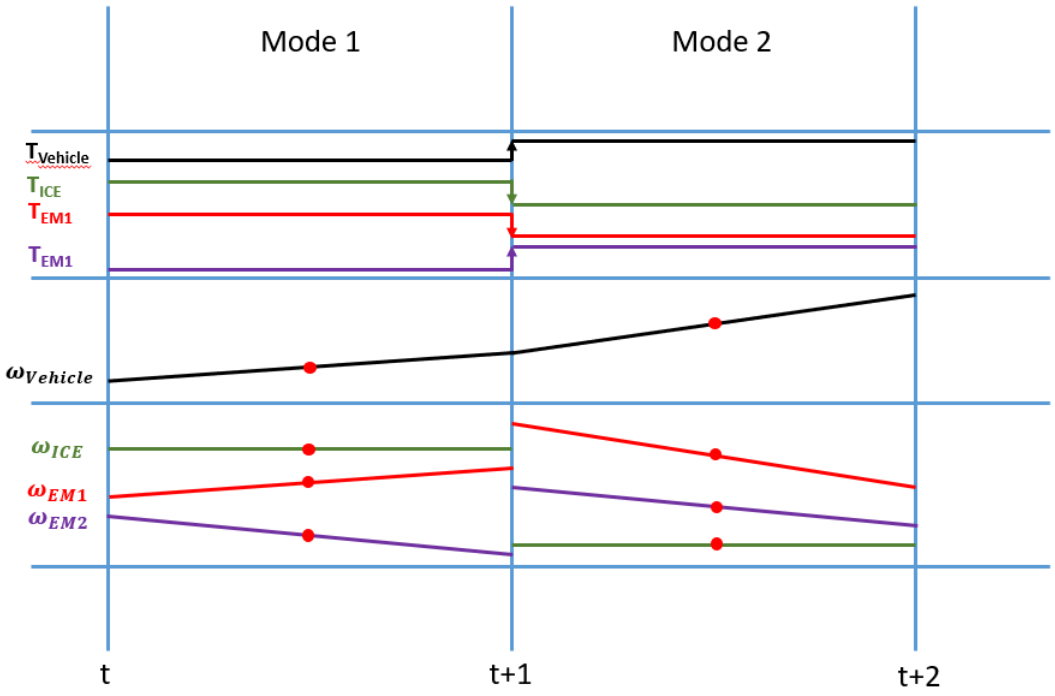

Figure 8.2: Speed and Torque Signals at the High Level Mode Shift Control.

Although the assumption of a step change in the speed signals simplifies the fuel economy simulations, the feasibility of the respective mode shift and the effect of transients on the fuel economy results are ignored. The inclusion of the medium level control eliminates these drawbacks. Figure 8.3 shows how the medium level control is integrated with the high level control. Assuming the length of the mode transition is known, the medium level control starts changing the actuator torque commands before the next execution period of high level control begins. The medium level control has two main goals. The first is to evaluate whether or not the desired mode transition is feasible, since the actuator limits or current driver demand may not make

the transition possible in light of the performance constraints. If the mode transition is feasible, the second goal is to control actuator torque values such that the speed signals at the start of the mode transition approach the desired speed signals at the beginning of the next execution period of the high level control, where a step change in the speed signals is eliminated. How the feasibility analysis and mode transition control are performed will be explained in the following sections.

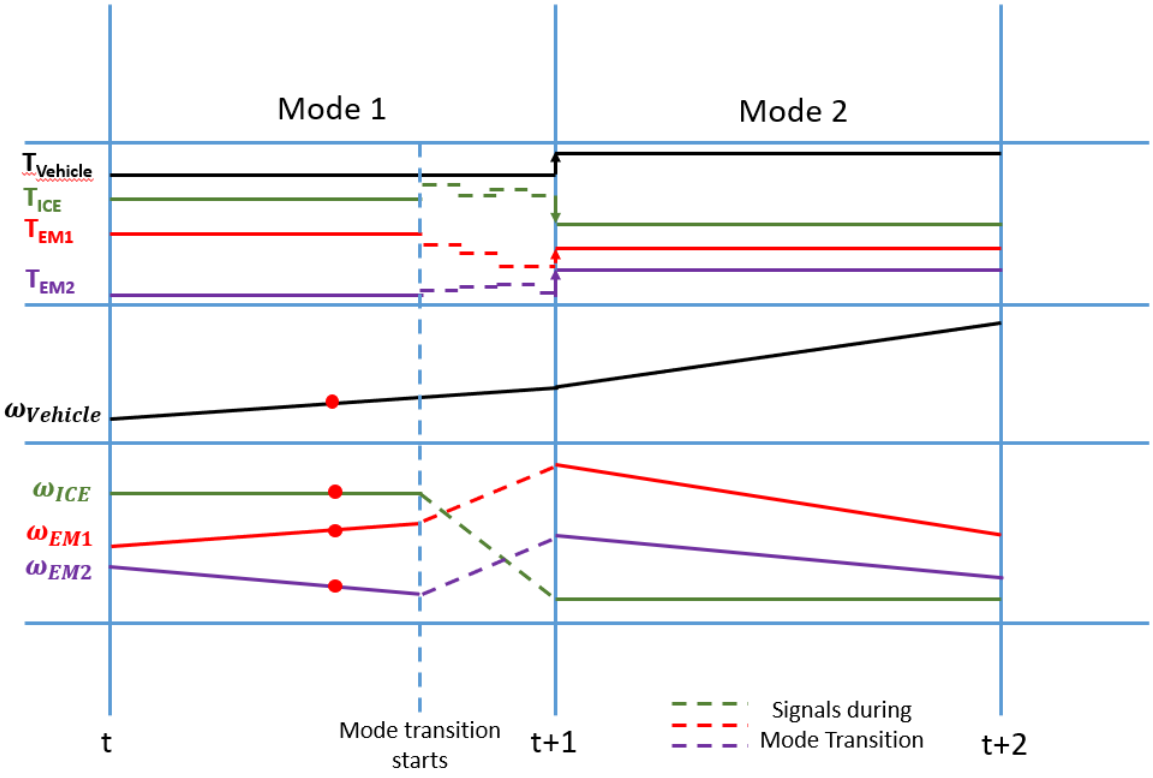

Figure 8.3: Speed and Torque Signals at the High and Medium Levels Mode Shift Control.

8.2 Mode Transition Feasibility and Control

In the previous section, mode transition is analyzed from the perspective of hierarchical control. In this section, the methods that are developed to achieve the goals of the medium level control will be explained. First, the fundamental gear shift con-

cepts used in conventional transmissions are adapted to the mode transition control in HEV powertrains. These concepts are then used to analyze the feasibility of mode transitions and to control clutch torque and speed for seamless mode transition.

8.2.1 Torque Transfer and Speed Control Phases in Mode Shift Control

Torque transfer and speed control concepts are widely used in the gear shifts of conventional transmissions. Since the engine is the only torque source in these transmissions, and the degrees of freedom are at most two during a shift, the use and order of these phases cannot be changed for a given vehicle torque and engine torque, and gear shift. However, electric machines in HEV powertrains provide additional torque sources and degrees of freedom. Hence, torque transfer and speed control phases can be used creatively in different ways during mode transitions. In this subsection, these possibilities will be explained for mode transitions that require one on-coming and one off-going clutches because the concepts for mode shifts with other clutch combinations will be derived from this development.

In the torque transfer phase, the torque on the off-going clutch is reduced to 0, while the slipping on-coming clutch is loaded to maintain the existing speed dynamics. In the speed control phase, the speed of clutch plates is controlled to make them equal and to close the open or slipping clutch. Since only the torque values of the actuators are changed during torque transfer without any involvement of the system dynamics, torque transfer is much faster than speed control. The design and its corresponding modes 1 and 2 in Figure 8.4 will be used as an example to show how torque transfer and speed control phases can be utilized during a mode shift in an HEV powertrain. Two possibilities exist for the application order of torque transfer and the speed control phases to the mode transition from mode 1 to mode 2:

1. First torque transfer phase, then speed control phase, as illustrated in Figure 8.5.

2. First speed control phase, then torque transfer phase, as illustrated in Figure 8.6.

In the first case, the on-coming clutch $C1$ is pressurized to have torque carrying capacity, while the off-going clutch $B1$ is unloaded. When $B1$ clutch torque reaches 0, $B1$ clutch is fully opened. At this moment, the system is in an intermediate mode, where slipping $C1$ clutch is carrying the torque transferred from the $B1$ clutch. However, $C1$ clutch cannot be closed due to the speed difference between its plates. Controlling the actuators' torque, the speed of $C1$ clutch plates are equalized, and then $C1$ clutch is closed. At the end of this process, the system is in mode 2, and the mode transition is complete.

In the second case, the speed difference between on-coming $C1$ clutch plates is nonzero at the beginning of the mode transition. In order to make this speed difference zero, the torque carrying capacity of the $B1$ clutch is reduced to cause it to slip and control the speed of $C1$ clutch plates. When the speeds of $C1$ clutch plates are equal, $C1$ clutch can be closed, while $B1$ clutch is slipping. Then the torque transfer phase begins where the torque on the slipping $B1$ clutch is transferred to the closed $C1$ clutch. Once $B1$ clutch is fully unloaded, it can be opened and the mode transition to mode 2 is complete.

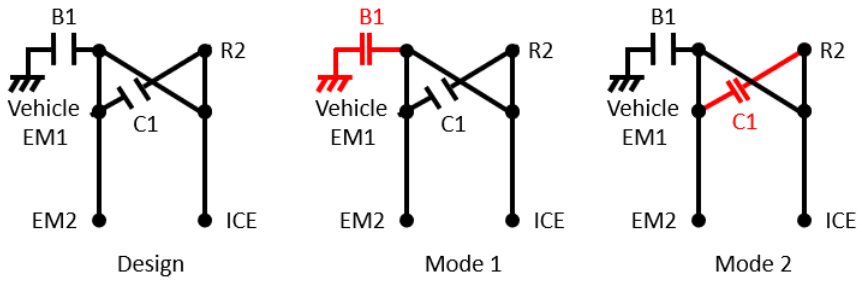

Figure 8.4: Example Design for Mode Shift Analysis and Control.

8.2.2 Mode Transition Strategy

After laying the groundwork for the mode transition concept in the previous sections, the general strategy for achieving the mode transitions is described in this section.

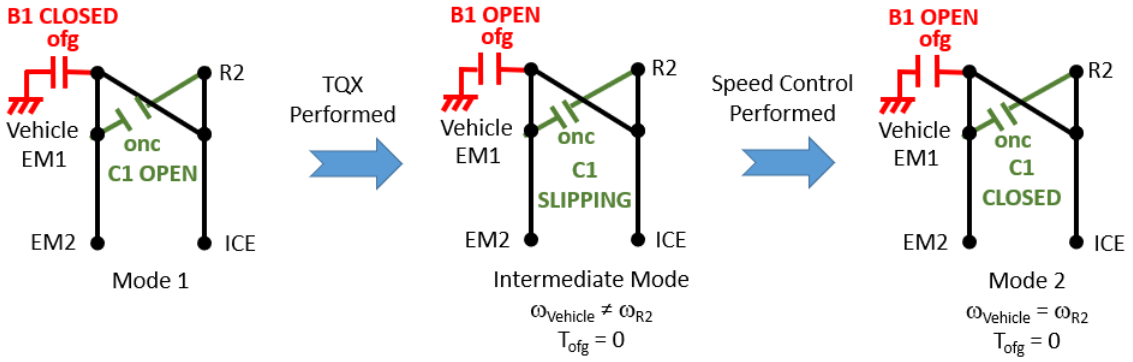

Figure 8.5: First Torque Transfer Phase, then Speed Control Phase in the Transition from Mode 1 to Mode 2.

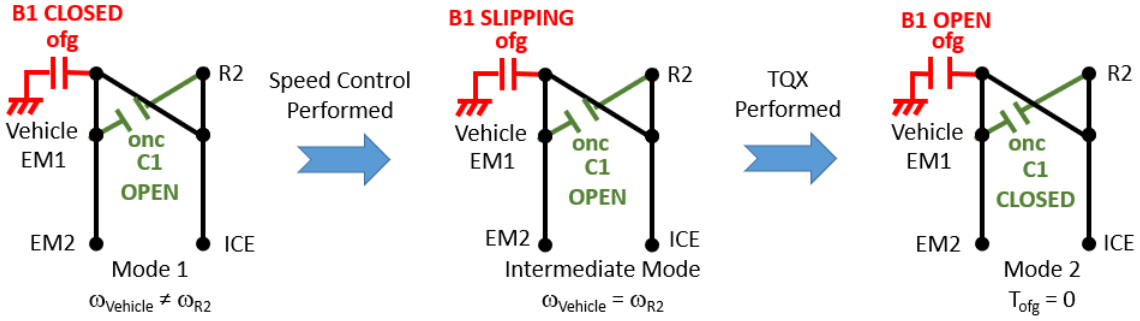

Figure 8.6: First Speed Control Phase, then Torque Transfer Phase in the Transition from Mode 1 to Mode 2.

This control strategy and related constraints can be summarized as follows:

- During a mode transition, $T_{Vehicle}$ and $\dot{\omega}_{Vehicle}$ should be kept constant in order to prevent any adverse effect of mode transition on drivability.

- The base control mechanisms in the medium level mode transition are speed control and torque transfer phases. In a mode transition, they are applied sequentially, and the order of application depends on the speed differential between clutch plates and the controllable torque range of off-going and on-coming clutches.

- The speed dynamics of the current mode should not change during the torque transfer phase.

- Separate control algorithms should be developed for these three types of mode transitions: 1 off-going mode transition, 1 on-coming mode transition, and 1 off-going, 1 on-coming mode transition. The other types of mode transitions should be achieved using combinations of these control algorithms.

In this study, all HEV powertrain designs that can be constructed with at most three clutches have been investigated. Hence, the on-coming and off-going clutches that are involved in any mode transition of a design have the combinations depicted in Figure 8.7. 1 on-coming clutch, 1 off-going clutch, 1 on-coming and 1 off-going clutches are considered the fundamental clutch combinations; the other clutch combinations can be constructed by using these three combinations, as shown in Figure 8.7. Furthermore, control algorithms, which will be explained in the next section, are developed solely for the fundamental clutch combinations, as the control of other clutch combinations can be achieved using these control algorithms in the given sequence of fundamental clutch combinations.

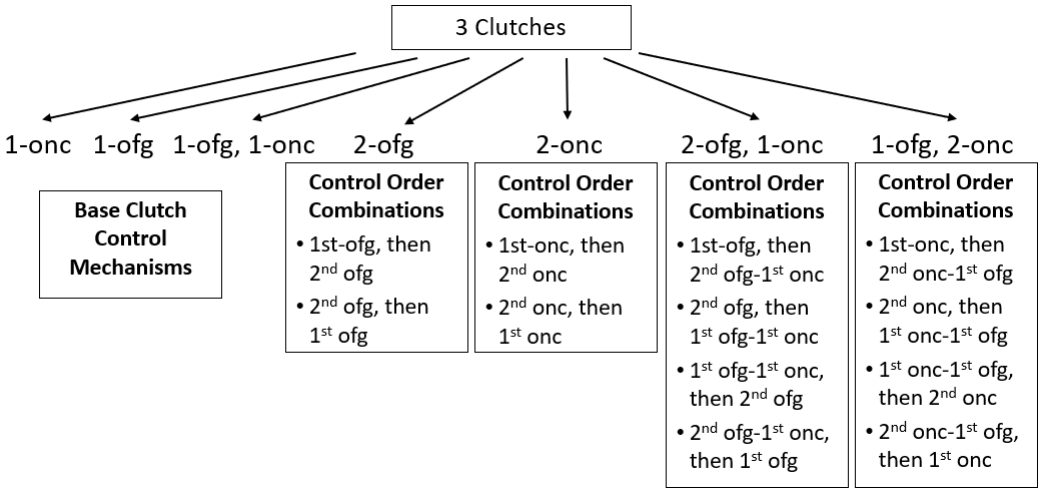

Figure 8.7: All On-coming and Off-going Clutch Combinations in a Mode Transition of a 3-clutch Design.

8.2.3 Feasibility of Torque Transfer and Speed Control Phases

Subsection 8.2.1 describes how the clutch speed and torque are controlled to achieve mode transitions at a high level using torque transfer and speed control phases. However, the feasibility of these phases and their implementation order in a mode transition are not discussed. In this subsection, the feasibility algorithms for the three fundamental clutch combinations in a mode transition are developed.

8.2.3.1 Feasibility of Mode Transition with 1 Off-going Clutch

In a mode transition from mode 1 to mode 2 with 1 off-going clutch, two control possibilities exist:

1. First torque transfer (TQX) phase, then speed control phase

2. First speed control phase, then torque transfer phase

In the first case, the torque on the off-going clutch is initially removed (torque transfer phase), while $T_{Vehicle}$ is kept constant. Then the off-going clutch is opened. From then on, the active mode in the design is mode 2. Using speed control algorithms, the component speeds are driven to their final desired values (speed control phase).

In the second case, the component speeds are initially driven to their final desired values, reducing the torque capacity of the off-going clutch and causing slip on that clutch. Once the desired speeds are attained, the torque on the off-going clutch is removed completely (torque transfer phase) and the off-going clutch is opened.

The flow chart of the algorithm that evaluates the feasibility of a mode transition with 1 off-going clutch is shown in Figure 8.8. The first step in the algorithm is to derive the speed and torque equations of the start mode (Mode 1) using the techniques in Section 3.2. Using the speed equations, the speed at each PG node after 0.8 seconds of the current simulation time ($t+0.8s$) is calculated by assuming the mode transition starts at $t + 0.8s$ and lasts $0.2s$. Then two linear programs (LPs) that include speed

and torque equations, components' torque and speed limits, and mode transition constraints (constant $T_{Vehicle}$ and $\dot{\omega}_{Vehicle}$) are setup, as explained in Section 6.4. Two LPs calculate minimum and maximum torque of the off-going clutch (T_{ofgmin}, T_{ofgmax}). If LP does not have a solution, that is, constant $T_{Vehicle}$ cannot be sustained, the mode transition is not feasible. If it has a solution and T_{ofgmin} and T_{ofgmax} have opposite signs, it means that T_{ofg} can be set to 0 without violating the transition constraints and the torque transfer phase can be implemented first. If T_{ofgmin} and T_{ofgmax} have the same signs, the torque transfer phase cannot be implemented.

If T_{ofgmin} and T_{ofgmax} have opposite signs, the speed control phase can be implemented first as well because T_{ofg} should also be positive for a positive clutch slip or vice versa. The sign of the slip will be determined according to the speed differential between clutch plates (ω_{ofg-}) and (ω_{ofg+}) at the end mode (Mode 2). When T_{ofgmin} and T_{ofgmax} have opposite signs, the speed control phase can be implemented regardless of the sign of the clutch slip. However, if T_{ofg} cannot change its sign and it contradicts the clutch plates' speed differential $\omega_{ofg+} - \omega_{ofg-}$, the speed control phase cannot be implemented before the torque transfer phase.

8.2.3.2 Feasibility of Mode Transition with 1 On-coming Clutch

Since an off-going clutch does not exist in the mode transition with 1 on-coming clutch, the torque transfer phase is not implemented. To match the speeds of on-coming clutch plates, the speed control phase is implemented. Hence, the component speeds are driven to their final desired values and the on-coming clutch is closed. If $T_{Vehicle}$ cannot be kept constant during the speed control phase, the mode transition is not feasible.

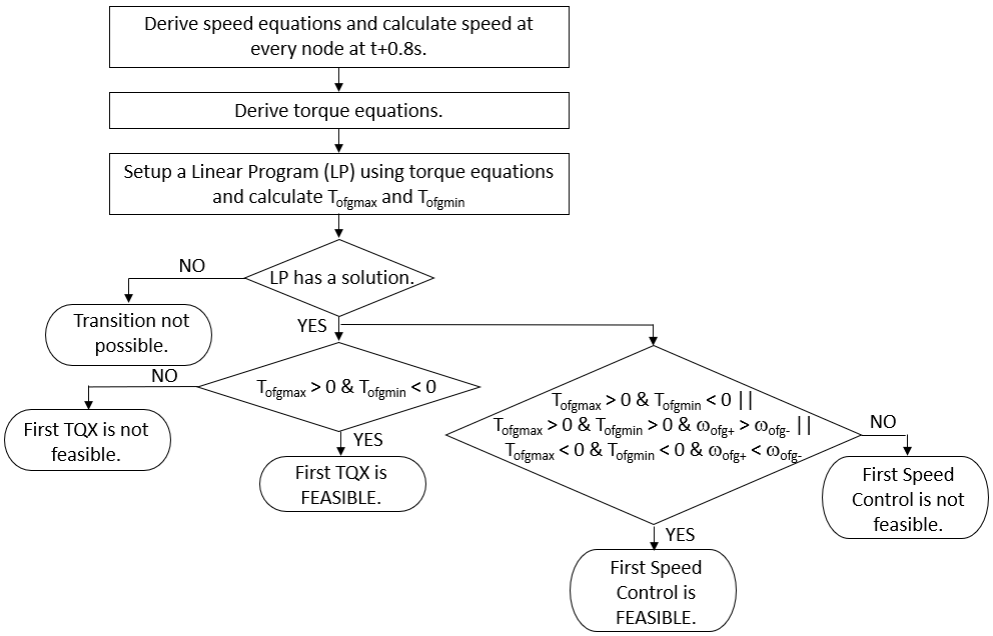

Figure 8.8: Mode Transition Feasibility Algorithm for a Mode Transition with 1 Off-going Clutch.

8.2.3.3 Feasibility of Mode Transition with 1 Off-going and 1 On-coming Clutches

The flow charts of the algorithm that evaluates the feasibility of a mode transition with 1 off-going and 1 on-coming clutches, and the order of torque transfer and speed control phases are shown in Figures 8.9 and 8.10. The initial steps in the algorithms are the same as those in Figure 8.8 until the setup of the linear program. Then four linear programs (LPs) that include speed and torque equations, components' torque and speed limits, and mode transition constraints (constant $T_{Vehicle}$ and $\dot{\omega}_{Vehicle}$) are set up, as explained in Section 6.4. Two LPs calculate minimum and maximum torque of the off-going clutch (T_{ofgmin}, T_{ofgmax}) when the torque on the on-coming clutch is zero $T_{onc} = 0$, that is, the current mode is the start mode (Mode 1). Moreover, two more LPs calculate minimum and maximum torque of the on-coming clutch (T_{oncmin}, T_{oncmax}) when the torque on the off-going clutch is zero $T_{ofg} = 0$, that is, the current mode is the end mode (Mode 2). If LP does not have a solution, that is, constant

$T_{Vehicle}$ cannot be sustained, the mode transition is not feasible.

For the feasibility of the first torque transfer phase and then the speed control phase, the speed differential between on-coming clutch plates (ω_{onc-} and ω_{onc+}) at the start mode (Mode 1) is compared to T_{oncmin} and T_{oncmax}. If T_{oncmax} and the slip speed of the on-coming clutch are positive, or T_{oncmin} and the slip speed of the on-coming clutch are negative, the torque transfer phase can be implemented first since the torque can be transferred from the off-going clutch to the slipping on-coming clutch. However, since the torque transfer cannot occur instantaneously, the solution of intermediate T_{onc}, T_{ofg} torque values should also be examined, as shown in Figure 8.9.

For the feasibility of the first speed control phase and then the torque transfer phase, the speed differential between off-going clutch plates (ω_{ofg-} and ω_{ofg+}) at the end mode (Mode 2) is compared to T_{ofgmin} and T_{ofgmax}. If T_{ofgmax} and the slip speed of the off-going clutch are positive or T_{ofgmin} and the slip speed of the off-going clutch are negative, the speed control phase can be implemented first since the torque capacity of the off-going clutch can be reduced in order to slip it and control the speed of the other nodes. Moreover, speed control can be performed through the off-going clutch's slip regardless of the difference between ω_{ofg-} and ω_{ofg+} if T_{ofgmax} and T_{ofgmin} have opposite signs because T_{ofg} can be set to any sign depending on ω_{ofg-} and ω_{ofg+}.

8.2.4 Speed Control Algorithm

In the speed control phase, the speed of PG nodes are controlled to the values at the start of high level control's next time step $(t + 1)$. However, the initial values of the speed variables are not known, since the instant when the mode transition starts during the high level control's current time step is also not known. Hence, this known-final-state and unknown-initial-state control problem can be solved by starting

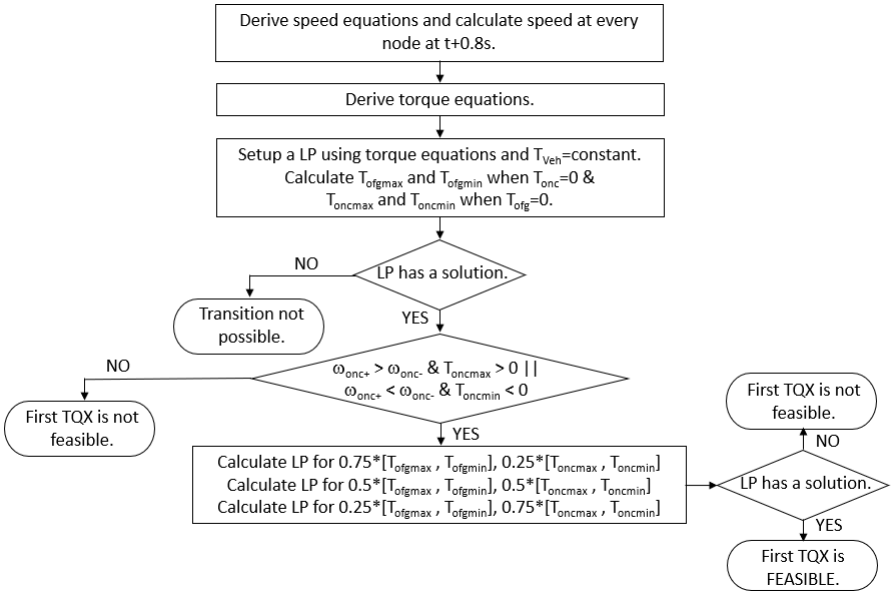

Figure 8.9: Mode Transition Feasibility Algorithm for a Mode Transition with 1 Off-going and 1 On-coming Clutches, where Torque Transfer Phase executes before Speed Control Phase.

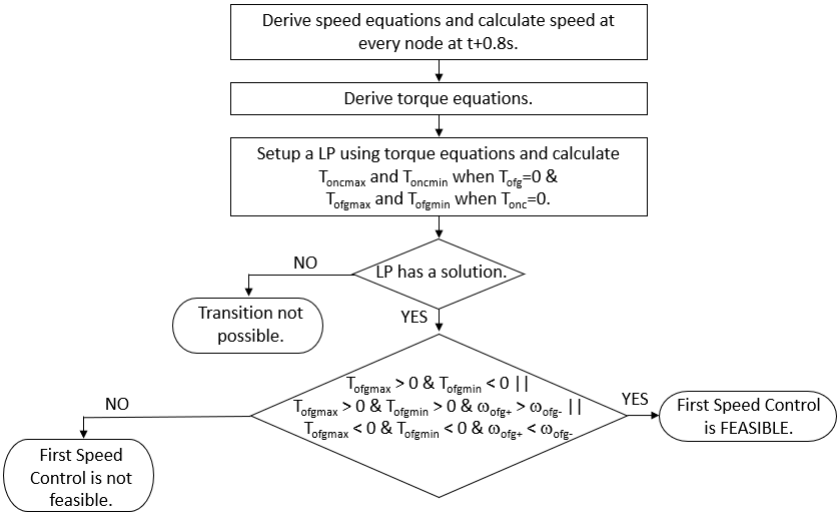

Figure 8.10: Mode Transition Feasibility Algorithm for a Mode Transition with 1 Off-going and 1 On-coming Clutches, where Speed Control Phase executes before Torque Transfer Phase.

from the final state and going backwards in time until a solution is found. The length in which the solution is found is subtracted from $t + 1$ to calculate the instant the

speed control should start between t and $t+1$.

The flow chart of the designed control algorithm is shown in Figure 8.11. The first step in the algorithm is to derive the dynamic equation of the mode in the format, as in Eq. (8.1), using the technique explained in Section 3.3, where $\dot{\Omega}$ is the vector of each PG node's rotational acceleration, U is the vector of torque inputs, A is the inertia matrix, B is the torque input matrix, and C is the speed constraint matrix. Since the requirement of the feasible mode transition is constant $\dot{\omega}_{Vehicle}$ in $\dot{\Omega}$, and constant $T_{Vehicle}$ in U during a mode transition, the columns corresponding to these variables can be carried to the right side of the equation after their summation as a constant vector. Then the application of the reduced row echelon form on this set of linear equations reveals the independent and dependent control inputs, as shown in Eq. (8.2), which is reformulated in Eq. (8.3) for the successive steps. Furthermore, the independent speed variables called controlled states are also determined using $C \cdot \Omega = 0$. The maximum size of $U_{independent}$ vector can be two because the maximum number of independent torque variables can be three in any mode, as shown in Chapter IV and one of these variables $T_{Vehicle}$ is constant during a mode transition. All control combinations of $U_{independent}$ are generated within their limits and $U_{dependent}$ is calculated using Eq. (8.3). The control combinations that cause any element of $U_{dependent}$ to be out of its limits are excluded from the possible solution set. If any feasible control combination is not left after this elimination, the mode transition is declared an infeasible mode transition.

$$\begin{bmatrix} A & B \\ C & 0 \end{bmatrix} \begin{bmatrix} \dot{\Omega} \\ U \end{bmatrix} = D \begin{bmatrix} \dot{\Omega} \\ U \end{bmatrix} = 0 \tag{8.1}$$

$$D \begin{bmatrix} \dot{\Omega} \\ U_{dependent} \\ U_{independent} \end{bmatrix} = b \tag{8.2}$$

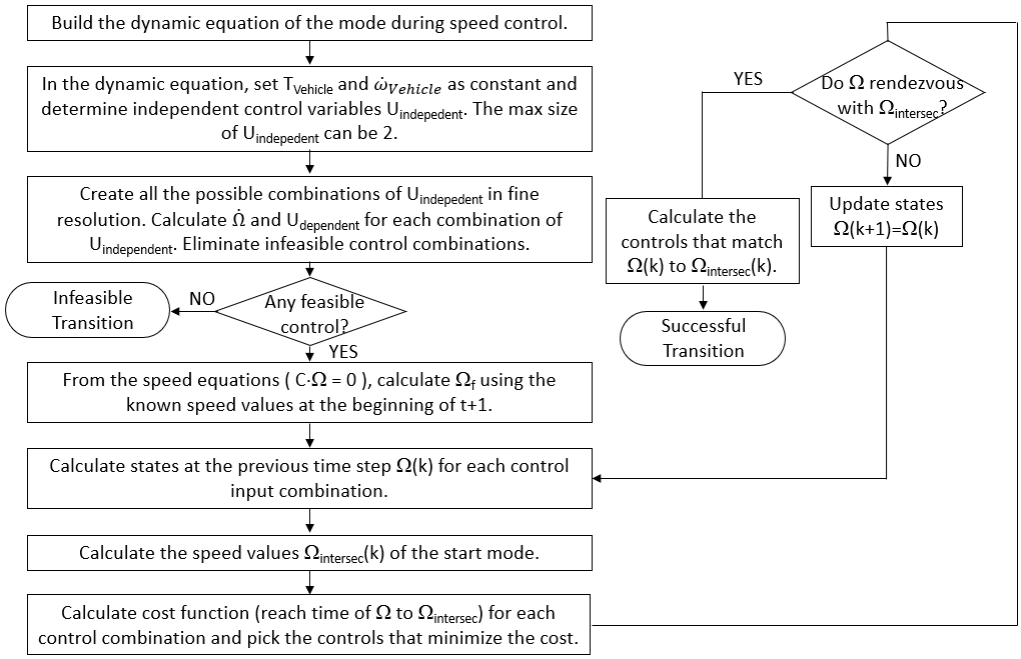

Figure 8.11: Speed Control Algorithm.

$$\begin{bmatrix} \dot{\Omega} \\ U_{dependent} \end{bmatrix} = \begin{bmatrix} E_1 \\ E_2 \end{bmatrix} U_{independent} + \begin{bmatrix} F_1 \\ F_2 \end{bmatrix} b \tag{8.3}$$

If any feasible control combination exists, final state values Ω_f at the beginning of $t+1$ are calculated from the $C \cdot \Omega = 0$. Then the state equation in Eq. (8.3) is discretized to the form in Eq. (8.4) in order to start calculating the controls solution backwards in time. In this equation, Δt and $k \cdot \Delta t$ are the execution period and one time step before the current time in the time domain of the medium level control, respectively. The state values at the previous time step are calculated using latest state values $\Omega(k+1)$, all feasible control combinations, and Eq. (8.4). The control input combinations that cause any state in $\Omega(k)$ to go out of its bound or to an undesired direction are eliminated.

$$\begin{bmatrix} \Omega(k) \\ U_{dependent}(k) \end{bmatrix} = \begin{bmatrix} \Omega(k+1) \\ 0 \end{bmatrix} + \begin{bmatrix} -\Delta t \cdot E_1 \\ E_2 \end{bmatrix} U_{independent}(k) + \begin{bmatrix} -\Delta t \cdot F_1 \\ F_2 \end{bmatrix} b(k) \tag{8.4}$$

Assuming the speed control phase of the mode transition starts at time $t + k \cdot \Delta t$, the speed at every PG node of the start mode $\Omega_{intersec}(k)$ is calculated using the speed equations of the start mode and the acceleration at each PG node without medium level control. Using this information and previous results, the feasible control combination that minimizes the time the controlled states reach their corresponding elements in $\Omega_{intersec}(k)$ simultaneously is selected as the control commands at time $t + k \cdot \Delta t$. When all controlled states reach their rendezvous points in $\Omega_{intersec}$ with the selected controls, $t + k \cdot \Delta t$ is set as the time the mode transition should start and $t + 1 - (t + k \cdot \Delta t) = 1 - k \cdot \Delta t$ becomes the duration of the speed control. If the controlled states cannot reach their rendezvous points less than a preset time threshold, the control effort is abandoned and the mode transition is defined as an infeasible transition.

8.3 Integration of Mode Transition Control into Fuel Economy Simulations

The previous section laid out the concepts for controlling a mode transition in an HEV transmission. However, it did not explain how these concepts can be used in a design process. A mode transition requires the dynamic control of actuators, and affects the fuel economy benefit of a design. Hence, making the mode transition a part of the fuel economy simulations enhances the accuracy of the design process. In this section, how the mode transition algorithms are integrated into the PEARS fuel economy simulation algorithm and related simulation results are discussed.

8.3.1 Integration of Mode Transition Control into PEARS

As the other fuel economy simulation algorithms, PEARS optimizes the decision of mode selection for maximum fuel economy at the high level of hierarchy explained in Section 8.1. The optimization is performed in two main steps, as shown in Figure 8.12. In the first step, the target drive cycle is discretized into a 2D table with the X and Y axes being the vehicle speed and vehicle torque demand, respectively. Then the most efficient modes and the operating points of the components in these modes are identified for EV, HEV, and regenerative HEV operations in each cell of this table. The completion of the table is a computationally intensive task due to its size and the large number of solution candidates. In the second step, the mode that optimizes fuel economy is selected at each time instant of the drive cycle using the dynamic programming (DP) technique. The cost function at each time instant k in the DP is chosen as $C(x_{i,k}, u_k = x_{j,k+1}) = Fuel\_Rate(x_{j,k+1})$, where m, and $x_{i,k}$ $i = 1, ..., m$ are the number of modes and the selected mode at time instant k, respectively. The control signal u_k that sets the value of the cost function is the mode at the next time instant $x_{j,k+1}$ $j = 1, ..., m$. Since the cost function does not depend on the start mode $x_{i,k}$ and the operating points of the components in each selected mode have already been calculated in the first step, the execution time of the second step is much shorter than that of the first step.

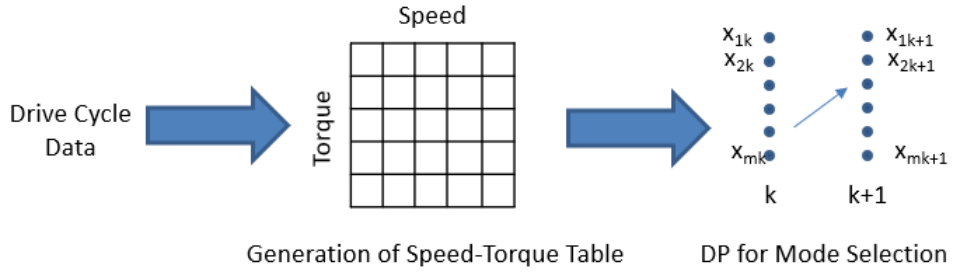

Figure 8.12: Phases of PEARS Algorithm.

The lack of the start mode in the cost function makes it unsuitable for integrating

the mode transition algorithms into PEARS. Hence, the cost function is modified as $C(x_{i,k}, u_k = x_{j,k+1}) = Fuel\_Rate(x_{j,k+1}) \cdot (1 - \Delta t_{transition}) + Fuel\_Rate(\Delta t_{transition}) + Fuel\_Rate(x_{j,k+1})$, where $\Delta t_{transition}$ and $Fuel\_Rate(\Delta t_{transition})$ are the duration of the corresponding mode transition and the fuel consumed during the mode transition, respectively.

In contrast to the original formulation, the cost function should be calculated for each mode transition combination $(x_{i,k}, x_{j,k+1})$. Furthermore, the feasibility and control of all mode transition options need to be evaluated for each mode transition combination. Therefore, the cost function calculation is computationally intensive and lengthens the fuel economy simulations considerably. The execution of the PEARS algorithm is accelerated by modifying PEARS through an iterative method as follows.

1. Execute the PEARS without mode transition algorithms.

2. Save the vehicle speed and torque table generated in the first phase of PEARS for the next run, since this table is independent from mode transition algorithms.

3. Identify mode transition combinations $(x_{i,k}, x_{j,k+1})$ from the fuel economy simulation data of PEARS without mode transition algorithms and record them in a mode transition table.

4. Execute the modified PEARS by using recorded vehicle speed and torque table, and evaluating the fuel penalty of mode transitions in the previously recorded transition table.

5. Compare the new mode transition data to the one in the transition table and update the transition table to cover all mode transition combinations in the previous simulations.

6. Repeat the cycle of running the modified PEARS with the updated transition table until the transition table covers all mode transitions in a simulation.

8.3.2 Simulation Results

To validate and explore the effect of mode transitions on fuel economy simulation results, the modified PEARS algorithm is executed for the best 10 designs, depicted in Figures 7.5-7.6. As shown in Tables 8.1-8.2, the fuel economy penalties of including mode transitions in the UDDS and HWFET simulations vary between 1.78mpg-0.25mpg (average=0.75mpg) and 0.64mpg-0.06mpg (average=0.29mpg), respectively. The following observations can be made about the results.

- The duration of mode transitions falls generally in the range of tens of milliseconds, which is shorter than expected duration of a few hundreds of milliseconds because the power requirements of the drive cycles are much lower than the capability of competent designs and, hence, the engine and electric machines have sufficient torque reserves to control mode transition dynamics in a fast manner without deteriorating vehicle output torque. As a result, mode transitions do not have a major effect on fuel economy results most of the time.

- Since the duration of the HWFET drive cycle is shorter than the one of the UDDS, and the speed and load in the HWFET drive cycle do not vary as much as in the UDDS drive cycle, the fuel economy decrease due to mode transitions is not large in the HWFET drive cycle.

- Two interwoven factors play a key role in the deterioration of fuel economy due to the inclusion of mode transitions. The first factor is the fuel cost of feasible mode transitions, as some mode transitions require longer time spent at inefficient operating points in contrast to other efficient mode transitions that last very short. For example, Design 40 and Design 43 have the same number of feasible modes and the penalty of the inclusion of mode transitions in Design 43 is twice of the penalty in Design 40 (1.17mpg vs. 0.56mpg) although in Design 40 the modes selected by PEARS have changed at the 41% of the UDDS time

instants due to the inclusion of mode transition algorithms in contrast to Design 43, where the modes have changed at the 34% of the UDDS time instants. The second factor is the availability of fuel efficient modes in a design. Some designs have more alternative fuel-efficient modes to each drive cycle load and speed point. If a mode transition penalizes the fuel economy at a time instant, PEARS can select the alternative fuel-efficient mode that requires less mode transition effort for that time point. For example, Design 37 has just five feasible modes, whereas Design 40 has seven feasible modes. Although in Design 40 the modes selected by PEARS have changed at the 41% of the UDDS time instants in contrast to 24% of the time instants in Design 37, the fuel economy penalty in Design 40 is much less than the one in Design 37 (0.56mpg vs. 1.78mpg).

- Some mode transitions may have a positive effect on the fuel economy if the mode transition at any simulation time is from a less efficient mode to a much more efficient one, since longer time is spent on more efficient operating points during mode transition.

Table 8.1: UDDS Fuel Economy Results of Ten Competent Designs without and with Mode Transition Algorithms

Design No	UDDS Fuel Economy without Mode Transitions (mpg)	UDDS Fuel Economy with Mode Transitions (mpg)	Δ
Design 43	37.61	36.44	1.17
Design 37	36.89	35.11	1.78
Design 4	37.12	36.23	0.89
Design 5	35.85	35.60	0.25
Design 2	36.79	36.14	0.65
Design 40	37.79	37.23	0.56
Design 1	36.20	35.78	0.42
Design 36	35.42	34.67	0.75
Design 23	35.88	35.23	0.65
Design 34	35.41	35.01	0.40

In the original PEARS, four mode transition penalty terms, whose coefficients are set by trial and error, have been added to the cost function to prevent frequent

Table 8.2: HWFET Fuel Economy Results of Ten Competent Designs without and with Mode Transition Algorithms

Design No	HWFET Fuel Economy without Mode Transitions (mpg)	HWFET Fuel Economy with Mode Transitions (mpg)	Δ
Design 43	27.15	26.83	0.32
Design 37	25.62	24.98	0.64
Design 4	27.20	26.70	0.50
Design 5	26.71	26.41	0.30
Design 2	26.19	26.04	0.15
Design 40	27.16	27.05	0.11
Design 1	25.83	25.69	0.14
Design 36	25.65	25.52	0.13
Design 23	25.68	25.62	0.06
Design 34	26.95	26.42	0.53

mode transitions and their unknown effects, as no analysis about mode transitions has been done during the development of PEARS. Since the problem of mode transition feasibility and control is solved analytically in this study, the mode transition penalty terms are removed during the simulations. However, the cost of the inclusion of the mode transitions is long simulation time, which makes the execution of the modified PEARS for each competent design impractical. This dilemma can be solved by first running PEARS with the mode transition algorithms for only a few of the competent designs and then executing the original PEARS several times for various penalty terms until the fuel economy numbers between modified and original PEARS are close to each other. This way, mode transition penalty terms are calibrated analytically and the cost of long simulation time is avoided.

CHAPTER IX

Conclusions and Future Work

9.1 Conclusions

In this dissertation, a systematic hybrid electric powertrain design process with strategically placed phases is presented. The major contribution of this design methodology is to develop the necessary HEV powertrain analysis and synthesis methods to overcome the challenges of achieving all the following design benefits.

- The design methodology relies on an exhaustive search of the design space to prevent the possibility of skipping any useful design candidate.
- All performance criteria utilized in a realistic powertrain design process are included. Hence, the optimal designs are superior in terms of both fuel economy and performance.
- Optimal component-sizing is involved in the process.
- Mode transition dynamics becomes a part of the fuel economy evaluation in the process.

The key reason for the success of the proposed design process is to create and order the design phases strategically. In the first and most critical phase, powertrain modes are chosen as the constituents of the design space, as this choice generates a

design space in a manageable size that enables the screening all possible designs in a time-efficient manner. In the second phase, algorithms independent of the size of any component are developed to analyze the feasibility and powertrain type of each mode. Removing the infeasible modes from the design space in the early stage allows the subsequent phases to deal with a smaller design space. In the third phase, the feasible modes are grouped according to their forward-speed and backward-speed capability for the engine-on condition. This grouping made another strategic cut to the size of the design space since the initial focus in the design process is forward-speed capable modes. In the fourth phase of the process, the performance of each forward-speed capable mode is evaluated against gradeability, long-hauling, acceleration time, and top speed criteria for each planetary gearset (PG) gear ratio combination. The maximum output torque used in gradeability and acceleration time calculations is assessed using a novel problem formulation suitable to the application of linear programming (LP) techniques. New LP solvers specific to each powertrain type are developed to accelerate the processing time of solving maximum output torque problem. These solvers enable completing the performance analysis of all feasible modes for all PG gear ratio combinations within practical time limits. At the end of this phase, each forward-speed capable mode possesses its performance map. The fifth phase identifies the combination of modes called competent designs that meet the performance requirements, along with the clutches that make the mode transitions possible. Moreover, each competent design is evaluated in terms of backward-speed capability by analyzing whether any auxiliary mode in the design is backward-speed capable or the design can be integrated with another backward-speed capable mode without exceeding the clutch number limit. At the end of this phase, the number of competent designs is low enough to conduct the time-consuming fuel economy simulations. In the last phase, the fuel economy benefit of each competent design for each PG gear ratio combination is assessed using an algorithm that approximates dynamic

programming optimization. The high performing designs with high fuel economy benefits are presented at the end of the process.

In addition to the design process, novel algorithms about mode transition feasibility and control are developed and then integrated into the fuel economy simulations to obtain more accurate results.

To sum up, the introduced design process with its analysis and synthesis phases solves the problem of identifying high performing and fuel efficient PG-based HEV powertrain designs.

9.2 Future Work

The design process is applied to HEV powertrains with simple PGs. When a second pinion is inserted between the sun and ring gears of a simple PG, the resultant device is called a double-pinion PG. The governing speed and torque equations of double-pinion PGs are equivalent to those of simple PGs if α and β terms are replaced by $-\alpha$ and $-\beta$. Therefore, modes constructed with double-pinion PGs can be included in the design space by just extending the range of simple PG gear ratios to the negative domain. In the future, the contribution of modes with double-pinion PGs to the final set of fuel efficient competent designs should be investigated.

Section 5.2 shows that the coefficients in the torque equations are monotonic functions of PG gear ratios by utilizing only two-PG modes. This proof should be extended to cover modes with any number of PGs.

Although the proposed design process and its methods are applied to modes that can be generated with two PGs, one engine, two electric machines, three brakes, and three clutches, the process can be adapted to modes that can be constructed with any number of components. Increasing the number of electric machines or engines in an HEV powertrain is not practical due to their cost. However, the PG number can be increased to three, as most of today's conventional transmissions have three PGs and

PGs are not costly hardware. Hence, as an extension of this dissertation, the design process needs to be updated to solve the following complications of three-PG modes.

- Mode-based design space grows from 50,000 modes to 5 million modes when the PG number in a design increases from two to three. Therefore, new compression techniques similar to that in Section 3.4 should be developed to accelerate mode feasibility analysis.

- Some modes in the design space are not implementable due to the physical constraints imposed by the way the PG nodes are connected to each other. Hence, a new computationally efficient method should be developed to determine the implementability of each feasible mode.

- In three-PG modes, an actuator can be connected to more than one PG node at the same time. The mode generation phase should take these modes into account as well.

In Section 8.2, all feasible control methods to perform mode transitions are developed. In most of them, an on-coming- or off-going clutch slips while transferring torque during a certain period of the transition. However, undesired heat energy is dissipated during this phenomenon. As an improvement to the mode transition control, a simple clutch heating model should be integrated into the mode transition control algorithms in PEARS, and the weight of the mode transition penalty term in the mode selection phase of PEARS should start from zero at the beginning of the fuel economy simulation. As the total heat dissipated through a slipping clutch increases during the fuel economy simulation, the mode transition penalty term should be gradually increased. This mechanism will maximize the fuel economy benefit of a design by facilitating as many mode transitions as possible without exceeding practical hardware limits.

BIBLIOGRAPHY

BIBLIOGRAPHY

[1] Ernest H. Wakefield. *History of the Electric Automobile: Hybrid Electric Vehicles*. Society of Automotive Engineers (SAE), 1998.

[2] Jeff Cobb. December 2016 Hybrid Car Sales Numbers. `http://www.hybridcars.com/december-2016-dashboard/`, 2017. [Online; accessed 20-August-2017].

[3] Environmental Protection Agency (EPA) and Department of Transportation (DOT). Light-duty vehicle greenhouse gas emission standards and corporate average fuel economy standards. Federal Register 199, 2012.

[4] Brandon Schoettle and Michael Sivak. A comparison of CAFE standards and actual CAFE performance of new light-duty vehicles: An update through model year 2014. Technical report, University of Michigan, Transportation Research Institute (UMTRI), 10 2014.

[5] National Highway Traffic Safety Administration (NHTSA). NHTSA and EPA set standards to improve fuel economy and reduce greenhouse gases for passenger cars and light trucks for model years 2017 and beyond. Technical report, 2012.

[6] The U.S. automotive market and industry in 2025. Technical report, Center for Automotive Research (CAR), 06 2011.

[7] Parisa Bastani, John B. Heywood, and Chris Hope. Potential for meeting light-duty vehicle fuel economy targets, 2016-2025. Technical report, Massachusetts Institute of Technology, 01 2012.

[8] Environmental Protection Agency (EPA). Joint Technical Support Document: Final Rulemaking for 2017-2025 Light-Duty Vehicle Greenhouse Gas Emission Standards and Corporate Average Fuel Economy Standards. Technical report, 2012.

[9] WardsAuto Corp. U.S. Car and Truck Sales, 1931-2016. `http://wardsauto.com/public-data`, 2017. [Online; accessed 20-August-2017].

[10] Tim Grewe, Brendan Conlon, and Alan Holmes. Defining the General Motors 2-Mode Hybrid Transmission, 2007-01-0273. Society of Automotive Engineers World Congress, Detroit, USA, 2007.

[11] M. Schulz. Circulating Mechanical Power in a Power-split Hybrid Electric Vehicle Transmission. *Journal of Automobile Engineering*, 218:1419–1425, 2004.

[12] Howard L. Benford and Maurice B. Leising. The Lever Analogy: A New Tool in Transmission Analysis, 810102. Society of Automotive Engineers World Congress, Detroit, USA, 1981.

[13] Epicyclic Gearing. `http://en.wikipedia.org/wiki/Epicyclic_gearing`, 2003. [Online; accessed 04-April-2015].

[14] Edward J. Haug. *Intermediate Dynamics*. Prentice Hall, 1992.

[15] M. Maegi. A General New Approach for Characterization and Analysis of Planetary Gear Trains. *VDI Berichte*, (1460):77–91, 1999.

[16] Shushan Bai, Joel Maguire, and Huei Peng. *Dynamic Analysis and Control System Design of Automatic Transmissions*. SAE International, 1st edition, 2013.

[17] Thomas R. Kane and David A. Levinson. *Dynamics: Theory and Applications*. Mcgraw-Hill, 1985.

[18] F. Freudenstein and A. T. Yang. Kinematics and Statics of a Coupled Epicyclic Spur-Gear Train. *Mechanism and Machine Theory*, 7:263–275, 1972.

[19] E. Pennestri and F. Freudenstein. The Mechanical Efficiency of Epicyclic Gear Trains. *ASME Journal of Mechanical Design*, 115:645–651, 1993.

[20] D. C. Karnopp, D. L. Margolis, and R. Rosenberg. *System Dynamics - a Unified Approach*. John Wiley and Sons, New York, 1990.

[21] Andy Ruina and Rudra Pratap. *Introduction to Statics and Dynamics*. Oxford University Press, 2002.

[22] D. Zhang, J. Chen, T. Hsieh, J. Rancourt, and M. R. Schmidt. Dynamic Modelling and Simulation of Two-Mode Electric Variable Transmission. *Proceedings of the IMechE, Part D*, 215:1217–1223, 2001.

[23] Namdoo Kim, Richard Carlson, Forrest Jehlik, and Aymeric Rousseau. Tahoe HEV Model Development in PSAT, 2009-01-1307. Society of Automotive Engineers World Congress, Detroit, USA, 2009.

[24] M. Cipek, J. Deur, and J. Petric. Bond Graph Modelling and Power Flow Analysis of Series-Parallel HEV Transmissions. *International Journal of Powertrains*, 1(4):396–419, 2012.

[25] Jinming Liu and Huei Peng. Modeling and Control of a Power-Split Hybrid Vehicle. *IEEE Transactions on Control Systems Technology*, 16(6):1242–1251, 2008.

[26] Fazal Syed, Ming L. Kuang, John Czubay, and Hao Ying. Derivation and Experimental Validation of a Power-Split Hybrid Electric Vehicle Model. *IEEE Transactions on Vehicular Technology*, 55(6):1731–1747, 2006.

[27] Aimin Du and Hongwei Cai. An Analytic Foundation for the Two-Mode Hybrid Transmission with a Comparison to Other Hybrid Vehicle Power Split Transmissions. International Conference on Transportation, Mechanical, and Electrical Engineering, Changchun, China, 2011.

[28] Michael A. Miller, Alan G. Holmes, Brendan M. Conlon, and Peter J. Savagian. The GM "Voltec" 4ET50 Multi-Mode Electric Transaxle. Society of Automotive Engineers World Congress, Detroit, USA, 2011.

[29] Jinming Liu and Huei Peng. A Systematic Design Approach for Two Planetary Gear Split Hybrid Vehicles. *Vehicle System Dynamics*, 48(11):1395–1412, 2010.

[30] Madhusudan Raghavan, Norman Bucknor, Joel Maguire, James Hendrickson, and Tejinder Singh. The Design of Advanced Transmissions. FISITA World Automotive Congress, Yokohama, Japan, 2006.

[31] Kai Loon Cheong, Perry Y. Li, and Thomas R. Chase. Optimal Design of Power-Split Transmissions for Hydraulic Hybrid Passenger Vehicles. American Control Conference, San Francisco, CA, 2011.

[32] Xiaowu Zhang, Huei Peng, Jing Sun, and Shengbo Li. Automated Modeling and Mode Screening for Exhaustive Search of Double-Planetary-Gear Power Split Hybrid Powertrains. ASME Dynamic Systems and Control Conference, San Antonio, Texas, 2014.

[33] Minkuk Kang, Hyunjun Kim, and Dongsuk Kum. Systematic Configuration Selection Methodology of Power-Split Hybrid Electric Vehicles with a Single Planetary Gear. In *SAE Technical Paper*, Proceedings of the ASME Dynamic Systems and Control Conference, San Antonio, TX, 10 2014.

[34] Emilia Silvas, Theo Hofman, Alexander Serebrenik, and Maarten Steinbuch. Functional and Cost-Based Automatic Generator for Hybrid Vehicle Topologies. *IEEE/ASME Transactions on Mechatronics*, 20(4):1561–1572, 2015.

[35] Xiaowu Zhang, Shengbo E. Li, Huei Peng, and Jing Sun. Efficient Exhaustive Search of Power-Split Hybrid Powertrains with Multiple Planetary Gears and Clutches. *Journal of Dynamic Systems, Measurement, and Control*, 137(12), 2015.

[36] Alparslan E. Bayrak, Namwoo Kang, and Panos Y. Papalambros. Decomposition-Based Design Optimization of Hybrid Electric Powertrain Architectures: Simultaneous Configuration and Sizing Design. *Journal of Mechanical Design*, 138(7), 2016.

[37] Weichao Zhuang, Xiaowu Zhang, D. Zhao, Huei Peng, and Liangmo Wang. Optimal Design of Three-Planetary-Gear Power-Split Hybrid Powertrains. *International Journal of Automotive Technology*, 17(2):299–309, 2016.

[38] Weichao Zhuang, Xiaowu Zhang, Huei Peng, and Liangmo Wang. Rapid Configuration Design of Multiple-Planetary-Gear Power-Split Hybrid Powertrain via Mode Combination. *IEEE/ASME Transactions on Mechatronics*, 21(6):2924–2934, 2016.

[39] Xiaowu Zhang, Chiao-Ting Li, Dongsuk Kum, and Huei Peng. Prius+ and Volt-: Configuration Analysis of Power-Split Hybrid Vehicles with a Single Planetary Gear. *IEEE Transactions on Vehicular Technology*, 61(8):3544–3552, 2012.

[40] Kai Loon Cheong, Perry Y. Li, Stephen Sedler, and Thomas R. Chase. Comparison between Input Coupled and Output Coupled Power-Split Configurations in Hybrid Vehicles. International Fluid Power Exhibition, Las Vegas, NV, 2011.

[41] Richard Bellman. *Dynamic Programming*. Princeton University Press, Princeton, NJ, 1957.

[42] Dimitri P. Bertsekas. *Dynamic Programming and Optimal Control*, volume 1. Athena Scientific, Belmont, MA, 3rd edition, 2005.

[43] C. C. Lin, Huei Peng, Jessy W. Grizzle, and Jun-mo Kang. Power Management Strategy for a Parallel Hybrid Electric Truck. *IEEE Transactions on Control Systems Technology*, 11(6):839–849, 2003.

[44] C. Mansour and D. Clodic. Optimized Energy Management Control for the Toyota Hybrid System Using Dynamic Programming on a Predicted Route with Short Computation Time. *International Journal of Automotive Technology*, 13(2):309–324, 2012.

[45] Laura V. Perez, Guillermo Bossio, Diego Moitre, and Guillermo Garcia. Optimization of Power Management in an Hybrid Electric Vehicle using Dynamic Programming. *Mathematics and Computers in Simulation*, 2006.

[46] A. Sciarretta and L. Guzzella. Optimal Control of Parallel Hybrid Electric Vehicles. *IEEE Transactions on Control System Technology*, 12(3):352–363, 2004.

[47] Michiel Koot, J. T. B. A. Kessels, Bram de Jager, W. P. M. H. Heemels, P. P. J. van den Bosch, and Maarten Steinbuch. Energy Management Strategies for Vehicular Electric Power Systems. *IEEE Transactions on Vehicular Technology*, 54(3):771–782, 2005.

[48] Oguz H. Dagci, Huei Peng, and Jessy W. Grizzle. Power-split hybrid electric powertrain design with two planetary gearsets for light-duty truck applications. *IFAC-PapersOnLine*, 28(15):8–15, 9 2015.

[49] S. Delprat, T. Guerra, G. Paganelli, J. Lauber, and M. Delhom. Control Strategy Optimization for an Hybrid Parallel Powertrain. American Control Conference, Arlington, TX, 2001.

[50] G. Paganelli, S. Delprat, T. Guerra, J. Rimaux, and J. Santin. Equivalent Consumption Minimization Strategy for Parallel Hybrid Powertrains. IEEE Vehicular Technology Conference, Atlantic City, NJ, 2001.

[51] Lorenzo Serrao, Simona Onori, and Giorgio Rizzoni. ECMS as a Realization of Pontryagin's Minimum Principle for HEV Control. American Control Conference, St. Louis, MO, 2009.

[52] Donald E. Kirk. *Optimal Control Theory - An Introduction*. Dover Publications, Mineola, NY, 2004.

[53] Namwook Kim and Aymeric Rousseau. Sufficient Conditions of Optimal Control based on Pontryagin's Minimum Principle for Use in Hybrid Electric Vehicles. *Journal of Automobile Engineering*, 226(9):1160–1170, 2012.

[54] N. Murgovski, L. Johannesson, J. Sjoberg, and B. Egardt. Component Sizing of a Plug-in Hybrid Electric Powertrain via Convex Optimization. *Mechatronics*, 22(1):106–120, 2012.

[55] X. Hu, N. Murgovski, L. Johannesson, and B. Egardt. Energy Efficiency Analysis of a Series Plug-in Hybrid Electric Bus with different Energy Management Strategies and Battery Sizes. *Applied Energy*, 111:1001–1009, 2013.

[56] N. Murgovski, X. Hu, L. Johannesson, and B. Egardt. *Combined Design and Control Optimization of Hybrid Vehicles*. 2014.

[57] M. Pourabdollah, N. Murgovski, A. Grauers, and B. Egardt. Optimal Sizing of a Parallel PHEV Powertrain. *IEEE Transactions on Vehicular Technology*, 62(6):2469–2480, 2013.

[58] Xiaowu Zhang, Huei Peng, and Jing Sun. A Near-Optimal Power Management Strategy for Rapid Component Sizing of Power Split Hybrid Vehicles with Multiple Operating Modes. American Control Conference, Washington DC, 2013.

[59] M. Goetz, M. C. Levesley, and D. A. Crolla. Integrated powertrain control of gearshifts on twin clutch transmissions. In *SAE Technical Paper*. SAE International, 03 2004.

[60] Shushan Bai, Daniel Brennan, Donald Dusenberry, Xuefeng Tao, and Zhen Zhang. Integrated powertrain control. In *SAE Technical Paper*. SAE International, 04 2010.

[61] Qingkai Wei, Yulong Lei, Xingzhong Li, Boqin Hu, Zhengwei Liu, and Bin Song. Integrated control strategy in the power-on upshift process of automatic transmission based on transmission output torque. In *SAE Technical Paper*. SAE International, 04 2015.

[62] Yunjiang Cheng, Xiangyang Xu, Shuhan Wang, and Yang Liu. Generic Control Flow for the Four Types of Clutch-to-Clutch Shifts. *Advances in Mechanical Engineering*, 8(5):1–16, May 2016.

[63] Zeng Xiaohua, Yang Nannan, Wang Junnian, Song Dafeng, Zhang Nong, Shang Mingli, and Liu Jianxin. Predictive-model-based Dynamic Coordination Control Strategy for Power-Split Hybrid Electric Bus. *Mechanical Systems and Signal Processing*, 60-61:785–798, 2015.

[64] Chen Wang, Zhiguo Zhao, Tong Zhang, and Mengna Li. Mode Transition Coordinated Control for a Compound Power-Split Hybrid Car. *Mechanical Systems and Signal Processing*, 87:192–205, 2017.

[65] Sangjoon Kim, Joonyoung Park, Jeongho Hong, Myungwon Lee, and Hyunsung Sim. Transient control strategy of hybrid electric vehicle during mode change. In *SAE Technical Paper*. SAE International, 2009.

[66] Li Chen, Gang Xi, and Jing Sun. Torque Coordination Control during Mode Transition for a Series-Parallel Hybrid Electric Vehicle. *IEEE Transactions on Vehicular Technology*, 61(7):2936–2949, 2012.

[67] Hu Zhang, Yong Zhang, and Chengliang Yin. Hardware-in-the-Loop Simulation of Robust Mode Transition Control for a Series-Parallel Hybrid Electric Vehicle. *IEEE Transactions on Vehicular Technology*, 65(3):1059–1069, 2016.

[68] Arash M. Gavgani, Aldo Sorniotti, John Doherty, and Carlo Cavallino. Optimal Gearshift Control for a Novel Hybrid Electric Drivetrain. *Mechanism and Machine Theory*, 105:352–368, 2016.

[69] Kyuhyun Sim, Sang-Min Oh, Choul Namkoong, Ji-Suk Lee, Kwan-Soo Han, and Sung-Ho Hwang. Control Strategy for Clutch Engagement during Mode Change of Plug-in Hybrid Electric Vehicle. *International Journal of Automotive Technology*, 18(5):901–909, 2017.

[70] Jy-Jen F. Sah and Lawrence A. Kaminsky. Method for Controlling Multiple EVT Shifts in a Multi-Mode Hybrid Transmission, 11 2011. US Patent 8,068,948.

[71] Sungwha Hong, Woulsun Choi, Sunghyun Ahn, Yongjoo Kim, and Hyunsoo Kim. Mode Shift Control for a Dual-Mode Power-Split-Type Hybrid Electric Vehicle. *Journal of Automobile Engineering*, 228(10):1217–1231, 2014.

[72] Besim Demirovic, Pinaki Gupta, Lawrence A. Kaminsky, Ali K. Naqvi, Anthony H. Heap, and Jy-Jen Sah. Method and Apparatus for Executing an Asynchronous Clutch-to-Clutch Shift in a Hybrid Transmission, 08 2014. US Patent 8,801,567.

[73] Kun Huang, Changle Xiang, Yue Ma, Weida Wang, and Reza Langari. Mode Shift Control for a Hybrid Heavy-Duty Vehicle with Power-Split Transmission. *Energies*, 10(2), 2017.

[74] Muammer Yolga and Markus Bachinger. Novel shift control without clutch slip in hybrid transmissions. In *SAE Technical Paper*. SAE International, 03 2017.

[75] Xiaowu Zhang, Shengbo E. Li, Huei Peng, and Jing Sun. Design of Multimode Power-Split Hybrid Vehicles - A Case Study on the Voltec Powertrain System. *IEEE Transactions on Vehicular Technology*, 65(6):4790–4801, 2016.

[76] Emilia Silvas, Theo Hofman, Nikolce Murgovski, Pascal Etman, and Maarten Steinbuch. Review of Optimization Strategies for System-Level Design in Hybrid Electric Vehicles. *IEEE Transactions on Vehicular Technology*, 66(1):57–70, 2017.

[77] R. Mathis and Y. Remond. A New Approach to Solving the Inverse Problem for Compound Gear Trains. *Journal of Mechanical Design*, 121:98–106, 1999.

[78] Ali Emadi, Kaushik Rajashekara, Sheldon S. Williamson, and Srdjan M. Lukic. Topological Overview of Hybrid Electric and Fuel Cell Vehicular Power System Architectures and Configurations. *IEEE Transactions on Vehicular Technology*, 54(3):763–770, May 2005.

[79] John M. Miller. Hybrid Electric Vehicle Propulsion System Architectures of the e-CVT Type. *IEEE Transactions on Power Electronics*, 21(3):756–767, May 2006.

[80] C. M. Chan, Alain Bouscayrol, and Keyu Chen. Electric, Hybrid, and Fuel-Cell Vehicles: Architectures and Modeling. *IEEE Transactions on Vehicular Technology*, 59(2):589–598, 2010.

[81] Chris Mi, Abul M. Masrur, and David W. Gao. *Hybrid Electric Vehicles - Principles and Applications with Practical Perspectives*. John Wiley & Sons, West Sussex, UK, 2011.

[82] Oguz H. Dagci and Huei Peng. A Method for the Exploration of Hybrid Electric Powertrain Architectures with Two Planetary Gearsets. *SAE Int. J. Alt. Power.*, 5:94–108, 04 2016.

[83] Society of Automotive Engineers (SAE). SAE Standard J2807: Performance Requirements for Determining Tow-Vehicle Gross Combination Weight Rating and Trailer Weight Rating, 2012.

[84] Hamdy A. Taha. *Operations Research - An Introduction*. Pearson, London, UK, 9 edition, 2010.

[85] Xiaowu Zhang. *Design of Power Split Hybrid Powertrains with Multiple Planetary Gears and Clutches*. PhD thesis, The University of Michigan, Ann Arbor, MI, 2015.

[86] Weichao Zhuang, Xiaowu Zhang, Huei Peng, and Liangmo Wang. Simultaneous Optimization of Topology and Component Sizes for Double Planetary Gear Hybrid Powertrains. *Energies*, 9(411), May 2016.